I

THE CRYSTAL STRUCTURE OF THE INTERMETALLIC COMPOUND $Mg_{12}Ce$

II

REACTION PRODUCTS OF γ-PICOLINE AND IODINE

Thesis by

Arthur Miller

In Partial Fulfillment of the Requirements

For the Degree of

Doctor of Philosophy

California Institute of Technology

Pasadena, California

1957

ACKNOWLEDGEMENTS

The production of a thesis involves the efforts of many people other than its author. It is a pleasant task to acknowledge the help I have received. I have profited through my association with Professor Gunnar Bergman, my thesis advisor. He has provided the criticism, encouragement, and instruction necessary for the completion of my main research project, has painstakingly examined the manuscript which follows, and has made many valuable editorial suggestions. In addition, his guidance has helped to develop my attitudes and skills for scientific research. To Professor Bergman go my sincerest thanks. I am also grateful to Professor Linus Pauling for his suggestions and aid during my stay at Caltech.

Part of the work described in this thesis was done in collaboration with Dr. Donald Glusker. He has been a friend as well as a worthy research partner. Both Dr. Glusker and I are grateful to Professor Verner Schomaker for his critical discussions with us and for his help in preparing our work for publication. I wish to express my appreciation to the many other members of the Faculty and to the graduate students who have helped make this thesis possible.

The investigation of the crystal structure of $Mg_{12}Ce$ was supported by the Office of Naval Research. The California Institute of Technology, the National Science Foundation, the Consumer's Union, and E. I. du Pont de Nemours and Company have contributed generously in the form of fellowships, assistantships, and scholarships.

Finally, I would like to extend my thanks to my parents for their encouragement and forbearance, and to the friends who have made pleasant my stay in Pasadena.

ABSTRACT

I. The structure of the intermetallic compound $Mg_{12}Ce$ has been investigated by x-ray diffraction methods. The diffraction photographs seem to indicate that the structure has hexagonal symmetry, but further considerations reveal that the true symmetry is orthorhombic, and that the space group is very probably D^1_{2h}. The orthorhombic unit cell, with dimensions a_o=35.52Å, b_o=10.28Å, and c_o=10.28Å, contains 156 atoms. The diffraction maxima with the Miller index 1 even can be indexed on the basis of a smaller pseudo-hexagonal unit cell containing only 13 atoms. In this subcell, the arrangement of the atoms is related to those found in the $CaZn_5$ and $TiBe_{12}$ structures.

The structure of the crystal is partially disordered in a complex fashion. A theory based on crystal growth has been devised which successfully accounts for the gross features of the disorder.

II. Two distinct addition compounds, with formulas $C_{12}H_{14}N_2I_2$ and $C_6H_7NI_2$ have been isolated from the reaction products of iodine and γ-picoline. The second of these compounds is analogous to the well-known addition compound of pyridine and iodine. It has been of interest to determine whether the complexing forces between iodine and the organic base are sufficient to break the iodine-iodine covalent bond. X-ray radial distribution analyses showed that in the first compound the covalent bond had been broken, leading to an ionic structure, whereas in the second compound the covalent bond remained intact.

TABLE OF CONTENTS

PART PAGE

I. The Crystal Structure of the Intermetallic Compound $Mg_{12}Ce$.

A. Introduction.

The binary alloy system Mg-Ce was first studied by Vogel, who used thermal and metallographic methods (1). He reported four distinct intermetallic compounds, to which he assigned the formulas $MgCe_4$, MgCe, Mg_3Ce, and Mg_9Ce. It was decided to investigate the last of these compounds, Mg_9Ce, by x-ray diffraction methods, since ordered structures of the type X_9Y had not been reported in the literature, and the difference in the metallic radii of cerium and magnesium makes substitutional disorder unlikely. The present investigation indicates that the formula of the phase is $Mg_{12}Ce$. Phases with the composition $X_{12}Y$ have been studied by other investigators, but the structure type represented by $Mg_{12}Ce$ has not been observed previously. However, the resemblance between the x-ray diffraction patterns of $Mg_{12}Ce$ and those produced by $TiBe_{12}$ is striking (2,3).

Some interesting features of the investigation are as follows. The structure was determined in spite of its great complexity and the fact that the reciprocal lattice indicated by the x-ray diffraction photographs is not the one corresponding to a coherently scattering domain in the crystal. The interesting distribution of the very large number of absent reflections other than those corresponding to the space group made the determination of the structures particu-

larly challenging. In a typical crystal structure investigation, the principal problem is to determine the positions of the atoms. In this investigation, the coordinates of the sites where atoms could be located were found very easily, but there were more of these sites than there were atoms, and the main efforts were devoted to finding the relationships involving the probabilities of occupancy of each site. The methods which had to be devised to cope with such a situation are different from those ordinarily used in crystal structure analysis, and are applicable to other structures where similar occupancy problems arise. A theoretical investigation was made to attempt to explain the curious disorder phenomena occurring in the $Mg_{12}Ce$ structure. This investigation resulted in the formulation of a set of principles which are applicable not only to the $Mg_{12}Ce$ phase, but to several known structures as well.

B. Preparation of the alloys.

The materials used in the preparation of the melts were 99.5% pure cerium supplied by Dr. F. H. Spedding and chemically pure magnesium (purity otherwise unspecified) obtained from Eimer and Amend. Both metals were in rod form. According to the phase diagram reported by Vogel, primary crystals of the magnesium-rich phase are formed from melts within the range of composition from 65 weight percent of magnesium, where liquidus curve of the Mg_3Ce phase intersects the liquidus curve of the Mg_9Ce phase to 73 weight percent

magnesium, which is the composition of the Mg_9Ce-Mg eutectic. Accordingly, the melts were prepared having a composition near 70 weight percent of magnesium. It is reported that the magnesium-rich phase melts incongruently at 620°C. forming Mg_3Ce and liquid. The temperature corresponding to the Mg_9Ce-Mg eutectic point is 590°C.

The initial preparation was sealed under vacuum in a quartz tube and fused with a gas-oxygen torch. After cooling, the tube was cracked open. A silicide layer which formed at the interface between the melt and the quartz was ground off. Spectrographic analysis* of the melt showed only 0.25% silicon to be present. Subsequent melts were prepared by fusing the elements at approximately 750°C. in hard-sintered alundum thimbles in an atmosphere of argon. This method of preparation is superior to the first inasmuch as there is no change of composition due to reaction with the walls of the vessel. A total of five to ten grams of the metals was used in preparing the melts. A few milligrams of magnesium in excess of the desired composition were included to compensate for vaporization. There was no oxidation or contamination of the melts prepared in this way. The fusion was carried out in an induction furnace. The melts thus prepared were homogeneous, due to the induction stirring effect.

Some of the melts prepared in the induction furnace were

---

*The analysis was carried out by the Smith-Emery Company of Los Angeles.

quenched, and after sealing the thimble in an evacuated Pyrex tube, annealed for several weeks at 535°C. It was possible to obtain satisfactory single crystals both from annealed melts and from melts which were allowed to cool naturally to room temperature.

C. X-ray diffraction photographs.

Samples of the melts were crushed in a steel mortar and powdered in an agate mortar. The preparations were sufficiently stable so that they could be mounted, using petrolatum as an adhesive, on the surface of glass fibers for x-ray powder photography. The powder photographs thus obtained were moderately complex, and attempts to index them with nomograms for the trigonal, hexagonal, and tetragonal systems (including the cubic system) were not successful. Thus, single crystal work was necessitated. It was fortunate that very little time was spent on these attempts, since in retrospect it is clear that it would have been impossible to determine a structure as complex as that of $Mg_{12}Ce$ solely from powder photographs.

Promising fragments of the crushed melts were attached to glass fibers with dry shellac, and Laue photographs were made to determine whether the fragments were single crystals. Several satisfactory crystals were found by this method. Comparison of single crystal photographs with powder photographs of an unannealed sample confirmed that the crystals selected were of the principal constituent of the melt.

Laue photographs were used to establish the Laue symmetry of the crystals as $D_{6h} = 6/mmm$, and to approximately orient the crystals for rotation, Weissenberg, and precession photography.

All photographs from which diffraction intensity data were taken were obtained with molybdenum K_α radiation. Relative intensities of the reflections were estimated visually using intensity strips and multiple films (4). The crystals were sufficiently small to make it unnecessary to correct the data for absorption.

D. The unit cell dimensions.

It was found that the reflections with the Miller index l even could be indexed on the basis of a hexagonal subcell with $A_o = a_o/\sqrt{48}$ and $C_o = c_o$. Approximate dimensions A_o and C_o of the subcell were found from rotation and Weissenberg photographs to be 5.9 and 10.2 Å, respectively. Precise unit cell dimensions were determined from (hk0) and (h0l) single crystal data obtained from two equatorial rotation photographs, using the Straumanis arrangement. When the two photographs (rotation about the c-axis and a-axis respectively) were superimposed on one another, it was found surprisingly that the positions of the spots on the two photographs coincided within the limits of accuracy of their measurement, even in the back-reflection region. (There was no question that the same photograph by mistake was taken twice; relative intensities on the two films differed.) This is the

case because the spacing of the (100) subcell planes is almost exactly equal to the spacing of the (002) planes. More will be said about this fortuitous equality in the discussion of the subcell structure. The precision determination of the unit cell dimensions involves the specification of only one parameter, namely d_{100}. This parameter was determined by a least squares fitting of the best straight line through a plot of d_{100} computed for each observation versus $\cos^2\theta\ (\frac{1}{\sin\theta} + \frac{1}{\theta})$, the Nelson-Riley function (5). Copper K_{α_1} radiation ($\lambda K_{\alpha_1} = 1.5405$ Å) was used, and equal weight was given to each observation. The value of $d_{100} \simeq d_{002}$ at approximately 22°C. obtained by extrapolation of the data in table 1 to $\cos^2\theta = 0$ was $5.142_2 \pm 0.001_5$ Å.*

Since in the hexagonal system

$$A_o = \frac{2\sqrt{3}}{3} d_{100} \qquad (1a,b)$$

$$C_o = 2 d_{002}$$

and

$$a_o = 8 d_{100} \qquad (2a,b)$$

$$c_o = 2 d_{002} ,$$

the dimensions of the subcell and the true unit cell are

---

*The limits of error quoted for this figure, as well as the limits of error given for all other quantities in this thesis are probable errors, equal to 0.6745σ (6).

Table 1. Data for determination d_{100}.

Subcell indices	θ, radians	$\sin\theta$	$\frac{(h^2+hk+k^2)^{\frac{1}{2}}\lambda}{2\sin\theta} = d_{100}$	$\cos^2\theta\left(\frac{1}{\sin\theta}+\frac{1}{\theta}\right)$
100	.1511	.15053	5.117 Å	12.961
110	.2630	.25998	5.131	7.132
200	.3055	.30077	5.122	6.001
210	.4086	.39732	5.129	4.180
300	.4674	.45057	5.128	3.474
220	.5457	.51902	5.141	2.746
400	.6436	.60008	5.134	2.060
320	.7117	.65312	5.141	1.684
500	.8530	.75326	5.113	1.082
330	.8877	.77562	5.160	0.963
420	.9159	.79311	5.139	0.873
510	.9838	.83261	5.151	0.680
600	1.1154	.89809	5.146	0.389
520	1.2106	.93583	5.140	0.235
610	1.3780	.98147	5.146	0.064

respectively

$$A_o = 5.938 \pm 0.002 \text{ Å}$$

$$C_o = 10.284 \pm 0.003 \text{ Å}$$

and

$$a_o = 41.14 \pm 0.01 \text{ Å}$$

$$c_o = 10.284 \pm 0.003 \text{ Å}.$$

E. The composition of the phase.

Attempts to prepare a melt consisting only of this phase were not successful. If, in accord with the phase diagram reported by Vogel (1), the magnesium-rich phase melts incongruently, crystals of Mg_3Ce are first formed upon cooling. The probable explanation for the failure to obtain melts consisting solely of $Mg_{12}Ce$ is that the heterogeneous reactions are slow below the peritectic temperature, and equilibrium was not achieved. Nor is it feasible to collect enough single crystals so that the composition of the phase can be established by chemical analysis. Nevertheless, there is very strong evidence, described in the paragraph below, that the formula of the phase is $Mg_{12}Ce$, and not Mg_9Ce as reported by previous investigators.

The density of the phase was found from flotation measurements on single crystals to be 2.302 gms./cm.^{3} at 22°C. From this figure, the molecular weight of the contents of the subcell with dimensions A_o = 5.938 Å, C_o = 10.284 Å is 435. It is estimated that this figure is in error by less than 2%, or 8 molecular weight units. The calculated formula weight of $Mg_{12}Ce$ is 431.97. The density calculated for the formula $Mg_{12}Ce$, on the assumption that the atomic volumes of cerium and magnesium in the alloy are the same as in the elements is 2.30 gms./cm.^{3}, which is in good agreement with the observed density.

In order to disprove the conclusion obtained from Vogel's investigation that the formula of the magnesium-rich phase is

Mg_9Ce, the thermal analysis results must be shown to be in error. The stoichiometric formula $Mg_{12}Ce$ corresponds by coincidence to nearly the composition reported for the eutectic of Mg_9Ce and Mg. A melt having this composition was prepared and analyzed chemically. The metallographic examination of the melt kindly performed by Paul Pietrokowsky of the Jet Propulsion Laboratory revealed that the alloy consisted of about 90% of primary crystals, rather than of the eutectic mixture which would have been expected if the thermal analysis investigation was correct.

A powder photograph of a melt having the stoichiometric composition $Mg_{12}Ce$ taken with copper radiation shows several weak lines in the front reflection region which cannot be associated with the magnesium-rich intermetallic compound. Their Bragg spacings, in Å, together with data for Mg_3Ce and Mg are tabulated below.

Table 2. Spurious lines observed on a powder photograph of an alloy having the composition $Mg_{12}Ce$

	Bragg spacings	
Spurious lines	Closest Mg_3Ce lines*	Closest strong Mg lines (3)
6.93 Å		
4.13 Å	4.26 Å	
3.86 Å	3.68 Å	
2.72 Å		2.77 Å
2.64 Å	2.61 Å	2.60 Å
2.48 Å		2.45 Å
2.08 Å	2.11 Å	

*Calculated from the data of Rossi (7).

The spurious lines, with the exception of the 6.93 Å spacing, may be interpreted as arising from Mg_3Ce and Mg impurities. The agreement is not good, but the lines were all weak, and the observations were made in the low precision front-reflection region. The presence of both Mg_3Ce and Mg in small amounts is consistent with the hypothesis that the phase, with the formula $Mg_{12}Ce$, is formed by an incomplete peritectic reaction between Mg_3Ce and the melt.

Additional evidence which supports the assignment of the formula $Mg_{12}Ce$ to the phase is the similarity of the diffraction patterns to those observed for the compound $TiBe_{12}$. The structure of the subcell found in this investigation is isomorphous to that reported for $TiBe_{12}$ (2).

In order to disprove that there are actually two magnesium-rich phases, having the formulas Mg_9Ce and $Mg_{12}Ce$, a melt having the composition of the former was prepared and a powder photograph was taken. This photograph was essentially identical to those made of the melts more rich in magnesium, showing that no new principal phase was present.

F. The absences in the reciprocal lattice and possible space groups.

Although most of the absences which occur in the x-ray diffraction patterns for $Mg_{12}Ce$ are not accountable for by space group symmetry elements, they are nevertheless of a systematic nature. The diffraction patterns are best described by considering planes in reciprocal space having

constant Miller index l. All such planes with even l have one configuration of absences, and all planes with odd l have another configuration. Throughout this thesis, the two types of planes will be referred to, respectively, as the even and odd layers. Figure 1 shows which reflections on odd and even layers are not ruled out by the absences.

A reciprocal lattice plot of diffraction data apparently showing large unit cell dimensions with many absences can sometimes be resolved into a set of simpler interpenetrating lattices, so that what was supposedly a single crystal is actually multiple. A three dimensional model of several layers of the $Mg_{12}Ce$ reciprocal lattice was constructed as a visual aid to determine whether such a resolution was possible. A model of this sort was useful in the investigation of the ζ-phase in the silver-zinc system (9). No lattices could be found however which could be combined to explain the majority of the absences in the reciprocal lattice for $Mg_{12}Ce$.

The Laue symmetry $D_{6h} = 6/mmm$ is consistent with the crystal classes $D_{3h} = \bar{6}2m$, $C_{6v} = 6mm$, $D_6 = 622$, and $D_{6h} = 6/mmm$ (10). The only absences in the reciprocal lattice which can be space group extinctions are the (001) absences with l odd. Space groups having c glide planes, or $6_1, 6_2, 6_4$, or 6_5 screw axes are therefore eliminated. The space groups which remain possible are $D^1_{3h} = C\bar{6}m$, $D^3_{3h} = C\bar{6}2m$, $C^1_{6v} = C6mm$, $D^1_6 = C62$, $D^6_6 = C6_32$, and $D^1_{6h} = C6/mmm$ (11). Further reduction of the number of possible space groups will be made by special methods to be described later.

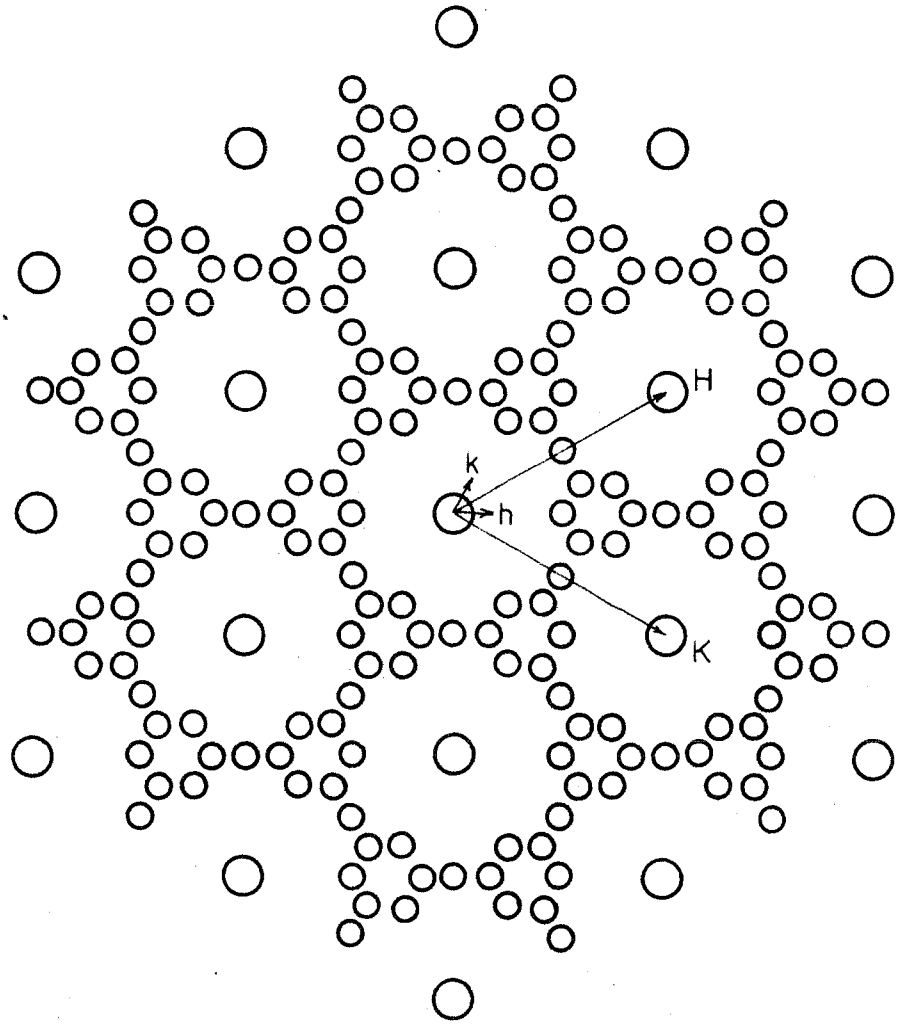

FIGURE I. HEXAGONAL RECIPROCAL LATTICE LAYERS FOR $Mg_{12}Ce$.

True cell reciprocal lattice vectors h,k and subcell reciprocal lattice vectors H, K are shown.

$\ell = 2n$

$\ell = 2n+1$

G. The structure determination.

1. Division of the problem.

In order to take advantage of the simplicity of the diffraction data with Miller index l even the method described by Raeuchle and Rundle (2) for the structure of $TiBe_{12}$ was used. If

$$\rho(x,y,z) = \frac{1}{V} \sum_h \sum_k \sum_l F_{hkl}\, e^{-2\pi i(hx+ky+lz)}, \qquad (3)$$

then

$$\rho(x,y,z+\tfrac{1}{2}) = \frac{1}{V} \sum_h \sum_k \sum_l F_{hkl}\, e^{-2\pi i[hx+ky+l(z+\frac{1}{2})]}$$

$$= \frac{1}{V} \sum_h \sum_k \sum_l F_{hkl}\,(-1)^l e^{-2\pi i(hx+ky+lz)}. \qquad (4)$$

From equations 3 and 4,

$$\tfrac{1}{2}[\rho(x,y,z)+\rho(x,y,z+\tfrac{1}{2})] = \frac{1}{V} \sum_h \sum_k \sum_l F_{hkl}\left[\frac{1+(-1)^l}{2}\right] e^{-2\pi i(hx+ky+lz)}$$

$$= \frac{1}{V} \sum_h \sum_k \sum_l{}' F_{hkl}\, e^{-2\pi i(hx+ky+lz)}, \qquad (5)$$

where the primed summation over l indicates that only those

terms with l even are included in the sum. Thus, the three-dimensionally periodic function formed by averaging the electron density at each point (x,y,z) with that at (x,y,z+$\frac{1}{2}$) is the Fourier transform of those structure factors having l even. The spacings on the even layer reciprocal space maps dictate that this function must have a periodicity corresponding to a hexagonal unit cell of dimensions A_o and $\frac{1}{2}C_o$. Once this averaged density is determined, the structure must be found by resolving the ambiguities arising from the fact that a peak at (x_o,y_o,z_o) in the function $\frac{1}{2}[\rho(x,y,z) + \rho(x,y,z+\frac{1}{2})]$ may arise from atoms situated either at (x_o,y_o,z_o), at $(x_o,y_o,z_o+\frac{1}{2})$, or at both positions. Resolution of these ambiguities must be based on an interpretation of the diffraction data with l odd.

2. Interpretation of the diffraction data with l even.*

a. The trial structure of the subcell.

The entire reciprocal lattice, with phases as well as intensities assigned to each point, and consequently the even layer reciprocal lattice, possesses one of the point symmetries consistent with Laue symmetry D_{6h}. Since the Fourier transformation preserves point symmetry, the electron density function $\frac{1}{2}[\rho(x,y,z) + \rho(x,y,z+\frac{1}{2})]$, which is the transform of the even layer reciprocal lattice, must also have such a symmetry. The space group of the function $\frac{1}{2}[\rho(x,y,z) +$

*In this section, all Miller indices used are based on the subcell edges A_o = 5.938 Å, C_o = 10.284 Å.

$\rho(x,y,z+\frac{1}{2})]$, which has a periodicity in the z direction equal to $\frac{1}{2}$ C_o, is therefore one of those possible for the overall structure after omission of D_6^6, as there are no systematic absences among the (0,0,21) reflections. The possible space groups are then $D_{3h}^1 = C\bar{6}m$, $D_{3h}^3 = C\bar{6}2m$, $C_{6v}^1 = C6mm$, $D_6^1 = C62$, and $D_{6h}^1 = C6/mmm$.

It was observed on the (hk0) photographs that the intensities of the reflections are related approximately by normal declines along the subcell reciprocal lattice vector with components (220). This suggests that the atoms are at (or near) the special positions for which the x and y coordinates are rational fractions of the subcell edge. The three sets of special positions in hexagonal plane groups that have rational coordinates are tabulated below.

Table 3. Some special positions in hexagonal plane groups.

1-fold	(a)	0,0
2-fold	(b)	1/3, 2/3; 2/3, 1/3.
3-fold	(c)	0, 1/2; 1/2, 0; 1/2, 1/2

For each of the positions in table 3, 2x + 2y is an integer, so that if the atoms were exclusively in these positions, there would indeed be the aforementioned normal declines of the observed intensities.

The following treatment confirms that the x,y coordinates of the atoms are essentially those of special positions above, and establishes the phases of the hk0 reflections. If all of the atoms have subcell x,y coordinates that place them in these special positions, then within each reciprocal lattice layer of constant l there must be groups of reflections related to each other by normal decline. It is possible to test whether the atoms have special x,y coordinates by examination of the relative intensities of the subcell hk0 reflections.

On the assumption that each atom in the subcell has one of the special x,y coordinates tabulated above, the geometrical structure factors G_{hk0} for the hk0 reflections can have one of only four values. It is equal to A + 2B + 3C when h-k = 3n and h and k are both even, A + 2B - C when h - k = 3n and h and k are not both even, A - B + 3C when h - k $\neq$ 3n and h and k are both even, and A - B - C when h - k $\neq$ 3n and h and k are not both even. Here A is the scattering power of the atoms associated with the position (a) in the table above, B the scattering power associated with each of positions (b), C the scattering power associated with each of positions (c), and n is an integer. The (hk0) reflections in each group of equal G_{hk0} for which intensity data are available are tabulated below.

Table 4. Grouping of observed hk0 reflections

G_{hk0}	Indices
A + 2B + 3C	220, 600, 440, 820, 660
A + 2B - C	110, 300, 410, 330, 520, 710, 630, 550, 900
A - B + 3C	200, 400, 420, 620, 800, 640, 10·0·0
A - B - C	100, 210, 310, 320, 500, 510, 430, 610, 530, 700, 540, 720, 810, 730, 650

If the approximation is made that the scattering powers of both magnesium and cerium fall off in the same way with increasing $\sin\theta/\lambda$, the intensities I_{hk0} of the hk0 reflections are given by the relationship

$$I_{hk0} = K\left[f\left(\frac{\sin\theta}{\lambda}\right)\right]^2 \left|G_{hk0}\right|^2 e^{-B\frac{\sin^2\theta}{\lambda^2}} L\,p, \qquad (6)$$

where K is a proportionality constant, $f\left(\frac{\sin\theta}{\lambda}\right)$ is the function describing the decline of scattering power of the atoms, G_{hk0} is the geometrical structure factor discussed above, $e^{-B\frac{\sin^2\theta}{\lambda^2}}$ is the temperature factor, L is the Lorentz factor, and p is the polarization factor.

The function $f\left(\frac{\sin\theta}{\lambda}\right)$ chosen was a weighted average of

the atomic scattering factors of magnesium and cerium, namely

$$f\left(\frac{\sin\theta}{\lambda}\right) = \frac{f_{Ce^{-2}}+12f_{Mg}}{Z_{Ce^{-2}}+12Z_{Mg}} \qquad (7)$$

Making the approximation that the K electrons of the cerium atom are not excited by molybdenum radiation, two electrons are subtracted from the atomic scattering factor for cerium. This modified scattering power for cerium shall henceforth be denoted simply as f_{Ce}.

Equation 6 may be rewritten

$$\log_{10}\left[\frac{I_{hk0}}{Lpf\left(\frac{\sin\theta}{\lambda}\right)}\right]^{\frac{1}{2}} = \log_{10}\left\{[K(Abs.)]^{\frac{1}{2}}|G_{hk0}|\right\}$$

$$- \frac{B}{2\log_e 10} \times \frac{\sin^2\theta}{\lambda^2} \qquad (8)$$

Within each group of reflections defined above, $|G_{hk0}|$ is constant. Therefore a plot of $\log_{10}\left[\frac{I_{hk0}}{Lpf(\sin\theta/\lambda)}\right]^{\frac{1}{2}}$ versus $\frac{\sin^2\theta}{\lambda^2}$ for each of the four families of reflections should be a straight line with slope $-\frac{B}{2\log_e 10}$ and intercept $\log_{10}\{[K(Abs.)]^{1/2}|G_{hk0}|\}$. Figure 2 shows the (hk0) intensity data plotted in this fashion. The intercepts on the plot indicate that the ratios of the absolute values of the geometrical structure factors $|A+2B+3C| : |A+2B-C| : |A-B+3C| : |A-B-C|$ are approximately 241:117:163:72. From the figures above, $|A+2B-C| > |A-B-C|$. Since A, B, and C are positive quantities, $A+2B-C > A-B-C$. Therefore A+2B-C is positive,

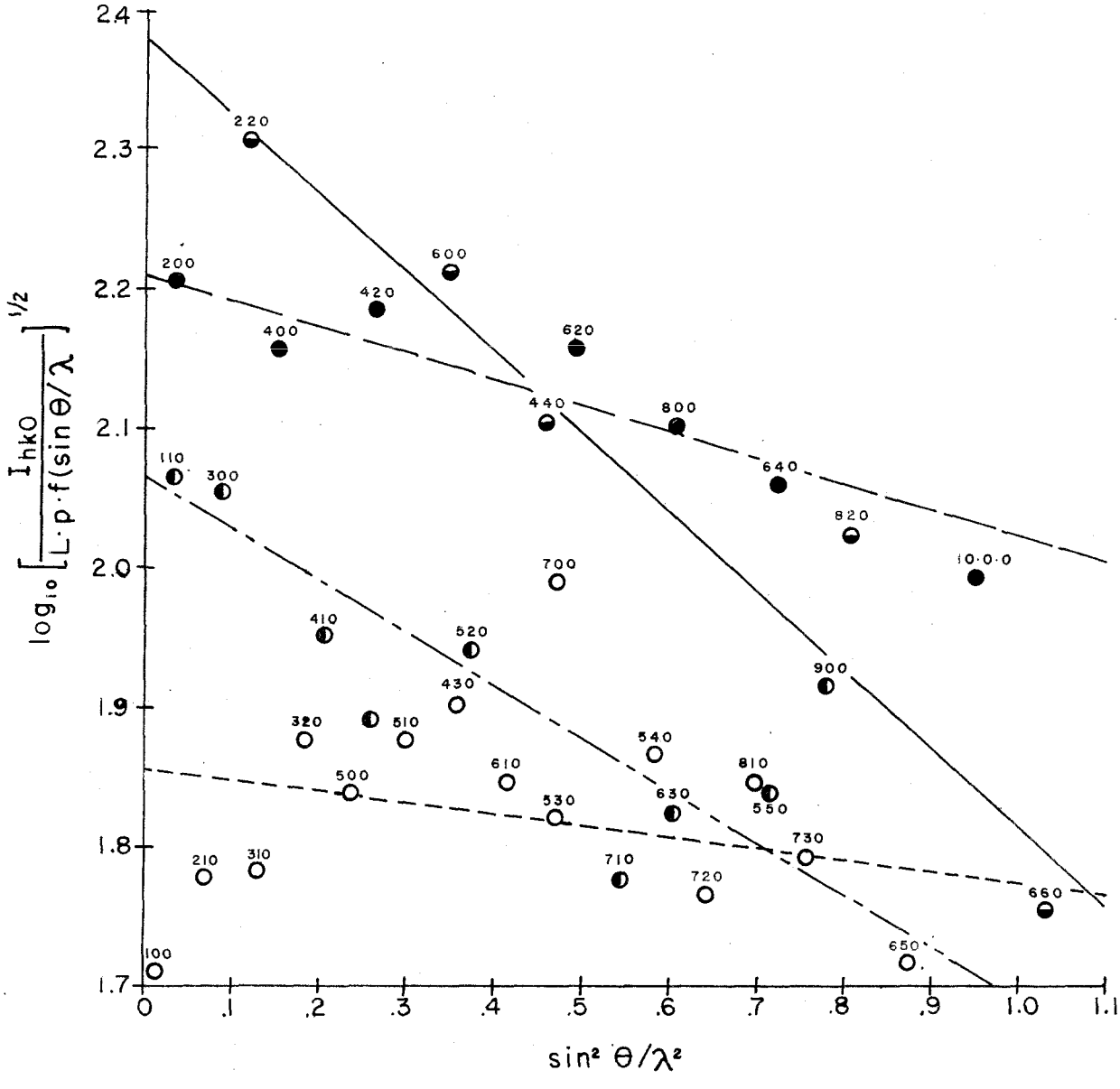

FIGURE 2. TREATMENT OF (hk0) INTENSITY DATA.

Points on plot are labelled with indices of reflections.

G_{hk0}

- ◒ A+2B+3C ——————
- ◐ A+2B−C ——·——
- ● A−B+3C —— ——
- ○ A−B−C - - - - - -

regardless of the sign of A-B-C. Similarly, $|A-B+3C| > |A-B-C|$ and $A-B+3C > A-B-C$ implies that A-B+3C is positive. Because A, B, and C are positive, A+2B+3C is positive also. Since the signs and relative magnitudes of A+2B+3C, A+2B-C, and A-B+3C are known, it is possible to compute the ratios between the quantities A, B, and C. The solution of the proportionalities

$$\begin{aligned} A + 2B + 3C &\propto 241 \\ A + 2B - C &\propto 117 \qquad (8) \\ A - B + 3C &\propto 163 \end{aligned}$$

is A:B:C::96:26:31, or 1:0.27:0.32. From this result it follows by substitution that A-B-C is greater than zero. It is therefore established that the sign of every hk0 reflection is positive.

There are features of the intensity data plotted on figure 2 which are not explained by the simple treatment. It is possible to account for the differences in the slopes of the lines by assigning to the atoms at each position a different temperature factor. Other data cannot be explained in this way. For instance, the intensities of the (530) and (700) reflections, which have equal Bragg angles and supposedly equal geometrical structure factors, differ from each other by a factor of more than two. The reason for the misbehavior of the data becomes apparent when a Fourier map of the hk0 structure factors is made. Punched card methods were used to

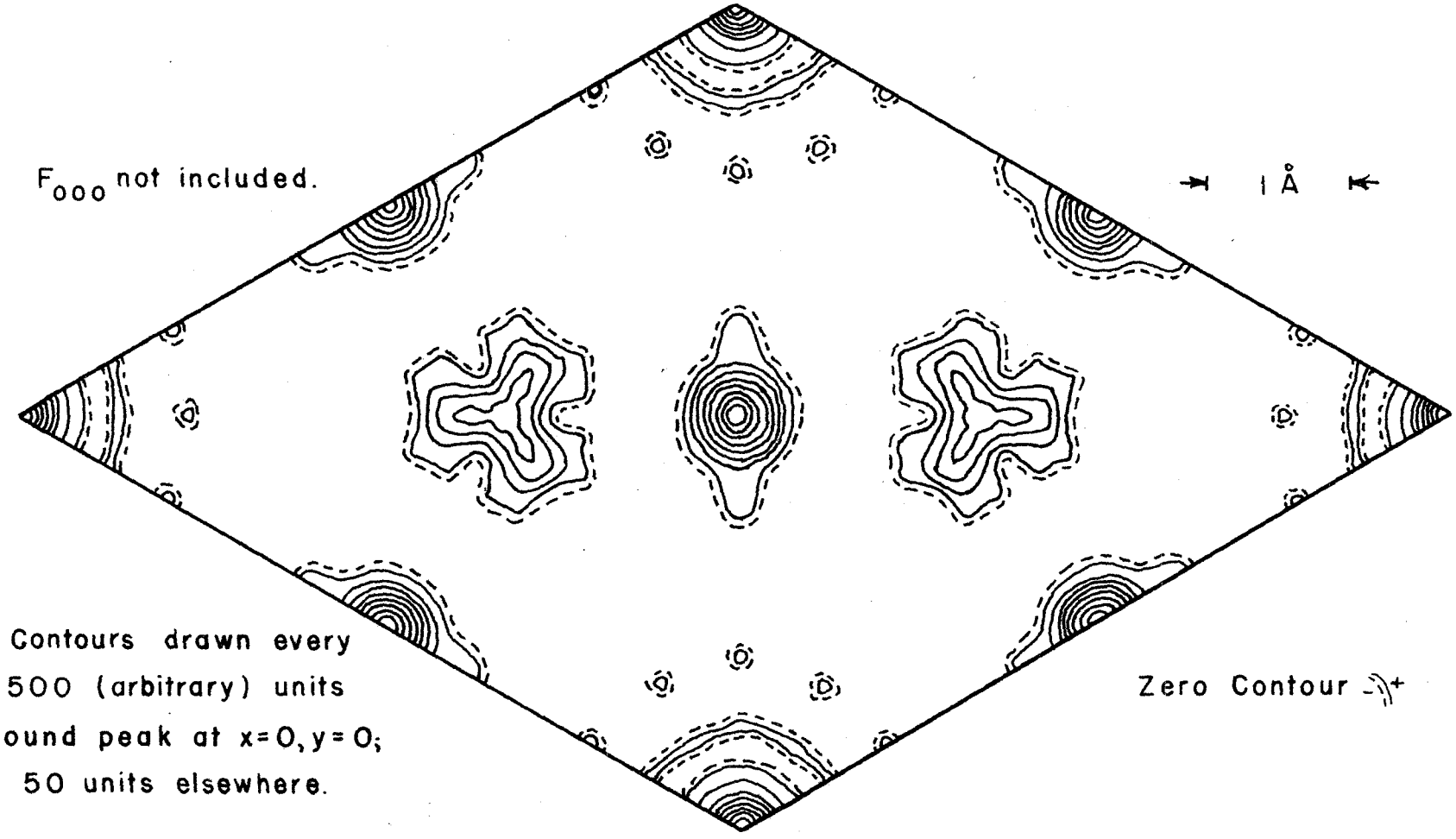

FIGURE 3. FOURIER PROJECTION ONTO SUBCELL x,y PLANE.

facilitate the Fourier calculations. The electron density projected onto the x,y plane of the subcell, with contours drawn at arbitrary intervals, is shown in figure 3. The distortion of the peaks in the Fourier projection at 1/3,2/3 from circular shape indicates that some of the atoms are displaced slightly in the x,y plane from these positions, with the direction of the displacements varying from one subcell to another.

There is considerable evidence which suggests that the subcell structure is isomorphous with that reported for $TiBe_{12}$(2). In addition to the aforementioned similarity between the x-ray diffraction patterns produced by the two compounds, the following arguments support the choice of the $TiBe_{12}$ subcell structure as a starting point for the refinement of the $Mg_{12}Ce$ structure. In the hypothesized structure there are two magnesium atoms and a cerium atom in a row both along the c-axis and the diagonal of the x,y plane. It would be expected that the cell dimensions in these directions would be slightly larger than $4r_{Mg} + 2r_{Ce}$, where r_{Mg} and r_{Ce} are respectively the metallic radii of magnesium and cerium. The value of this sum, which is 10.0 Å (12), using radii for coordination number 12, compares favorably with the observed cell dimensions in these directions, both of which are 10.284 Å.

All of the x,y coordinates of the atoms in the $TiBe_{12}$ structure correspond (or nearly correspond) to the special

positions listed in table 3. For $Mg_{12}Ce$ the numbers of electrons A, B, and C associated respectively with the atoms at positions (a), (b), and (c) (subtracting 2 from the atomic number of cerium) are in the ratios A:B:C::80:24:24, or 1:0.3:0.3. These figures are consistent with the ratios A:B:C::1:0.27:0.32 found from the analysis of the observed (hk0) intensities in the previous section.

The subcell coordinates, which are identical to those reported for $TiBe_{12}$(2), except that the parameters have been estimated using the metallic radii for magnesium and cerium (12), are listed in table 5.

Table 5. Atomic positions isomorphous with the $TiBe_{12}$ subcell structure

1 Ce in (a)	0,0,0; or (b) 0,0,1/2.
2 Mg in (e)	$0,0,z_1$; $0,0,-z_1$ z_1 approximately 0.35 or 0.85.
6 Mg in (i)	$1/2,0,z_2$; $0,1/2,z_2$; $1/2,1/2,z_2$; $1/2,0,-z_2$; $0,1/2,-z_2$; $1/2,1/2,z_2$
2 Mg in (c)	1/3,2/3,0; 2/3,1/3,0 z_2 approximately 0.25.
2 Mg in (d)	1/3,2/3,1/2; 2/3,1/3,1/2.

The coordinates tabulated above do not take into account the displacements of the magnesium from their "ideal" positions at 1/3, 2/3, 0, etc. (These displacements are observable not only on the (hk0) Fourier map for $Mg_{12}Ce$, but also on the corresponding map for $TiBe_{12}$ (2).) Furthermore, there are other atoms in the structure which can undergo similar displacements.

Satisfactory agreement between the calculated and observed structure factors is obtained if it is realized that the surroundings of the magnesium atoms in positions (c), (d), and (i) vary from one subcell to another, so that these atoms can be displaced from their ideal positions listed above. The cerium atoms in positions (a) or (b) and the magnesium atoms in position (e) form chains parallel to the c axis of the crystal which are ordered along their length, but which may be arranged either with a cerium atom at z = 0, or with a pair of magnesium atoms above and below the plane z = 0.

The displacements of the magnesium atoms in positions (c) and (d) will be discussed first. The gross way in which the surroundings of these atoms vary from one subcell to another can be described by considering only those nearest neighbors which lie in and about the plane through the atoms under consideration which is perpendicular to the c axis of the crystal. Changes in the configuration of the other neighboring atoms are perturbations produced by the gross

changes in the plane. Each magnesium atom in positions (c) or (d) is surrounded equilaterally by three of the aforementioned MgCeMg chains. The surroundings of the central magnesium atom in and about the plane are therefore n cerium atoms in the plane and 3-n pairs of magnesium atoms located above and below the plane, which are members of the MgCeMg chains.

It is reasonable to suppose that the magnitudes and directions of the displacements of the central atom from its ideal position at, e.g., 1/3,2/3,0 will be determined chiefly by the disposition of its three surrounding groups. There will be mirror planes through z = 0 and z = 1/2 whether or not the MgCeMg chains are translated, so that the central atoms will be displaced within these planes. It will be assumed that if the central atom is surrounded by two cerium atoms and one magnesium pair, it will be displaced from its ideal position by a distance δ_1, expressed in cell edge units, towards the magnesium pair. If it is surrounded by one cerium atom and two magnesium pairs, it will be displaced by δ_2 away from the cerium atom. It is evident from figure 3 that δ_1 is greater than δ_2. If the central atom is surrounded symmetrically by three cerium atoms, or by three magnesium pairs, it will be essentially unperturbed from its ideal position. In the discussion of the structure of $TlBe_{12}$(2), it is observed that steric considerations prohibit a central (beryllium) atom from being surrounded by three large

(titanium) atoms. This also prohibits the situation in which a central atom is surrounded by three beryllium atom pairs, inasmuch as the BeTiBe chains are ordered along their length (if the composition is exactly $TiBe_{12}$), so that a central atom with coordinates x,y,z being surrounded by three beryllium atom pairs would imply that the central atom at x,y,z+1/2 is surrounded by three titanium atoms. In this investigation it will be assumed that a central magnesium atom is surrounded by three cerium atoms or by three magnesium pairs only very rarely. The validity of this assumption will be discussed in detail in the analysis of the odd layer diffraction data. A consequence of this supposition is that there are virtually no central atoms which remain undisplaced. Furthermore, if an atom near the ideal position x,y,z is surrounded by two cerium atoms and a magnesium pair, the atom near the ideal position x,y,z+1/2 will be surrounded by two magnesium pairs and a cerium atom. Thus, for every central atom displaced by δ_1 from its ideal position there will be an atom translated from the first by nearly $\underset{\sim}{c}_0/2$ which is displaced from its ideal position by δ_2 in the opposite direction. Thus, equal numbers of atoms are displaced by δ_1 and δ_2. The hexagonal symmetry of the subcell requires that an equal number of atoms be displaced along each of the vertical mirror planes passing through the positions (c) and (d) in D^1_{6h}. Figure 4 shows in projection the disposition of the atoms of groups (c) and (d).

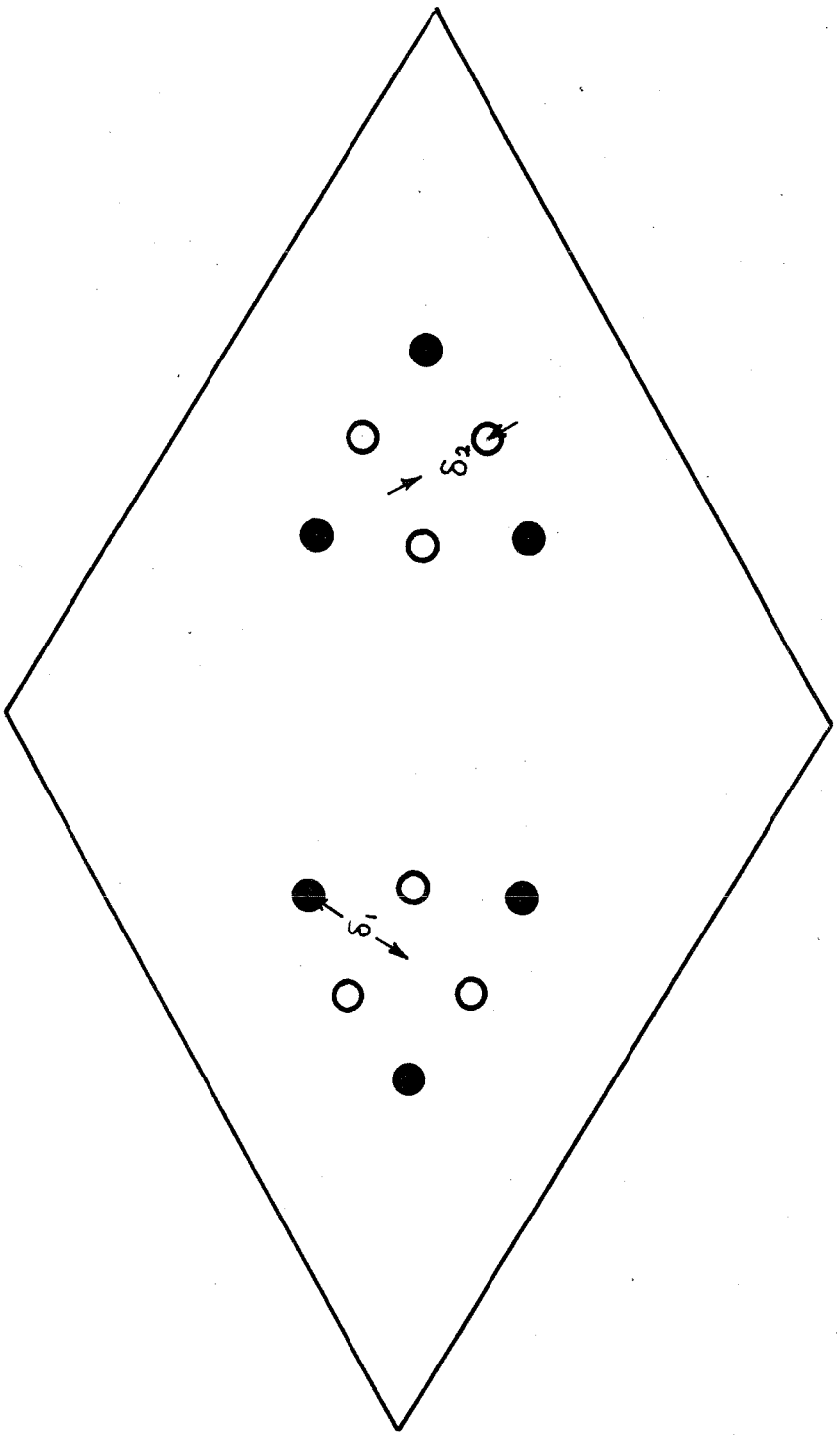

FIGURE 4. SITES FOR OCCUPANCY OF MAGNESIUM ATOMS NEAR $^1/_3, ^2/_3$ AND $^2/_3, ^1/_3$.

It was the conclusion of the preceding paragraph that each of the circles, open or closed, in the subcell projection shown in figure 4 will on the average be occupied by an equal number of atoms. There are twelve such circles and four atoms in groups (c) and (d), so each circle must represent one-third of a magnesium atom. Since the diffraction data with l even does not distinguish between atoms at z = 0 and z = 1/2, it suffices in discussing the structure of the subcell to place the twelve sites in the positions

$$(l)\ x_1,2x_1,0;\ -2x_1,-x_1 0;\ x_1,-x_1,0;\ -x_1,-2x_1,0;$$

$$2x_1,x_1,0;\ -x_1,x_1,0,$$

$$(m)\ x_2,2x_2,1/2;\ -2x_2-x_2,1/2;\ x_2,-x_2,1/2;\ -x_2,-2x_2,1/2;$$

$$2x_2,x_2,1/2;\ -x_2,x_2,1/2,$$

where

$$x_1 = 1/3 - \delta_1/\sqrt{3} \qquad (9a,b)$$

$$x_2 = 1/3 + \delta_2/\sqrt{3}$$

The positions (l) and (m) are meant to distinguish between the x coordinates rather than the z coordinates of the atoms. For example, it is permissible for an atom to have the co-

ordinates $x_2, 2x_2, 0$, and in the discussion of interatomic distances which will follow, such an atom will be described as being in position (m).

The displacement of the magnesium atoms from their ideal positions at (i), $1/2, 0, z_2$, etc., will now be discussed. Once again, it will be assumed that the disposition of each of these atoms depends only on the configuration of its neighboring MgCeMg chains. The displacements of these atoms will be described further in the discussion of the odd layer data. Figure 8 (page 111) shows the four possible configurations of the neighboring MgCeMg chains, and the way in which the atoms near the ideal positions (i) are displaced. For cases C and D in figure 8, the atoms undergo no displacement at all, so that their z coordinates remain 1/4 and 3/4. In cases A and B, the atoms are displaced in the z direction by a distance δ from their ideal positions, but the even layer data cannot distinguish whether the displacements are towards or away from the cerium atoms. (It will be shown later that the displacements are towards the cerium atoms.) Referring to figure 8, it is evident that the same number of atoms are displaced upward as downward. There remains to establish the ratio of displaced to undisplaced atoms, that is, the relative frequency of configurations such as A and B compared to that for C and D. In discussing the previous group of atoms it was assumed that configurations having three untranslated chains (i.e., a central magnesium atom surrounded by three cerium

atoms or by three magnesium pairs) occurred with negligible frequency. Therefore, virtually every triangle of chains has two similar members, and one dissimilar with respect to the z coordinate of the cerium atom. Thus, two of the faces of the triangular prism formed by the chains will resemble configurations C and D, and one of the faces will resemble configurations A and B. From this, it is concluded that one-third of the magnesium atoms are displaced from their ideal positions (one-sixth in each direction) and that two-thirds are undisplaced. Due to the sixfold symmetry of the subcell, it suffices to specify the coordinates of the six atoms as follows:

4 Mg atoms in (i_1) 1/2,0,1/4; 0,1/2,1/4; 1/2,1/2,1/4;
1/2,1/2,1/4; 1/2,0,3/4; 0,1/2,3/4; 1/2,1/2,3/4
(2/3 atom in each position.)

2 Mg atoms in (i_2) 1/2,0,z_2; 0,1/2,z_2; 1/2,1/2,z_2;
1/2,0,$-z_2$; 0,1/2,$-z_2$; 1/2,1/2,$-z_2$.
(1/3 atom in each position.)

The trial structure for the subcell which results when the perturbations of the atoms from their ideal positions is considered is summarized in table 6 below.

Individual subcells in the actual structure will not in general possess the high symmetry represented in table 6. There are, however, mirror planes through z = 0 and z = 1/2 in

Table 6. Trial structure for the subcell of $Mg_{12}Ce$.

Space group D_{6h}^{1}

In the true structure, there is an ambiguity of 1/2 in the z coordinate of each position listed.

---

1 Ce in (a) 000.

2 Mg in (e) $0,0,z_1$; $0,0,-z_1$. (a_1 approximately 0.35.)

4 Mg in (i_1) 1/2,0,1/4; 0,1/2,1/4; 1/2,1/2,1/4; 1/2,0,3/4; 0,1/2/,3/4; 1/2,1/2,3/4. (2/3 atom in each position.)

2 Mg in (i_2) 1/2,0,z_2; 0,1/2,z_2; 1/2,1/2,z_2; 1/2,0,$-z_2$; 0,1/2,$-z_2$;1/2,1/2,$-z_2$ (1/3 atom in each position. z_2 slightly less than 1/4.)

2 Mg in (l) $x_1,2x_1,0$; $-2x_1,-x_1,0$; $x_1,-x_1,0$; $-x_1,-2x_1,0$; $2x_1,x_1,0$; $-x_1,x_1,0$. (1/3 atom in each position. x_1 slightly less than 1/3.)

2 Mg in (m) $x_2,2x_2,1/2$; $-2x_2,-x_2,1/2$; $x_2,-x_2,1/2$; $-x_2,-2x_2,1/2$; $2x_2,x_2,1/2$; $-x_2,x_2,1/2$. (1/3 atom in each position. x_2 slightly more than 1/3.)

---

each subcell. As pointed out by Raeuchle and Rundle, the interchangeability of the coordinates of the atoms in positions (i_1) and (i_2) and the variation of the x,y coordinates of the atoms in positions (1) and (m) from one subcell to another constitute deviations from an ideal subcell structure (2). It might therefore be expected in case the structure was ordered that reflections other than those indexed on the basis of the subcell axes will appear on the even layers. However, a displacement in the parameters from ideal subcell positions which changes the structure factor F to $F+\Delta$ will change the square of the structure factor by $(F+\Delta)^2-F^2 = 2F\Delta+\Delta^2$. Since the observed intensities are proportional to F^2 it is possible, if Δ is small, that the deviation of atoms from their "ideal" positions at 1/3,2/3 and 2/3,1/3 can influence the observed intensities without causing other reflections, whose "ideal" structure factors are zero, to appear.

b. Refinement of the parameters

The expression for the hk0 structure factors corresponding to the coordinates listed in table 6 is

$$F^{(c)}_{hk0} = f_{Ce} + 8f_{Mg}A(h,k) + \tfrac{2}{3}f_{Mg}[D(2h+k)+D(h-k)+D(h+2k)], \quad (10)$$

where

$$D(n) = \cos 2\pi nx_1 + \cos 2\pi nx_2, \quad (11)$$

and A(h,k) is equal to one if h and k are both even, and is equal to zero otherwise. The observed values $F^{(o)}_{hk0}$ for the (hk0) structure factors are related within limits of error to $F^{(c)}_{hk0}$ by the equation

$$CF^{(o)}_{hk0} = F^{(c)}_{hk0}\, e^{-\frac{B_A}{2}\frac{\sin^2\theta}{\lambda^2}} \quad . \tag{12}$$

The values of the positional parameters x_1 and x_2 determined by least squares refinement of the observed intensity data were

$$x_1 = 0.285 \pm 0.002$$

$$x_2 = 0.360 \pm 0.002,$$

with B_A equal to 1.7Å^2. The observed structure factors were then corrected for secondary extinction in accordance with the relationship (13)

$$\frac{\rho'}{\rho} = 1 - 2g\rho' \tag{13}$$

where ρ' is the observed intensity, ρ is the intensity which would be observed if there were no extinction, and g is the coefficient of secondary extinction which, in this investigation, was determined graphically. The observed structure factors, denoted by F_{obs} (which are equal to $F^{(o)}_{hk1}$ multiplied by the scale factor and corrected for extinction) and $F^{(c)}_{hk0} e^{-\frac{B_A}{2}\frac{\sin^2\theta}{\lambda^2}}$, denoted as F_{calc}, are tabulated below.

Table 5A. Calculated and observed (hk0) structure factors

Index	F_{obs}	F_{calc}	Index	F_{obs}	F_{calc}	Index	F_{obs}	F_{calc}
100	28.3	31.9	430	21.7	20.0	640	20.2	19.9
110	66.4	75.6	440	30.1	32.5	650	8.6	6.1
200	104.1	96.8	500	22.6	20.5	660	8.6	13.8
210	31.4	29.9	510	22.7	23.9	700	22.7	18.3
220	89.4	92.7	520	23.0	17.0	710	12.9	11.9
300	46.5	50.5	530	15.3	15.3	720	11.2	12.0
310	24.8	24.9	540	15.1	13.5	730	10.8	10.1
320	28.3	25.8	550	12.4	10.6	800	25.2	25.4
330	24.7	23.3	600	42.4	41.7	810	12.7	11.7
400	72.2	71.9	610	17.4	15.9	820	17.7	17.0
410	32.4	28.3	620	32.5	32.8	900	13.9	8.2
420	49.5	49.8	630	13.3	11.8	10,0,0	15.4	14.3

The R factor $\frac{\Sigma|F_{obs} - F_{calc}|}{\Sigma|F_{obs}|}$ for these data is 0.076.

The expression for the (001) structure factors is

$$F_{00l}^{(c)} = f_{Ce} + 8f_{Mg}E(l) + 2f_{Mg}\cos 2\pi l z_1 + 2f_{Mg}\cos 2\pi l z_2, \qquad (14)$$

where E(l) is equal to one if l is divisible by four, and is equal to zero otherwise. Since the scattering power of a cerium atom is greater than the scattering power of four magnesium atoms for all values of $\sin\theta/\lambda$, the sign of F_{001} is always positive. The calculated and observed (001) structure factors are related by an expression analogous to equation 12. From least squares refinement of the observed 001 intensity data it was found that

$$z_1 = 0.353 \pm 0.002$$

$$z_2 = 0.215 \pm 0.001,$$

with B_C equal to 1.9 Å^2. Table 7 shows the observed (001) structure factors, corrected for extinction, and the calculated structure factors, including the temperature factor. The R factor for the data below is 0.038.

Table 7. Calculated and observed 00l structure factors.

Index	F_{obs}	F_{calc}	Index	F_{obs}	F_{calc}	Index	F_{obs}	F_{calc}
002	26.3	26.5	0,0,10	23.7	19.6	0,0,20	11.4	14.1
004	107.2	107.2	0,0,12	36.8	36.8	0,0,22	6.2	4.7
006	41.6	42.0	0,0,14	22.7	22.2	0,0,24	5.1	6.6
008	72.7	72.8	0,0,16	18.0	18.5	0,0,26	3.3	2.4
			0,0,18	11.1	9.0			

In order to check the trial structure and the determination of the parameters, it was decided to compare calculated and observed structure factors for all reflections with l even observed on molybdenum radiation photographs. Subcell (hkl) data were collected on several sets of films. Each set of multiple films had enough reflections which were in common with other sets to establish relative scale factors. The following procedure was used in correlating the data. For each set of films, observed intensities were converted into absolute values of the structure factors $|F^{\circ}_{\underset{\sim}{h}i}|$. The subscript $\underset{\sim}{h}$ denotes the index

of the reflection, and the subscript i denotes the film set from which the observed value was derived. There exist sets of values $\{|F_h|\}$ and $\{a_i\}$ which minimize the expression $\sum_{\underset{\sim}{h}} \sum_i w_{\underset{\sim}{h}i} (a_i |F_{\underset{\sim}{h}}| - |F^o_{\underset{\sim}{h}i}|)^2$. There are an infinite number of solutions, for if every a_1 is multiplied, and every $F_{\underset{\sim}{h}}$ is divided by the same constant, the value of the preceding expression is unchanged. These sets are unique however if the factor a_1 for one of the sets is fixed. The weight factor $w_{\underset{\sim}{h}1}$ was taken as $n_{\underset{\sim}{h}1}$, the number of times a reflection with index h is observed in the film set 1, divided by the observed relative value of the structure factor. The expression may therefore be rewritten as

$$P(\{|F_{\underset{\sim}{h}}|\},\{a_i\}) = \sum_{\underset{\sim}{h}} \sum_i \frac{n_{\underset{\sim}{h}i}}{|F^o_{\underset{\sim}{h}i}|} (a_i |F_{\underset{\sim}{h}}| - |F^o_{\underset{\sim}{h}i}|)^2 \qquad (15)$$

The factor a_1 for the (hk0) Weissenberg set was fixed, since the conversion factor for the relative hk0 data into absolute structure factors was established in the refinement of the (hk0) data discussed previously.

Setting the derivative of equation 16 with respect to $|F_{\underset{\sim}{h}}|$ equal to zero gives

$$|F_{\underset{\sim}{h}}| = \frac{\sum_i n_{\underset{\sim}{h}i} a_i}{\sum_i \frac{n_{\underset{\sim}{h}i}}{|F^o_{\underset{\sim}{h}i}|} a_i^2}, \qquad \text{for each } \underset{\sim}{h}. \qquad (16)$$

If a reflection with index $\underset{\sim}{h}$ occurs in only one film set, the

summations in equation 16 reduce to the trivial relationship

$$|F_{\underset{\sim}{h}}| = \frac{|F^{o}_{\underset{\sim}{h}i}|}{a_i} \quad . \tag{17}$$

It is therefore necessary to consider only those cases of equation 16 arising from reflections which occur in more than one set. Minimizing $P\left(\{|F_{\underset{\sim}{h}}|\}, \{a_i\}\right)$ with respect to each a_i except the one previously fixed for the hk0 Weissenberg film set gives the equations

$$a_i = \frac{\sum_{\underset{\sim}{h}} n_{\underset{\sim}{h}i} |F_{\underset{\sim}{h}}|}{\sum_{\underset{\sim}{h}} \frac{n_{\underset{\sim}{h}i}}{|F^{o}_{\underset{\sim}{h}i}|} |F_{\underset{\sim}{h}}|^2} \quad , \text{ for each } i. \tag{18}$$

An approximate set of values for $\{a_i\}$ was obtained by summing the observed structure factors within each set. These values were inserted in equation 16 to evaluate a set $\{|F_{\underset{\sim}{h}}|\}$. Application of equation 18 to the values of $\{|F_{\underset{\sim}{h}}|\}$ gave a new set $\{a_i\}$. Five alternate applications of equations 16 and 18 were sufficient for convergence of successive sets. When the final values for $\{a_i\}$ were obtained, the quantities $\{|F_{\underset{\sim}{h}}|\}$ for reflections which occurred on single film sets were evaluated. Each member of $\{|F_{\underset{\sim}{h}}|\}$ is denoted below as $|F_{obs}|$.

Combined structure and temperature factors for all observed reflections were calculated from values of the parameters x_1, x_2, z_1, z_2, B_A, and B_C previously determined, and

the equation

$$F_{calc} = F^{(c)}_{hkl}\, T^{1/2}_{hkl} = \{ f_{Ce} + 2 f_{Mg} [\cos 2\pi l z_1 + H(h,k) \cos 2\pi l z_2 + 2 H(h,k) L(l)$$

$$+ \tfrac{1}{3} D(2h+k) + \tfrac{1}{3} D(h-k) + \tfrac{1}{3} D(h+2k)] \} e^{-\frac{B_A (h^2+hk+k^2)}{8 d^2_{100}}} \; e^{-\frac{B_c l^2}{8 d^2_{001}}} , \qquad (19)$$

where D(n) has been defined in equation 11, and

$$\begin{aligned} &H(h,k) = 1 \text{ if } h \text{ and } k \text{ are both even,} \\ &H(h,k) = -1/3 \text{ if } h \text{ and } k \text{ are not both even,} \\ &L(l) = 1 \text{ if } l \text{ is divisible by four,} \\ &L(l) = -1 \text{ if } l \text{ is not divisible by four.} \end{aligned} \qquad (20a\text{-}d)$$

Values of F_{calc} and $|F_{obs}|$, including the (hk0) and (00l) reflections are tabulated below. Reflections which were too weak to be observed are denoted by dashed lines in the $|F_{obs}|$ column. Only the (hk0) and (00l) data have been corrected for extinction. The largest relative discrepancies between the observed and calculated data occur for the most intense reflections, and for weak reflections at small Bragg angles. The first discrepancies are accountable for by secondary extinction, for in every case $|F_{calc}|$ is greater than $|F_{obs}|$. The discrepancies between the calculated and observed intensities of the weak reflections at small Bragg angles are

probably due to the use of incorrect atomic form factors in the structure factor calculations. These discrepancies do not arise between calculated and observed (hk0) and (001) structure factors. For these reflections all the signs are positive, and all of the reflections at small Bragg angles are rather intense. On the whole, the agreement between the calculated and observed (hkl) reflections with l even is good enough to conclude that the trial structure and the values of the parameters which were determined are essentially correct. The R factor for the data in table 8 is 0.116.

c. Discussion of the subcell structure

Distances to the nearest neighbors of each atom were calculated, and are listed in table 9 below. The quantities n, p, q, r, s, t, and u are integers which vary between the limits prescribed in the table to take into account the ambiguities in the positions of the atoms.

The ligancy of cerium in the structure is twenty. The number of nearest neighbors around each magnesium atom is twelve or fourteen. Distances between cerium and magnesium atoms range between 3.63 and 3.93 Å, with a large number of distances near 3.70 Å. These interatomic separations are, as expected, considerably larger than 3.46 Å, the sum of the Pauling metallic radii for coordination number 12. Some of the distances between neighboring pairs of magnesium atoms, which vary from 2.87 to 3.63 Å, are significantly

Table 8. Calculated and observed subcell structure factors

Index	$\lvert F_{obs} \rvert$	F_{calc}	Index	$\lvert F_{obs} \rvert$	F_{calc}	Index	$\lvert F_{obs} \rvert$	F_{calc}
100	28.3	31.9	222	10.2	4.2	434	14.2	9.6
110	66.4	75.6	302	48.3	58.0	444	20.3	21.1
200	104.1	96.8	312	32.3	32.2	504	11.3	6.1
210	31.4	29.9	322	31.8	31.8	514	15.0	11.7
220	89.4	92.7	332	28.5	28.0	524	15.3	7.4
300	46.5	50.5	402	8.1	-4.5	534	9.0	7.3
310	24.8	24.9	412	35.7	33.9	544	10.7	7.3
320	28.3	25.8	422	-	-2.6	554	9.9	5.8
330	24.7	23.3	432	22.5	23.4	604	28.0	25.9
400	72.2	71.9	442	7.0	1.1	614	8.2	7.1
410	32.4	28.3	502	23.0	24.9	624	21.6	22.4
420	49.5	49.8	512	28.8	28.1	634	9.3	5.8
430	21.7	20.0	522	21.9	20.5	644	15.7	14.0
440	30.1	32.5	532	20.1	18.1	654	-	4.3
500	22.6	20.5	542	17.5	15.5	664	7.4	9.7
510	22.7	23.9	552	14.2	12.1	704	13.0	10.3
520	23.0	17.0	602	-	-0.8	714	6.6	5.3
530	15.3	15.3	612	19.6	19.0	724	9.8	6.4
540	15.1	13.5	622	-	3.8	734	9.1	5.7
550	12.4	10.6	632	16.1	13.7	804	16.5	16.8
600	42.4	41.7	642	-	2.4	814	-	6.8
610	17.4	15.9	702	20.0	21.1	824	12.2	11.5
620	32.5	32.8	712	18.5	14.2	904	9.2	9.8
630	13.3	11.8	722	12.4	13.9	10,0,4	10.3	10.0
640	20.2	19.9	732	15.1	11.7			
650	8.6	8.1	802	-	2.7	006	41.6	42.0
660	8.6	13.8	812	15.1	13.5	106	40.1	40.9
700	22.7	18.3	902	11.8	9.6	116	60.2	70.1
710	12.9	11.9				206	-	3.8
720	11.2	12.0	004	107.2	107.2	226	22.5	19.5
730	10.8	10.1	104	9.4	-1.5	306	49.1	53.0
800	25.2	25.4	114	36.3	37.0	336	27.0	28.1
810	12.7	11.7	204	42.6	49.9	406	14.1	11.2
820	17.7	17.0	214	9.3	3.8	506	23.6	25.7
900	13.9	8.2	224	50.5	56.6	606	12.7	8.3
10,0,0	15.4	14.3	304	28.0	23.6			
			314	10.3	4.6	008	72.7	72.8
002	26.3	26.5	324	14.1	8.9	108	21.5	17.2
102	35.8	43.8	334	9.0	9.6	118	41.7	41.1
112	61.0	83.2	404	39.7	42.2	208	35.8	38.8
202	22.8	-22.8	414	19.1	12.0	228	42.5	44.2
212	31.0	38.8	424	31.3	30.3	308	33.6	30.8

Table 8.--Continued

Index	$\|F_{obs}\|$	F_{calc}	Index	$\|F_{obs}\|$	F_{calc}	Index	$\|F_{obs}\|$	F_{calc}
338	17.8	16.8	3,3,10	13.4	12.8			
408	32.3	34.7	4,0,10	-	5.4	0,0,14	22.7	22.2
508	16.2	14.5	5,0,10	11.4	10.9	1,0,14	15.2	16.0
608	27.9	22.6				1,1,14	12.2	25.5
			0,0,12	36.8	36.8			
0,0,10	23.7	19.6	1,0,12	16.9	11.0	0,0,16	18.0	18.5
1,0,10	16.4	11.4	1,1,12	26.5	24.4	0,0,18	11.1	9.0
1,1,10	30.5	29.7	2,0,12	20.4	18.6	0,0,20	11.4	14.1
2,0,10	-	-0.7	2,2,12	25.0	23.6	0,0,22	6.2	4.7
2,2,10	14.7	10.1	3,0,12	22.4	19.3	0,0,24	5.1	6.6
3,0,10	25.1	22.8	4,0,12	19.2	18.5	0,0,26	3.3	2.4

Table 9. Interatomic distances in the $Mg_{12}Ce$ structure.

Central Atom		Ligands			Restraints
Kind	Position	Number & kind	Position	Interatomic Distance Angstroms	
Ce	(a)	2 Mg	(e)	3.63	
		(12-2n) Mg	(i_2)	3.70	$0 \leq n \leq 6$
		(6-p) Mg	(i_1)	3.70	$0 \leq p \leq 6$
		p Mg	(m)	3.71	
		2n Mg	(i_1)	3.93	
Mg	(e)	1 Mg	(e)	3.02	
		q Mg	(i_1)	3.15	$0 \leq q \leq 6$
		(6-q) Mg	(i_2)	3.30	
		(6-r) Mg	(i_2)	3.30	$0 \leq r \leq 6$
		r Mg	(m)	3.63	
		1 Ce	(a)	3.63	
Mg	(i_1)	s Mg	(i_1)	2.97	
		(4-s) Mg	(i_2)	2.99	$0 \leq s \leq 4$
		2 Mg	(1)	2.99	
		2 Mg	(e)	3.15	
		2 Mg	(m)	3.32	
		2 Ce	(a)	3.93	
Mg	(i_2)	4 Mg	(i_1)	2.99	
		2 Mg	(1)	3.12	
		2 Mg	(m)	3.27	
		2 Mg	(e)	3.30	
		2 Ce	(a)	3.70	
Mg	(1)	t Mg	(1)	2.93	
		4 Mg	(i_1)	2.99	$0 \leq t \leq 2$
		2 Mg	(i_2)	3.12	
		2 Mg	(e)	3.30	
		(2-t) Mg	(m)	3.32	
		2 Ce	(a)	3.70	
Mg	(m)	1 Mg	(m)	2.87	
		2 Mg	(i_2)	3.27	
		4 Mg	(i_1)	3.32	
		(2-u) Mg	(1)	3.32	$0 \leq u \leq 2$
		4 Mg	(e)	3.63	
		u Mg	(m)	3.71	
		1 Ce	(a)	3.71	

shorter than the sum of the metallic radii, which is 3.20 Å. However, reports of magnesium-magnesium distances considerably shorter than the sum of the radii for coordination number 12 are not uncommon in the literature, and a distance as short as 2.83 Å has been reported (14). In no case is an atom surrounded by an excessively large number of ligands at short distances. Nor is any atom contained in a framework that "fits too loosely." Varying the quantities n, p, q, r, s, t, and u does not, in general, make the configurations of ligands around the atoms overwhelmingly more or less desirable from the standpoint of interatomic distances. If the values of all of these quantities were sufficiently restricted, the phase would have a simple ordered structure. On the contrary, the ambiguities are of such a nature that leads to the complex odd-layer data.

There is a similarity between the structures of $Mg_{12}Ce$ and $CaZn_5$ (15). The latter structure has hexagonal layers consisting of a large (Ca) atom at (0,0,0) and small (Zn) atoms at 1/3,2/3,0 and 2/3,1/3,0 alternated with graphite-like layers consisting of small (Zn) atoms at 1/2,0,1/2; 0,1/2,1/2, and 1/2,1/2,1/2. The $Mg_{12}Ce$ structure results when half of the large atoms in the $CaZn_5$ configuration are replaced by pairs of small atoms with the axes of the pairs parallel to the c axis, and the remaining small atoms are displaced slightly from their ideal positions.

The relative constancy of the distribution of inter-

atomic distances has, in addition, the following consequence. The substitution of pairs of small atoms for large atoms in the $CaZn_5$ structure can take place in many ways, leading to a family of interrelated stable structures. Some examples of structures in addition to $Mg_{12}Ce$ and $TiBe_{12}$ which can be derived in this manner from the $CaZn_5$ configuration are those of $BaMg_x$, $ThMn_{12}$, Th_2Ni_{17}, Th_2Fe_{17}, and $MoBe_{12}$ (16,17,18). The last of these structures has an especially interesting relationship to the $Mg_{12}Ce$ structure. It can be regarded as an ordered modification of $Mg_{12}Ce$ with the disposition of heavy atom sites as depicted in figure 5. The configurations of the subcells in the two structures are identical, so that the subcell of $Mg_{12}Ce$ should have very nearly the same axial ratio as that for $MoBe_{12}$. But the $MoBe_{12}$ structure is tetragonal, having the space group D_{4h}^{17} = I4/mmm. The pseudo-tetragonality of the $Mg_{12}Ce$ structure is evidenced by the subcell (h0l) photographs which have nearly (but not quite) perfect tetragonal symmetry, and gives rise to the relationships between the axial dimensions that was mentioned previously.

3. The interpretation of the diffraction data with 1 odd.*

a. The search for an ordered hexagonal structure

In order to complete the description of the $Mg_{12}Ce$ structure the ambiguities regarding translation of the atoms by

---

*In this section, the Miller indices are based on the true cell edges a_o = 41.14 Å, c_o = 10.284 Å.

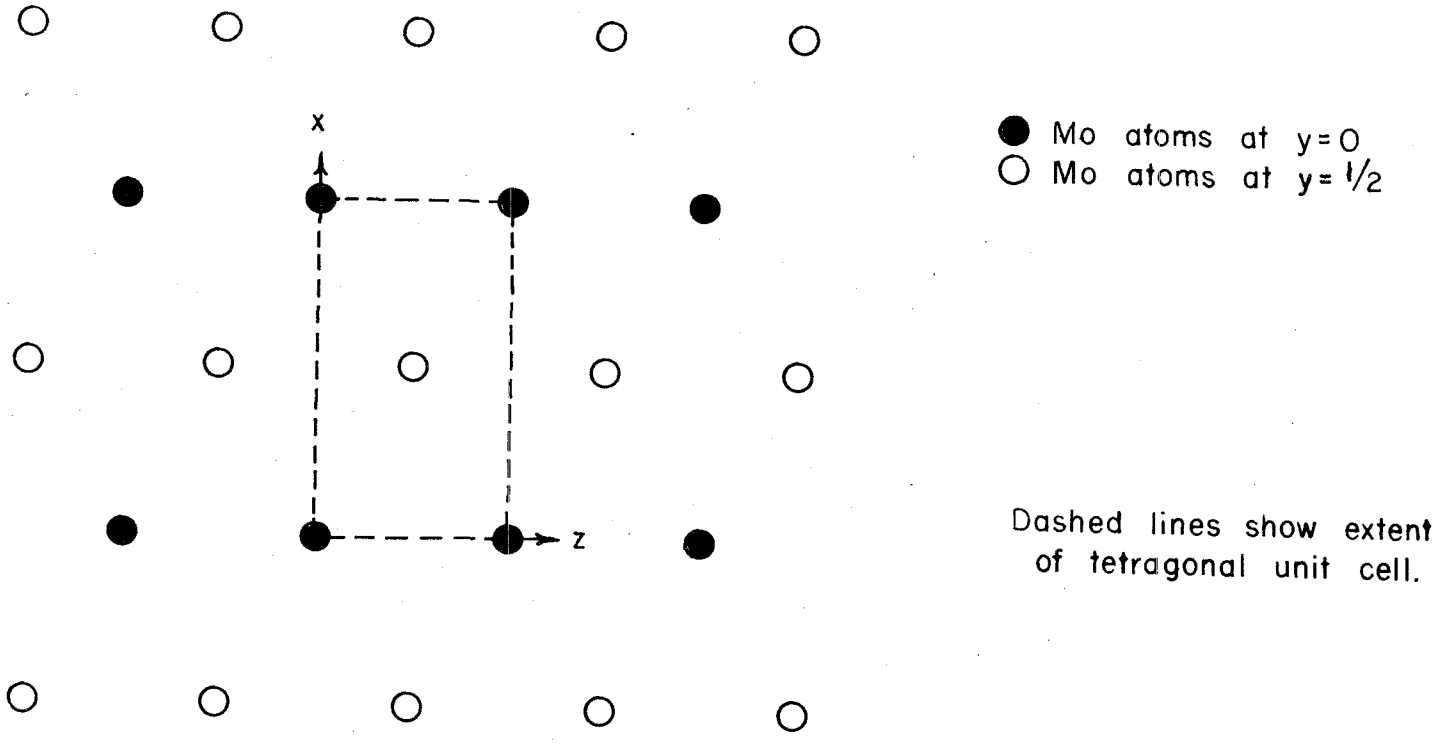

FIGURE 5. PROJECTION ALONG PSEUDO-HEXAGONAL AXIS OF $MoBe_{12}$, SHOWING CONFIGURATION OF THE Mo ATOMS.

1/2 c_o must be resolved. This description must involve the true periodicity of the structure, which has the axial dimension a_o = 41.14 A and contains forty-eight subcells. A nearly complete specification of the structure would result by removing the ambiguities associated with the cerium atoms only, inasmuch as this would also fix the positions of the magnesium atoms in subcell positions (1), and the parameter z_2 is sufficiently close to 1/4 so that the alternative z coordinates for the magnesium atoms at (i) virtually coincide.

Two cases are admissible. It may be possible to specify unequivocally the z coordinate of every atom in the unit cell, in which case the structure is ordered. On the other hand, it may only be possible to state, for instance, that there is a probability p that the z coordinate of a particular cerium atom in the true unit cell will be zero, and a probability 1-p that the z coordinate will be 1/2. For such a disordered structure, the array of probability assignments to the atomic sites in the unit cell must satisfy the symmetry and translational requirements imposed by the space group. Before disordered structures were considered, the possibilities for ordered structures were fully examined.

The reciprocal lattice layers of $Mg_{12}Ce$ with l odd present a complex but systematic pattern of absences which are not accountable for as space group extinctions. In attempting to interpret these absences, there arises quite naturally the notion of partial Fourier summation. The density of

electrons at the vector position $\underset{\sim}{r}$ in a crystal is related to the array of structure factors $\{F_{\underset{\sim}{h}}\}$ by the Fourier inversion

$$\rho(\underset{\sim}{r}) = \frac{1}{V} \sum_{\underset{\sim}{h}} F_{\underset{\sim}{h}} e^{-2\pi i \underset{\sim}{h}\cdot\underset{\sim}{r}} , \tag{21}$$

where V is the volume of the unit cell. In the circumstance that systematic (non-accidental) absences occur in the reciprocal lattice, a subset of the structure factors will be either exactly or virtually equal to zero. Then the electron density can be expressed as

$$\rho(\underset{\sim}{r}) = \frac{1}{V} \sum_{\underset{\sim}{h}}{}' F_{\underset{\sim}{h}} e^{-2\pi i \underset{\sim}{h}\cdot\underset{\sim}{r}} , \tag{21'}$$

where the primed summation is over the non-vanishing structure factors. The right hand side of equation 21' is a typical partial Fourier summation.

The following theorem on partial Fourier summations is useful in treating some of the absences that occur in the $Mg_{12}Ce$ structure. If $\rho(x)$ is a piecewise continuous one-dimensional function with unit periodicity it can be expressed as a Fourier series

$$\rho(x) = \sum_{h=-\infty}^{\infty} a_h e^{-2\pi i h x} . \tag{22}$$

It will be shown that the function $\rho_n(x)$, defined, in terms

of the same coefficients a_h, as

$$\rho_n(x) = \sum_{h=-\infty}^{\infty}{}' a_h e^{-2\pi i h x} \tag{23}$$

where the primed summation denotes that only those values of h which are integral multiples of some integer n are included in the sum, is expressible in a simple manner in terms of $\rho(x)$. The theorem states that

$$\rho_n(x) = \frac{1}{n} \sum_{p=1}^{n} \rho\left(x + \frac{p}{n}\right). \tag{24}$$

This relationship is easily verified. From equation 22,

$$\rho\left(x + \frac{p}{n}\right) = \sum_{h=-\infty}^{\infty} a_h e^{-2\pi i h\left(x + \frac{p}{n}\right)}. \tag{25}$$

Substitution of equation 25 into equation 24 gives

$$\rho_n(x) = \frac{1}{n} \sum_{p=1}^{n} \sum_{h=-\infty}^{\infty} a_h e^{-2\pi i h\left(x + \frac{p}{n}\right)}. \tag{26}$$

Any function $\rho(x)$ which will be encountered in crystallography

will be finite and continuous so that series such as equations 22, 25, and 26 converge uniformly. Equation 26 may therefore be rewritten

$$\rho_n(x) = \sum_{h=-\infty}^{\infty} \left[\frac{1}{n} \sum_{p=1}^{n} \left(e^{-\frac{2\pi i h}{n}} \right)^p \right] a_h e^{-2\pi i h x} \qquad (27)$$

The quantity $e^{-\frac{2\pi i h}{n}}$ is equal to one if h is an integral multiple of n, and is otherwise equal to some other n-th root of one. By considering the vector representation of complex numbers, it is evident that

$$\delta(h,n) = \frac{1}{n} \sum_{p=1}^{n} \left(e^{-\frac{2\pi i h}{n}} \right)^p \qquad (28)$$

is equal to one if h is an integral multiple of n, and is otherwise equal to zero. Since equation 27 can be written

$$\rho_n(x) = \sum_{h=-\infty}^{\infty} \delta(h,n)\, a_h e^{-2\pi i h x} , \qquad (29)$$

it is seen that $\rho_n(x)$ satisfies definition 23. Equation 5 is merely the special case of the theorem for which n equals 2.

It will now be shown with the aid of this theorem that there is a unique (but nevertheless unacceptable) ordered assignment of the z coordinates of the forty-eight cerium atoms in the unit cell that is consistent with the observed odd layer (hhl) and h0l) absences. Each space group consistent

with the Laue symmetry of the crystal and the observed absences in its reciprocal lattice has at least a threefold axis perpendicular to the x,y plane through 0,0. There are two ways of assigning x,y coordinates to the cerium atoms in the true unit cell which are consistent with this symmetry and the presence of a subcell. These are illustrated in figures 6 and 7. The existence of a threefold axis makes it possible to separate the forty-eight cerium atoms in each assignment into sixteen sets of three. These sets are denoted by the letters A through P on each of figures 6 and 7. The absence of 001 reflections when l is odd indicates that for every atom at height z there is somewhere an equivalent atom at $z+\frac{1}{2}$. (If this were not the case, e.g., if there were 25 Ce atoms at z=0 and 23 atoms at $z=\frac{1}{2}$, there would be a contribution of $2f_{Ce}$ to each of the 001 reflections with l odd. For some orders at least, these contributions would not be cancelled by those from magnesium atoms. The resultant intensities could readily have been observed, but were not.) Therefore, twenty-four of the cerium atoms are at z=0, and twenty-four are at $z=\frac{1}{2}$. The sites denoted by A in figure 6, the assignment with a cerium atom at the origin, are not a threefold set by symmetry. However, if there are to be twenty-four cerium atoms in an ordered structure at z=0, and twenty-four at $z=\frac{1}{2}$, then the A atoms must all be at z=0, or they must all be at $z=\frac{1}{2}$. This argument is not valid if the arrangement of cerium atoms is disordered.

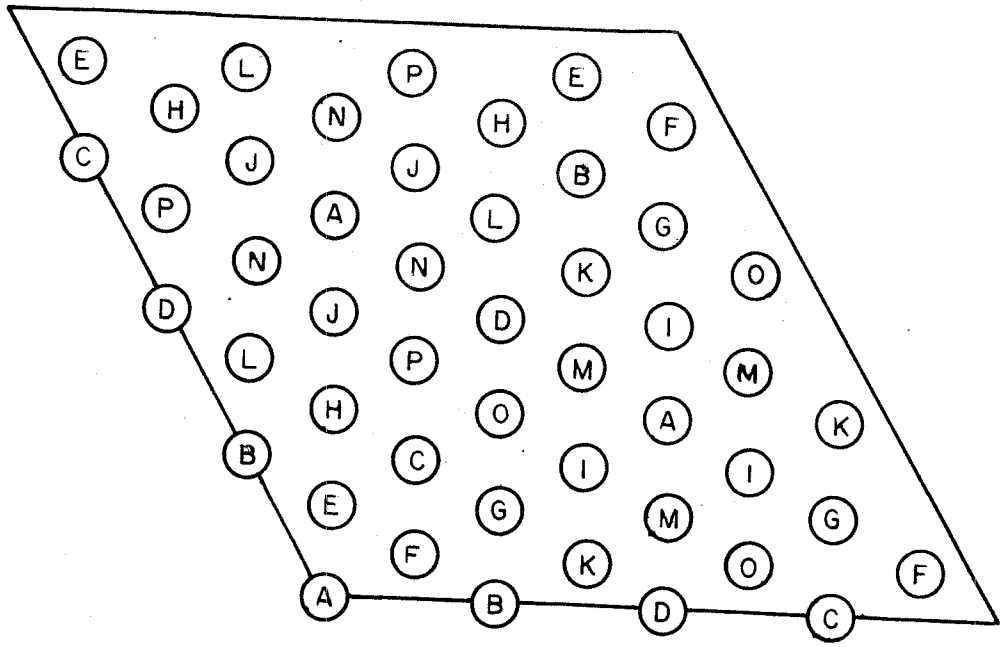

FIGURE 6. ASSIGNMENT OF CERIUM ATOMS ONTO THE (x,y) PLANE. CERIUM AT ORIGIN.

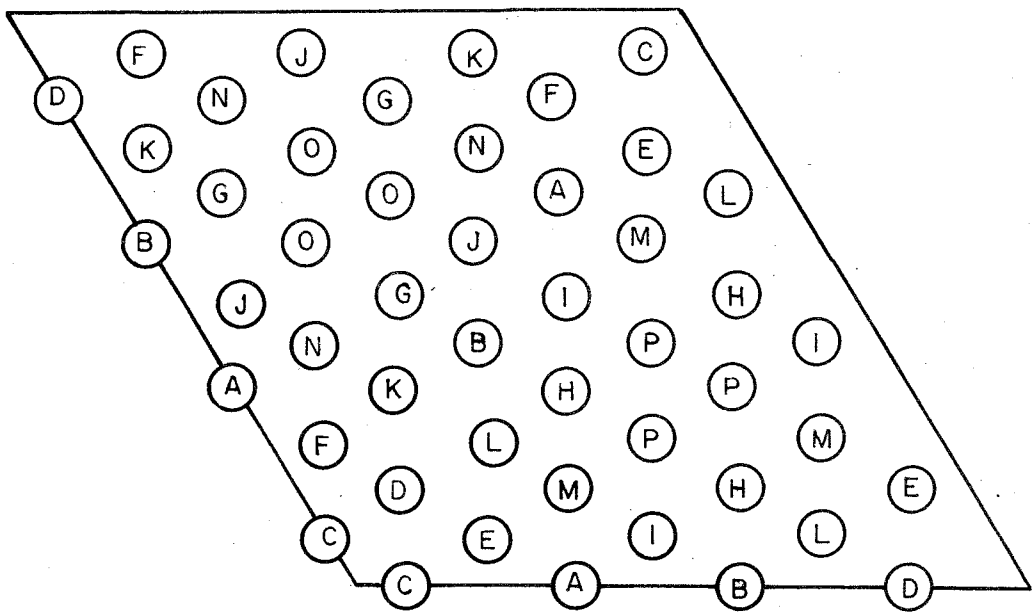

FIGURE 7. ASSIGNMENT OF CERIUM ATOMS ONTO THE (x,y) PLANE. CERIUM NOT AT ORIGIN.

(The discussion of the structure of $TlBe_{12}$ is in error on this point.)

An ordered structure with a cerium atom having x,y coordinates 0,0, as in figure 6 will be considered first. The only hhl reflections with l odd are those for which h=4n+2, where n is an integer. The conditions on the configuration of the cerium atoms which are imposed by the hhl absences derived as follows. The sum

$$\frac{1}{V}\sum_{h}\sum_{l} F_{hhl}\, e^{-2\pi i(ha+lz)} = \int_{o}^{1} \rho(a-y,y,z)\,dy, \qquad (30)$$

where V is the unit cell volume, ρ is the electron density, and a=x+y. The integral on the right hand side of equation 30 is the projection of the electron density onto the hhl plane. The object of this derivation is to make use of equation 24, to express as a function of ρ the partial Fourier summation over the hhl reflections with l odd which contains only the absent reflections, and then to equate this function to zero.

Using brackets to indicate sets of integers, the set of all odd numbers, $\{2n+1\}$, may be expressed as

$$\{2n+1\} = \{n\} - \{2n\} \qquad (31)$$

where n ranges over all positive and negative integers. The partial Fourier summation over any subset of the integers

which can be expressed, as above, as combinations of arithmetic progressions containing zero can be treated with theorem (24). Thus, from equations 24 and 30,

$$\frac{1}{V}\sum_{h}\sum_{l=2n} F_{hhl}\, e^{-2\pi i(ha+lz)} = \int_0^{\frac{1}{2}} [\rho(a-y,y,z)+\rho(a-y,y,z+\tfrac{1}{2})]\,dy. \qquad (32)$$

Subtracting equation 32 from equation 30 gives

$$\frac{1}{V}\sum_{h}\sum_{l\,odd} F_{hhl}\, e^{-2\pi i(ha+lz)} = \int_0^{\frac{1}{2}} [\rho(a-y,y,z)-\rho(a-y,y,z+\tfrac{1}{2})]\,dy \equiv G(a,z). \qquad (33)$$

The summation over h on the left hand side of equation 33 must be further restricted so as to include only the terms which are absent in the (hhl) data with l odd. The values of h corresponding to these absences, again using set notation, are

$$\{n\} - \{4n+2\} = \{n\} - \{2n\} + \{4n\}. \qquad (34)$$

From equations 33 and 34,

$$\frac{1}{V}\sum_{h=2n}\sum_{l\,odd} F_{hhl}\, e^{-2\pi i(ha+lz)} = \tfrac{1}{2}[G(a,z)+G(a+\tfrac{1}{2},z)], \qquad (35)$$

and

$$\frac{1}{V}\sum_{h=4n}\sum_{l\,odd}F_{hhl}\,e^{-2\pi i(ha+lz)}=\frac{1}{4}\left[G(a,z)+G(a+\tfrac{1}{4},z)+G(a+\tfrac{1}{2},z)+G(a+\tfrac{3}{4},z)\right]. \qquad (36)$$

Subtraction of equation 35 from the sum of equations 33 and 36 gives the partial Fourier summation involving only the absent hhl reflections with odd l

$$\frac{1}{V}\sum_{h=\{n\}-\{4n-2\}}\sum_{l\,odd}F_{hhl}\,e^{-2\pi i(ha+lz)}=$$

$$\frac{3}{4}G(a,z)+\frac{1}{4}G(a+\tfrac{1}{4},z)-\frac{1}{4}G(a+\tfrac{1}{2},z)+\frac{1}{4}G(a+\tfrac{3}{4},z). \qquad (37)$$

The right hand side of equation 37 may be expressed in its integral form according to the definition of G(a,z) in equation 33 and is set equal to zero in equation 38.

$$\frac{1}{8}\int_0^1\Big\{3\left[\rho(a-y,y,z)-\rho(a-y,y,z+\tfrac{1}{2})\right]+\left[\rho(a+\tfrac{1}{4}-y,y,z)-\rho(a+\tfrac{1}{4}-y,y,z+\tfrac{1}{2})\right]$$

$$-\left[\rho(a+\tfrac{1}{2}-y,y,z)-\rho(a+\tfrac{1}{2}-y,y,z+\tfrac{1}{2})\right]+\left[\rho(a+\tfrac{3}{4}-y,y,z)-\rho(a+\tfrac{3}{4}-y,y,z+\tfrac{1}{2})\right]\Big\}\,dy \qquad (38)$$
$$=0.$$

It will be assumed in this analysis that the structure factors of the systematically absent reflections are rigorously zero. (The validity of this assumption will be dis-

cussed later.) The absences occur over too wide a range of $\sin\theta/\lambda$ to result from the fortuitous cancellation of scattering from magnesium and cerium atoms. It follows that the reciprocal lattice constructed from the portions of the structure factors involving only the contributions from the cerium atoms must also contain these absences. Therefore, equation 38 is valid when ρ_{Ce}, the partial electronic density due to the cerium atoms in the structure, is substituted for ρ, the total electronic density.

To each of the forty-eight cerium sites shown in figure 6 may be assigned a value of a=x+y, the parameter appearing in equation 38. Since, from equation 33, G(a,z) = G(a+1,z), the range of the parameter a may be restricted from 0 to 1. The value of a for each of the cerium sites in figure 6 is 0, 1/4, 1/2, or 3/4. Table 10 is prepared from figure 6, and shows the x and y coordinates and the value for a of the cerium atoms in each of the threefold sets. Equation 38 expressed in terms of ρ_{Ce} is valid for every value of a and z, so in particular, it must be valid for a=0,1/4,1/2 and 3/4, z=0 and 1/2, the positions of the cerium peaks in the (hhl) projection. For values of a and z corresponding to a cerium peak position, the integral $\int_0^1 \rho_{Ce}(a-y,y,z)dy$ is proportional to the number of cerium atoms associated with that peak, so that equation 38 can be written in the discrete form

Table 10. Coordinates of cerium atoms with cerium assigned to origin.

Set	x	y	a	x	y	a	x	y	a
A	0	0	0	1/3	2/3	0	2/3	1/3	0
B	1/4	0	1/4	0	1/4	1/4	3/4	3/4	1/2
C	3/4	0	3/4	0	3/4	3/4	1/4	1/4	1/2
D	1/2	0	1/2	0	1/2	1/2	1/2	1/2	0
E	1/12	1/6	1/4	1/12	11/12	0	5/6	11/12	3/4
F	1/6	1/12	1/4	11/12	1/12	0	11/12	5/6	3/4
G	1/3	1/6	1/2	5/6	2/3	1/2	5/6	1/6	0
H	1/6	1/3	1/2	2/3	5/6	1/2	1/6	5/6	0
I	1/2	1/4	3/4	3/4	1/2	1/4	3/4	1/4	0
J	1/4	1/2	3/4	1/2	3/4	1/4	1/4	3/4	0
K	5/12	1/12	1/2	11/12	1/3	1/4	2/3	7/12	1/4
L	1/12	5/12	1/2	1/3	11/12	1/4	7/12	2/3	1/4
M	7/12	1/6	3/4	5/6	5/12	1/4	7/12	5/12	0
N	1/6	7/12	3/4	5/12	5/6	1/4	5/12	7/12	0
O	2/3	1/12	3/4	11/12	7/12	1/2	5/12	1/3	3/4
P	1/12	2/3	3/4	7/12	11/12	1/2	1/3	5/12	3/4

$$3[m(a,z)-m(a,z+\tfrac{1}{2})] + [m(a+\tfrac{1}{4},z)-m(a+\tfrac{1}{4},z+\tfrac{1}{2})z - [m(a+\tfrac{1}{2})-m(a+\tfrac{1}{2},z+\tfrac{1}{2})] + [m(a+\tfrac{3}{4},z)-m(a+\tfrac{3}{4},z+\tfrac{1}{2})] = 0, \quad (39)$$

where a is an integral multiple of one quarter, z is zero or one-half, and m(a,z) is the number of cerium atoms associated with the peak in the hhl projection at a,z.

Defining α, β, γ, and δ as

$$\alpha = \tfrac{1}{2}[m(0,0) - m(0,\tfrac{1}{2})] \quad (40a)$$

$$\beta = \tfrac{1}{2}[m(\tfrac{1}{4},0) - m(\tfrac{1}{4},\tfrac{1}{2})] \quad (40b)$$

$$\gamma = \tfrac{1}{2}[m(\tfrac{1}{2},0) - m(\tfrac{1}{2},\tfrac{1}{2})] \quad (40c)$$

$$\delta = \tfrac{1}{2}[m(\tfrac{3}{4},0) - m(\tfrac{3}{4},\tfrac{1}{2})], \quad (40d)$$

and substituting the values z=0 and a=0,1/4,1/2 and 3/4 successively into equation 39 give the simultaneous equations

$$3\alpha + \beta - \gamma + \delta = 0 \quad (41a)$$

$$\alpha + 3\beta + \gamma - \delta = 0 \quad (41b)$$

$$-\alpha + \beta + 3\gamma + \delta = 0 \quad (41c)$$

$$\alpha - \beta + \gamma + 3\delta = 0. \quad (41d)$$

Equations 41 have the trivial solution $\alpha=\beta=\gamma=\delta=0$, but since the value of the determinant of the coefficients in equations 41 is zero, a non-trivial solution exists. This solution is

$$\alpha = -\beta = \gamma = -\delta \tag{42}$$

Equations 40 may therefore be written, leaving α as a parameter, as

$$m(0,0)-m(0,\tfrac{1}{2}) = 2\alpha \tag{43a}$$

$$m(\tfrac{1}{4},0)-m(\tfrac{1}{4},\tfrac{1}{2}) = -2\alpha \tag{43b}$$

$$m(\tfrac{1}{2},0)-m(\tfrac{1}{2},\tfrac{1}{2}) = 2\alpha \tag{43c}$$

$$m(3/4,0)-m(3/4,1/2) = -2\alpha \tag{43d}$$

Let the quantities $p_A, p_B, \ldots p_O, p_P$ be the probabilities that the cerium atoms in the threefold sets A,B,..... O,P, respectively, have the coordinate z=0. It was established in the section on the subcell structure that each cerium site in the x,y plane the occurrence of cerium atoms at z=0 and $z=\frac{1}{2}$ are exhaustive and mutually exclusive events, so that the probabilities of finding the atoms at $z=\frac{1}{2}$ are $1-p_A, 1-p_B, \ldots 1-p_O, 1-p_P$. In an ordered assignment of the z coordinates of the cerium atoms, each of the probabilities $p_A, p_B, \ldots p_O, p_P$ must be zero or one. With the aid of table 10,

it is possible to evaluate the quantities appearing on the l.h.s. of equations 43 in terms of these probabilities. Table 10 shows, for instance, that there are three sites in the threefold set A, and one site each in the sets D, E, F, G, H, I, J, M, and N for which the parameter a is zero, so that

$$m(0,0) = 3p_A + p_D + p_E + p_F + p_G + p_H + p_I + p_J + p_M + p_N, \tag{44}$$

and

$$m(0,\tfrac{1}{2}) = 3(1-p_A) + (1-p_D) + (1-p_E) + (1-p_F) + (1-p_G) + (1-p_H) + (1-p_I) + (1-p_J) + (1-p_M) + (1-p_N). \tag{45}$$

The values for m thus obtained are actual values in the case of an ordered structure, and expectation values in the case of a disordered structure.

Substitution of equations 44 and 45 into equation 43a and division by 2 gives

$$3p_A + p_D + p_E + p_F + p_G + p_H + p_I + p_J + p_M + p_N = 6 + \alpha \tag{46a}$$

Equations 43b, 43c, and 43d may similarly be expressed in terms of the probabilities, leading to the relationships

$$2p_B + p_E + p_F + p_I + p_J + 2p_K + 2p_L + p_M + p_N = 6 - \alpha \tag{46b}$$

$$p_B + p_C + 2p_D + 2p_H + p_K + 2p_G + p_L + p_O + p_P = 6+\alpha \qquad (46c)$$

$$2p_C + p_E + p_F + p_I + p_J + p_M + p_N + 2p_O + 2p_P = 6-\alpha. \qquad (46d)$$

Equations 46 are the final expressions for the consequences of the hhl absences with l odd for the assignment of cerium sites having a cerium atom at the origin.

Further relations involving the probabilities can be obtained by considering the (h0l) absences with l odd. Making use of the Fourier analysis theorem and equation 24, it is possible to express the Fourier transform of the h0l structure factors with l odd as

$$\frac{1}{V}\sum_h \sum_{l\,odd} F_{h0l}\, e^{-2\pi i(hx+lz)} = \int_0^{\frac{1}{2}} [\rho(x,y,z) - \rho(x,y,z+\tfrac{1}{2})]\, dy \equiv H(x,z). \qquad (47)$$

From figure 1, odd-layer h0l reflections with h modulo 12 = 0,1,2,4,8,10, and 11 are absent. It is not possible to express this set of absences as combinations of arithmetic progressions containing zero. However, if consideration of the absences with h modulo 12 = 1 and 11 is postponed for the present, the remaining set, h modulo 12 = 0,2,4,8, and 10 is expressible in a form which can be interpreted with the partial Fourier summation theorem. In set notation

$$\{12n\} + \{12n+2\} + \{12n+4\} + \{12n+8\} + \{12n+10\} = \{2n\} - \{6n\} + \{12n\}. \qquad (48)$$

Using equation 24, the partial Fourier summation over the h0l reflections with l odd and h modulo 12 = 0,2,4,8, and 10 becomes

$$\frac{1}{V}\sum_{\substack{h \bmod 12 \\ =0,2,4,8,10}} \sum_{l \text{ odd}} F_{h0l}\, e^{-2\pi i(hx+lz)}$$

$$= \frac{1}{2}\sum_{p=1}^{2} H\left(x+\frac{p}{2},z\right) - \frac{1}{6}\sum_{p=1}^{6} H\left(x+\frac{p}{6},z\right) + \frac{1}{12}\sum_{p=1}^{12} H\left(x+\frac{p}{12},z\right). \qquad (49)$$

The right hand side of equation 49 may be expressed in its integral form according to the definition of H(x,z) in equation 47 and when equated to zero, gives

$$\frac{1}{24}\int_0^1 \Big\{5\left[\rho(x,y,z)-\rho(x,y,z+\tfrac{1}{2})\right]+\left[\rho(x+\tfrac{1}{12},y,z)-\rho(x+\tfrac{1}{12},y,z+\tfrac{1}{2})\right]$$
$$-\left[\rho(x+\tfrac{1}{6},y,z)-\rho(x+\tfrac{1}{6},y,z+\tfrac{1}{2})\right]+\left[\rho(x+\tfrac{1}{4},y,z)-\rho(x+\tfrac{1}{4},y,z+\tfrac{1}{2})\right]-\left[\rho(x+\tfrac{1}{3},y,z)-\rho(x+\tfrac{1}{3},y,z+\tfrac{1}{2})\right]$$
$$+\left[\rho(x+\tfrac{5}{12},y,z)-\rho(x+\tfrac{5}{12},y,z+\tfrac{1}{2})\right]+5\left[\rho(x+\tfrac{1}{2},y,z)-\rho(x+\tfrac{1}{2},y,z+\tfrac{1}{2})\right]+\left[\rho(x+\tfrac{7}{12},y,z)-\rho(x+\tfrac{7}{12},y,z+\tfrac{1}{2})\right]$$
$$-\left[\rho(x+\tfrac{2}{3},y,z)-\rho(x+\tfrac{2}{3},y,z+\tfrac{1}{2})\right]+\left[\rho(x+\tfrac{3}{4},y,z)-\rho(x+\tfrac{3}{4},y,z+\tfrac{1}{2})\right]-\left[\rho(x+\tfrac{5}{6},y,z)-\rho(x+\tfrac{5}{6},y,z+\tfrac{1}{2})\right]$$
$$+\left[\rho(x+\tfrac{11}{12},y,z)-\rho(x+\tfrac{11}{12},y,z+\tfrac{1}{2})\right]\Big\}dy = 0. \qquad (50)$$

For reasons mentioned previously, equation 50 shall be considered valid when ρ_{Ce} is substituted in each term for ρ. From table 10, the x coordinate of each cerium atom is an integral multiple of one-twelfth. Since for values of x which are integral multiples of 1/12 and for z = 0 or 1/2, the positions of the cerium peaks on the h0l projections, the integral $\int_0^1 \rho_{Ce}(x,y,z)\,dy$ is proportional to the number of cerium atoms

associated with each peak, equation 50 can be written in the form

$$5[n(x,z)-n(x,z+\tfrac{1}{2})]+[n(x+\tfrac{1}{12},z)-n(x+\tfrac{1}{12},z+\tfrac{1}{2})]-[n(x+\tfrac{1}{6},z)-n(x+\tfrac{1}{6},z+\tfrac{1}{2})]+[n(x+\tfrac{1}{4},z)-n(x+\tfrac{1}{4},z+\tfrac{1}{2})]$$
$$-[n(x+\tfrac{1}{3},z)-n(x+\tfrac{1}{3},z+\tfrac{1}{2})]+[n(x+\tfrac{5}{12},z)-n(x+\tfrac{5}{12},z+\tfrac{1}{2})]+5[n(x+\tfrac{1}{2},z)-n(x+\tfrac{1}{2},z+\tfrac{1}{2})]$$
$$+[n(x+\tfrac{7}{12},z)-n(x+\tfrac{7}{12},z+\tfrac{1}{2})]-[n(x+\tfrac{2}{3},z)-n(x+\tfrac{2}{3},z+\tfrac{1}{2})]+[n(x+\tfrac{3}{4},z)-n(x+\tfrac{3}{4},z+\tfrac{1}{2})]$$
$$-[n(x+\tfrac{5}{6},z)-n(x+\tfrac{5}{6},z+\tfrac{1}{2})]+[n(x+\tfrac{11}{12},z)-n(x+\tfrac{11}{12},z+\tfrac{1}{2})]=0, \qquad (51)$$

where x is an integral multiple of one-twelfth, z is zero or one-half, and n(x,z) is the number of cerium atoms associated with the peak in the h0l projection at x,z

Making the definitions

$$\epsilon = \tfrac{1}{2}[n(0,0)-n(0,\tfrac{1}{2})] \qquad (52a)$$

$$\zeta = \tfrac{1}{2}[n(\tfrac{1}{12},0)-n(\tfrac{1}{12},\tfrac{1}{2})] \qquad (52b)$$

$$\eta = \tfrac{1}{2}[n(\tfrac{1}{6},0)-n(\tfrac{1}{6},\tfrac{1}{2})] \qquad (52c)$$

$$\theta = \tfrac{1}{2}[n(\tfrac{1}{4},0)-n(\tfrac{1}{4},\tfrac{1}{2})] \qquad (52d)$$

$$\iota = \tfrac{1}{2}[n(\tfrac{1}{3},0)-n(\tfrac{1}{3},\tfrac{1}{2})] \qquad (52e)$$

$$\kappa = \tfrac{1}{2}[n(\tfrac{5}{12},0)-n(\tfrac{5}{12},\tfrac{1}{2})] \qquad (52f)$$

$$\lambda = \tfrac{1}{2}[n(\tfrac{1}{2},0)-n(\tfrac{1}{2},\tfrac{1}{2})] \qquad (52g)$$

$$\mu = \tfrac{1}{2}[n(\tfrac{7}{12},0)-n(\tfrac{7}{12},\tfrac{1}{2})] \qquad (52h)$$

$$\nu = \tfrac{1}{2}\left[n\left(\tfrac{2}{3},0\right) - n\left(\tfrac{2}{3},\tfrac{1}{2}\right)\right] \qquad (52i)$$

$$\xi = \tfrac{1}{2}\left[n\left(\tfrac{3}{4},0\right) - n\left(\tfrac{3}{4},\tfrac{1}{2}\right)\right] \qquad (52j)$$

$$o = \tfrac{1}{2}\left[n\left(\tfrac{5}{6},0\right) - n\left(\tfrac{5}{6},\tfrac{1}{2}\right)\right] \qquad (52k)$$

$$\pi = \tfrac{1}{2}\left[n\left(\tfrac{11}{12},0\right) - n\left(\tfrac{11}{12},\tfrac{1}{2}\right)\right], \qquad (52l)$$

and substituting the values z=0, and x=0,1/12,1/6,1/4,1/3, 5/12,1/2,7/12,2/3,3/4,5/6, and 11/12 successively into equation 51 lead to the simultaneous equations

$$5\epsilon + \zeta - \eta + \theta - \iota + \kappa + 5\lambda + \mu - \nu + \xi - o + \pi = 0 \qquad (53a)$$

$$\epsilon + 5\zeta + \eta - \theta + \iota - \kappa + \lambda + 5\mu + \nu - \xi + o - \pi = 0 \qquad (53b)$$

$$-\epsilon + \zeta + 5\eta + \theta - \iota + \kappa - \lambda + \mu + 5\nu + \xi - o + \pi = 0 \qquad (53c)$$

$$\epsilon - \zeta + \eta + 5\theta + \iota - \kappa + \lambda - \mu + \nu + 5\xi + o - \pi = 0 \qquad (53d)$$

$$-\epsilon + \zeta - \eta + \theta + 5\iota + \kappa - \lambda + \mu - \nu + \xi + 5o + \pi = 0 \qquad (53e)$$

$$\epsilon - \zeta + \eta - \theta + \iota + 5\kappa + \lambda - \mu + \nu - \xi + o + 5\pi = 0 \qquad (53f)$$

$$5\epsilon + \zeta - \eta + \theta - \iota + \kappa + 5\lambda + \mu - \nu + \xi - o + \pi = 0 \qquad (53g)$$

$$\epsilon + 5\zeta + \eta - \theta + \iota - \kappa + \lambda + 5\mu + \nu - \xi + o - \pi = 0 \qquad (53h)$$

$$-\epsilon+\zeta+5\eta+\theta-\iota+\kappa-\lambda+\mu+5\nu+\xi-o+\pi=0 \tag{53i}$$

$$\epsilon-\zeta+\eta+5\theta+\iota-\kappa+\lambda-\mu+\nu+5\xi+o-\pi=0 \tag{53j}$$

$$-\epsilon+\zeta-\eta+\theta+5\iota+\kappa-\lambda+\mu-\nu+\xi+5o+\pi=0 \tag{53k}$$

$$\epsilon-\zeta+\eta-\theta+\iota+5\kappa+\lambda-\mu+\nu-\xi+o+5\pi=0. \tag{53l}$$

Equations 53 are not linearly independent. However, most of their redundancy can be removed if the substitutions

$$g_1=\epsilon+\lambda \tag{54a}$$

$$g_2=\zeta+\mu \tag{54b}$$

$$g_3=\eta+\nu \tag{54c}$$

$$g_4=\theta+\xi \tag{54d}$$

$$g_5=\iota+o \tag{54e}$$

$$g_6=\kappa+\pi \tag{54f}$$

are made. Equations 53a-53f then become identical to equations 53g-53l. The new equations are

$$5g_1 + g_2 - g_3 + g_4 - g_5 + g_6 = 0 \tag{55a}$$

$$g_1 + 5g_2 + g_3 - g_4 + g_5 - g_6 = 0 \tag{55b}$$

$$-g_1 + g_2 + 5g_3 + g_4 - g_5 + g_6 = 0 \tag{55c}$$

$$g_1 - g_2 + g_3 + 5g_4 + g_5 - g_6 = 0 \tag{55d}$$

$$-g_1 + g_2 - g_3 + g_4 + 5g_5 + g_6 = 0 \tag{55e}$$

$$g_1 - g_2 + g_3 - g_4 + g_5 + 5g_6 = 0. \tag{55f}$$

The determinant of the coefficients of equations 55 is equal to zero. In addition to the trivial solution $g_1 = g_2 = g_3 = g_4 = g_5 = g_6 = 0$, there is the solution

$$g_1 = -g_2 = g_3 = -g_4 = g_5 = -g_6 \tag{56}$$

Substituting equations 54 and 52 successively in equation 56 and retaining q_1 as a parameter results in the equations

$$n(0,0) - n(0,\tfrac{1}{2}) + n(\tfrac{1}{2},0) - n(\tfrac{1}{2},\tfrac{1}{2}) = g_1 \tag{57a}$$

$$n(\tfrac{1}{12},0) - n(\tfrac{1}{12},\tfrac{1}{2}) + n(\tfrac{7}{12},0) - n(\tfrac{7}{12},\tfrac{1}{2}) = -g_1 \tag{57b}$$

$$n(\tfrac{1}{6},0) - n(\tfrac{1}{6},\tfrac{1}{2}) + n(\tfrac{2}{3},0) - n(\tfrac{2}{3},\tfrac{1}{2}) = g_1 \tag{57c}$$

$$n(\tfrac{1}{4},0) - n(\tfrac{1}{4},\tfrac{1}{2}) + n(\tfrac{3}{4},0) - n(\tfrac{3}{4},\tfrac{1}{2}) = -q_1 \qquad (57d)$$

$$n(\tfrac{1}{3},0) - n(\tfrac{1}{3},\tfrac{1}{2}) + n(\tfrac{5}{6},0) - n(\tfrac{5}{6},\tfrac{1}{2}) = q_1 \qquad (57e)$$

$$n(\tfrac{5}{12},0) - n(\tfrac{5}{12},\tfrac{1}{2}) + n(\tfrac{11}{12},0) - n(\tfrac{11}{12},\tfrac{1}{2}) = -q_1 . \qquad (57f)$$

The quantities n(x,z) appearing in equations 57 can be expressed with the aid of table 10 in terms of the probabilities $p_A, p_B, \cdots p_O, p_P$ by a method analogous to the evaluation of the quantities n(a,z). Substituting these values in equations 57 gives

$$p_A + p_B + p_C + 3p_D + p_I + p_J = 4 + q_1 \qquad (58a)$$

$$2p_E + 2p_L + 2p_M + 2p_P = 4 - q_1 \qquad (58b)$$

$$p_A + p_F + 3p_H + p_K + p_N + p_O = 4 + q_1 \qquad (58c)$$

$$2p_B + 2p_C + 2p_I + 2p_J = 4 - q_1 \qquad (58d)$$

$$p_A + p_E + 3p_G + p_L + p_M + p_P = 4 + q_1 \qquad (58e)$$

$$2p_F + 2p_K + 2p_N + 2p_O = 4 - q_1 \qquad (58f)$$

Equation 59 is obtained by adding equations 58a and 58d.

$$p_A + 3(p_B + p_C + p_D + p_I + p_J) = 8. \qquad (59)$$

If the assignment of cerium atoms is ordered, all of the p's are either zero or one. Therefore, $p_B + p_C + p_D + p_I + p_J$ should be an integer N, between zero and five. Equation 58 can therefore be rewritten

$$3N = 8 - p_A . \tag{60}$$

However, no integer N satisfies the relations

$$3N = 8 \quad \text{or} \quad 3N = 7 , \tag{61}$$

so there can be no ordered structures having the first arrangement of x and y coordinates of the cerium atoms. It must be concluded that any ordered arrangement of cerium atoms that is consistent with the observed absences in the reciprocal lattice must conform with the assignment of cerium atoms in figure 7 with no cerium atom on the z axis.

Of the space groups which are possible for the $Mg_{12}Ce$ structure, only $D_{3h}^3 = C\bar{6}2m$ is compatible with the second choice of x,y coordinates for the cerium atoms. The symmetry element m in this space group requires the following relationships between the probabilities to be valid.

$$p_E = p_F \tag{62a}$$

$$p_G = p_H \tag{62b}$$

$$p_I = p_J \tag{62c}$$

$$p_K = p_L \tag{62d}$$

$$p_M = p_N \tag{62e}$$

$$p_O = p_P. \tag{62f}$$

The sixteen threefold groups in figure 7 may therefore be reclassified into four threefold sets A,B,C, and D, and six sixfold sets E,G,I,K,M, and O. Table 11 gives the x and y coordinate, and the values of a=x+y for the sites in each set.

The values of x are all integral multiples of one-twelfth, and the values of a are all one-twelfth plus integral multiples of one quarter. The derivations of equations 39 and 51 do not depend on the choice of origin in the x,y plane, and are valid as long as the arguments a and z in equation 39 and x and z in equation 51 correspond respectively to cerium peak positions in the (hhl) and (h0l) projections. Equations 39 and 51 are therefore applicable to the assignment of cerium atoms according to table 11 when a is 1/12,1/3,7/12, or 5/6, x is an integral multiple of one-twelfth, and z is zero or one-half. The development of expressions involving the probabilities of finding the atoms in the new sets of zero proceeds identically with the derivations of equations 46 and 58. The four equations analogous to equation 46 which express the consequences of the (hhl) absences in the present assignment are

Table 11. Coordinates of cerium atoms with no cerium assigned to origin.

Set	x	y	a	x	y	a	x	y	a
A	1/3	0	1/3	0	1/3	1/3	2/3	2/3	1/3
B	7/12	0	7/12	0	7/12	7/12	5/12	5/12	5/6
C	1/12	0	1/12	0	1/12	1/12	11/12	11/12	5/6
D	5/6	0	5/6	0	5/6	5/6	1/6	1/6	1/3
E	1/4	1/12	1/3	11/12	1/6	1/12	5/6	3/4	7/12
	1/12	1/4	1/3	1/6	11/12	1/12	3/4	5/6	7/12
G	1/3	1/2	5/6	1/6	2/3	5/6	1/2	5/6	1/3
	1/2	1/3	5/6	2/3	1/6	5/6	5/6	1/2	1/3
I	1/2	1/12	7/12	7/12	1/2	1/12	11/12	5/12	1/3
	1/12	1/2	7/12	1/2	7/12	1/12	5/12	11/12	1/3
K	1/4	1/3	7/12	1/12	3/4	5/6	2/3	11/12	7/12
	1/3	1/4	7/12	3/4	1/12	5/6	11/12	2/3	7/12
M	5/12	1/6	7/12	5/6	1/4	1/12	3/4	7/12	1/3
	1/6	5/12	7/12	1/4	5/6	1/12	7/12	3/4	1/3
O	1/4	7/12	5/6	1/3	3/4	1/12	5/12	2/3	1/12
	7/12	1/4	5/6	3/4	1/3	1/12	2/3	5/12	1/12

$$2p_C + 2p_E + 2p_I + 2p_M + 4p_O = 6-\alpha \qquad (63a)$$

$$3p_A + p_D + 2p_E + 2p_G + 2p_I + 2p_M = 6+\alpha \qquad (63b)$$

$$2p_B + 2p_E + 2p_I + 4p_K + 2p_M = 6-\alpha \qquad (63c)$$

$$p_B + p_C + 2p_D + 4p_G + 2p_K + 2p_O = 6+\alpha. \qquad (63d)$$

The expressions which are analogous to equations 58 are

$$p_A + p_B + p_C + p_D + 2p_G + 2p_I = 4+q_1 \qquad (64a)$$

$$p_B + p_C + p_E + 2p_I + p_K + p_M + p_O = 4-q_1 \qquad (64b)$$

$$p_A + p_D + p_E + 2p_G + p_K + p_M + p_O = 4+q_1 \qquad (64c)$$

$$2p_E + 2p_K + 2p_M + 2p_O = 4-q_1 \qquad (64d)$$

$$p_A + p_D + p_E + 2p_G + p_K + p_M + p_O = 4+q_1 \qquad (64e)$$

$$p_B + p_O + p_E + 2p_I + p_K + p_M + p_O = 4-q_1. \qquad (64f)$$

Equations 64e and 64f are identical to equations 64c and 64b, respectively. There is no simple combination of the equations similar to equations 59 that leads to an elimination of ordered structures in this assignment of cerium atoms. The eight equations 63a-63d and 64a-64d are underdetermined, inasmuch as they contain as unknowns α, q_1, and ten probabilities. However, because of the Diophantine nature of the solutions desired for ordered structures (the probabilities all being either zero or one), it is possible to find a unique

solution for the probabilities.

Some of the probabilities occur in fixed combinations throughout the four equations 63. They can be summed to form new variables. Defining

$$\rho = p_D + 2p_G \tag{65a}$$

$$\sigma = p_E + p_I + p_M \tag{65b}$$

$$\tau = p_C + 2p_O \tag{65c}$$

$$\upsilon = p_B + 2p_K, \tag{65d}$$

equations 63 become

$$2\sigma + 2\tau = 6 - \alpha \tag{66a}$$

$$\rho + 2\sigma = 6 + \alpha - 3p_A \tag{66b}$$

$$2\sigma + 2\upsilon = 6 - \alpha \tag{66c}$$

$$2\rho + \tau + \upsilon = 6 + \alpha. \tag{66d}$$

Equations 66 have the solution

$$\rho = 2 - p_A + \alpha \tag{67a}$$

$$\sigma = 2 - p_A \tag{67b}$$

$$\tau = 1 + p_A - \frac{\alpha}{2} \tag{67c}$$

$$\upsilon = 1 + p_A - \frac{\alpha}{2}. \tag{67d}$$

From equations 67 and definitions 65,

$$p_D + 2p_G = 2 - p_A + \alpha \tag{68a}$$

$$p_E + p_I + p_M = 2 - p_A \tag{68b}$$

$$p_C + 2p_O = 1 + p_A - \frac{\alpha}{2} \tag{68c}$$

$$p_B + 2p_K = 1 + p_A - \frac{\alpha}{2}. \tag{68d}$$

Using equation 64a to solve for q_1 and substituting in equations 64b, 64c, and 64d results in

$$p_A + 2p_B + 2p_C + p_D + p_E + 2p_G + 4p_I + p_K + p_M + p_O = 8 \tag{69a}$$

$$-p_B - p_C + p_E - 2p_I + p_K + p_M + p_O = 0 \tag{69b}$$

$$p_A + p_B + p_C + p_D + 2p_E + 2p_G + 2p_I + 2p_K + 2p_M + 2p_O = 8. \tag{69c}$$

The probabilities appearing in equations 69 may also be grouped. Defining

$$\varphi = p_E + p_K + p_M + p_O \tag{70a}$$

$$\chi = p_A + p_D + 2p_G \tag{70b}$$

$$\psi = p_B + p_C + 2p_I, \tag{70c}$$

equations 69 can be rewritten as

$$\varphi + \chi + 2\psi = 8 \tag{71a}$$

$$\varphi - \psi = 0 \tag{71b}$$

$$2\varphi + \chi + \psi = 8. \tag{71c}$$

According to equation 71b, $\varphi = \psi$. Substituting this in equations 71a and 71c gives rise to the same equation,

$$\chi = 8 - 3\varphi \tag{72}$$

From definitions 70, if the arrangement of cerium atoms is ordered, χ and φ must have integral values ranging between zero and four. Table 12 shows the values of χ corresponding to the possible values of φ .

Table 12. Values of φ and χ.

φ	$\chi = 8 - 3\varphi$
0	8
1	5
2	2
3	-1
4	-4

The only allowable set of values in view of the limits imposed on φ and χ, is

$$\varphi = \psi = 2, \qquad \chi = 2. \tag{73}$$

Equations 70 can therefore be rewritten

$$p_E + p_K + p_M + p_O = 2 \tag{74a}$$

$$p_A + p_D + 2p_G = 2 \tag{74b}$$

$$p_B + p_C + 2p_I = 2. \tag{74c}$$

Comparison of equation 74b with equation 68a shows that $\alpha = 0$.

Because twenty-four of the cerium atoms in the unit cell are at z=0, and twenty-four are at z=1/2, the arrangement formed by replacing zero probabilities with unit probabilities and vice-versa is identical to the original arrangement displaced by $c_0/2$. These complementary assignments of probabilities thus differ from each other only with respect to a choice of the origin. This redundancy can be circumvented by arbitrarily assigning to one of the symmetry-equivalent sets of cerium atoms a z coordinate of zero. Fixing the z coordinate of set A as zero, and substituting $p_A = 1$ and $\alpha = 0$ in equations 68 result in

$$p_D + 2p_G = 1 \tag{75a}$$

$$p_E + p_I + p_M = 1 \tag{75b}$$

$$p_C + 2p_O = 2 \tag{75c}$$

$$p_B + 2p_K = 2. \tag{75d}$$

In an ordered structure, all of the probabilities are either zero or one. The only ordered values of p_D and p_G consistent with equation 75a are

$$p_D = 1 \tag{76a}$$

$$p_G = 0 \tag{76b}$$

Similarly, equation 75c requires that

$$p = 0 \tag{77a}$$

$$p_O = 1 \, , \tag{77b}$$

and equation 75d implies

$$p_B = 0 \tag{78a}$$

$$p_K = 1 \tag{78b}$$

Substitution of the values for p_K and p_O in equation 74a gives

$$p_E + p_M = 0 \, , \tag{79}$$

from which it follows that

$$p_E = 0 \tag{80a}$$

$$p_M = 0 \tag{80b}$$

Because $p_A = 1$, equation 74b is identical with equation 75a. From equations 77a, 78a, and 74c,

$$p_I = 1 \tag{81}$$

All of the probabilities have now been fixed. The only equation in sets 74 and 75 which has not been used is equation 75b. Substitution of the values of p_E, p_I, and p_M in equation 75b shows that it is consistent with the solution for the probabilities. To the symmetry equivalent sets of cerium atoms listed in table 11 z coordinates may be assigned. The positions of the cerium atoms are tabulated below

Table 13. Ordered arrangement of cerium atoms consistent with observed (hhl) and (h0l) absences with l odd.

Set	Number of atoms	z coordinate
A	3	0
D	3	0
I	6	0
K	6	0
O	6	0
B	3	1/2
C	3	1/2
E	6	1/2
G	6	1/2
M	6	1/2

As has been stated previously, fixing the z coordinates of the cerium atoms results in a nearly complete description of the $Mg_{12}Ce$ structure. In the preceding development, the only assumption made was that the configuration of the cerium atoms in the unit cell was ordered. It is interesting that with the theorem on partial Fourier summations and Diophantine analysis of the resulting equations a unique ordered solution could be obtained from a consideration of only the absences in the reciprocal lattice, without regard to the intensities of the reflections with l odd.

With the exception of the atoms in the MgCeMg chains at subcell coordinates x,y = 0, each atom in the unit cell has a chemically equivalent atom displaced from it by a translation which is nearly 1/2 ζ_0 . Therefore the structure factors of reflections (close to the origin in reciprocal space) having the Miller index l odd should involve principally the scattering from the MgCeMg chains. If the coordinates of the cerium atoms listed in table 13 are correct, there should be approximate agreement between calculated and observed intensities. The structure factors of several reflections with l equal to one were computed, taking into account only the contributions from the aforementioned chains of atoms. Because the x and y coordinates of the MgCeMg chains are all rational multiples of the unit cell axes, it suffices to compute the structure factors for only the nine reflections listed in table 14. The intensities of the remaining odd-

layer reflections are related to those in the table by normal decline.

Table 14. Contributions from MgCeMg chains to odd layer structure factors.

Unique ordered configuration - Space group D_{3h}^3

The quantities G below are to be multiplied by $f_{Ce} + 2f_{Mg}\cos 2\pi l z_1$

Indices h,k	G	Observed intensity
0,0	0	absent
1,0	-4	absent
2,0	0	absent
3,0	8	weak
4,0	0	absent
1,1	0	absent
2,1	$-6-6\sqrt{3}i$	absent
3,1	$2+2\sqrt{3}i$	medium
2,2	0	weak

Their agreement with the observed intensities is completely unacceptable. With the exception of the systematic absences explicitly taken into account, the array of calculated structure factors bears little resemblance to the observed reciprocal lattice. It must therefore be concluded that the struc-

ture is disordered insofar as fractional probabilities of translation of the atoms by $\frac{1}{2}\underset{\sim}{c}_o$ are necessary for its description. The methods developed in this section have led expeditiously to an elimination of ordered hexagonal structures. In the study of $TiBe_{12}$, ordered structures were eliminated by computing structure factors for 6,435 ordered assignments of titanium atoms (2). Twice this number of configurations would have had to be considered in the present investigation.

b. The treatment of systematic absences.

By treating only a subset of the absences which occur in the x-ray diffraction patterns of the phase $Mg_{12}Ce$, it has been shown that there are no ordered hexagonal solutions for the structure. In order to cope with the complexities added by the presence of disorder, a method must be devised to interpret the entire pattern of absences. The necessary and sufficient conditions imposed on a crystal structure by the existence of the general case of systematic absences will be derived in this section.

Sets of absences can differ from each other in their dimensionality. Thus, the isolated absence of a single point in reciprocal space is zero-dimensional; the absences caused by a screw axis are one-dimensional; those caused by a glide plane are two-dimensional; and those caused by lattice centerings or by the special relationships between the site-occupancy probabilities encountered in the $Mg_{12}Ce$ structure are three-dimensional.

A set of absences shall be defined as <u>systematic</u> if the indices of the absent reflections form a finite number of one-, two-, or three-dimensional arithmetic progressions. Absences which are caused by an n-dimensional space group symmetry element have the property that the compliment of the n-dimensional arithmetic progressions (i.e., the n-dimensional set of present reflections) is a single n-dimensional arithmetic progression containing a zero term.

In order to clarify the notion of how n-dimensional arithmetic progressions can be used to express sets of reflections which are involved in, or unaffected by absences (this notion being important in the forthcoming treatment) some examples will be given.

A typical one-dimensional set of absences are those caused by a 6_1 screw axis. The absences occurring are among the (00l) reflections. Because these absences are due to a space group symmetry element, the class of present reflections along the (00l) axis is expressible as a one-dimensional arithmetic progression containing zero, namely

$$l = 6n, \tag{82}$$

where n is any integer.

As an example of a two-dimensional set of absences, consider those produced by an n glide plane perpendicular to the b axis. The absences for this symmetry element occur in the (h0l) plane, and only reflections for which h+l is even occur in this plane. The two-dimensional arithmetic progression expressing the set of present reflections is thus

$$\begin{aligned} h &= n_1 \\ l &= -n_1+2n_2 \end{aligned} \tag{83}$$

Here, n_1 and n_2 are integers (positive or negative) which vary independently.

Face centering is a typical symmetry element which produces a three-dimensional set of absences. In this case, the indices of reflections which occur can only be all even or

all odd. This relationship can be expressed algebraically by the condition

$$\begin{aligned} k+l &= 2n_1 \\ h+l &= 2n_2 \\ h+k &= 2n_3 \end{aligned} \tag{84}$$

Equations 84 can be brought into the form of a three-dimensional arithmetic progression by solving for h, k, and l.

$$\begin{aligned} h &= -n_1+n_2+n_3 \\ k &= n_1-n_2+n_3 \\ l &= n_1+n_2-n_3 \end{aligned} \tag{85}$$

The absences occurring in such compounds as $Mg_{12}Ce$, $BaMg_9$, and $TiBe_{12}$ differ from those above in that the sets of absent reflections (or the present reflections) cannot be completely expressed in the form of arithmetic progressions which contain no constant terms, such as those in equations 82, 83, and 85, but must instead by expressed in the general form of a three-dimensional arithmetic progression, which introduces constant terms a_o, b_o, and c_o:

$$\begin{aligned} h &= a_o + a_1 n_1 + a_2 n_2 + a_3 n_3 \\ k &= b_o + b_1 n_1 + b_2 n_2 + b_3 n_3 \\ l &= c_o + c_1 n_1 + c_2 n_2 + c_3 n_3. \end{aligned} \tag{86}$$

The approach to the treatment of a general three-dimensional set of absences will be as follows. The entire array of absences is broken down into one or more sets of absences whose indices form arithmetic progressions of the form of

equations 86. Because the quantities F_{hkl} are all zero (or virtually zero) in the expression

$$\sum_{hkl}{}' F_{hkl} e^{-2\pi i(hx+ky+lz)}, \tag{87}$$

where the primed summation indicates that only those indices which are members of one of the arithmetic progressions describing the absences are included, the sum itself may be equated to zero. It will be shown that this sum is expressible in a closed form as a function ρ' of the electron density $\rho(x,y,z)$ of the crystal. For each arithmetic progression describing a subset of absences, there will be an equation $\rho'=0$. The set of equations corresponding to all of the arithmetic progressions describing the absences will then be equivalent to the conditions imposed on the structure by the absences.

Deriving the result for a one-dimensional set of absences will facilitate the solution of the problem in higher dimensions. Let $f(x)$ be a function with unit periodicity that is expressible in the one-dimensional Fourier series

$$f(x) = \sum_{h=-\infty}^{\infty} F_h e^{-2\pi i h x}. \tag{88}$$

Then

$$F_h = \int_0^1 f(\xi) e^{2\pi i h \xi} d\xi. \tag{89}$$

We wish to evaluate

$$f'(x) = \sum_{h=-\infty}^{\infty}{}' F_h e^{-2\pi i h x}, \tag{90}$$

where the primed summation indicates that only those terms for which

$$h = a_0 + an \tag{91}$$

are included, where n ranges through all integers from $-\infty$ to ∞, and where a_0 and a are integers. From equations 89, 90, and 91,

$$f'(x) = \sum_{n=-\infty}^{\infty} \left[\int_0^1 f(\xi) e^{2\pi i (a_0 + an)\xi} d\xi \right] e^{-2\pi i (a_0 + an) x} \tag{92}$$

Equation 92 may be rewritten

$$f'(x) = \int_0^1 f(\xi) e^{2\pi i a_0 (\xi - x)} \sum_{n=-\infty}^{\infty} e^{2\pi i n [a(\xi - x)]} d\xi. \tag{93}$$

The properties of the sum

$$\sigma(\xi) = \sum_{n=-\infty}^{\infty} e^{2\pi i n[a(\xi-x)]} \tag{94}$$

shall now be investigated. By considering the vector representation of complex numbers, it is apparent that

$$\sigma(\xi) = 0 \text{ when } a(\xi-x) \text{ is not an integer, and}$$
$$\sigma(\xi) = \infty \text{ when } a(\xi-x) \text{ is an integer.} \tag{95}$$

Evidently, $\sigma(\xi)$ will have a infinite peaks per unit interval in ξ . The area under these a peaks is

$$\int_0^1 \sigma(\xi)\, d\xi = \int_0^1 \sum_{n=-\infty}^{\infty} e^{2\pi i n[a(\xi-x)]}\, d\xi$$
$$= \int_0^1 \left\{1 + 2\sum_{n=1}^{\infty} \cos 2\pi n[a(\xi-x)]\right\} d\xi = 1. \tag{96}$$

Therefore the area under each of the peaks in the function $\sigma(\xi)$ is $1/a$.

Because the integrand in equation 93 has unit periodicity, $f'(x)$ can be reexpressed as

$$f'(x) = \int_{x+\delta}^{1+x+\delta} f(\xi)\, e^{2\pi i a_o(\xi-x)} \sum_{n=-\infty}^{\infty} e^{2\pi i n[a(\xi-x)]}\, d\xi. \tag{97}$$

$$(0 < \delta < \tfrac{1}{a})$$

In the range $x+\delta \leq \xi \leq 1+x+\delta$, $a(\xi-x)$ assumes integral values when $\xi = x+\frac{p}{a}$, $p = 1, \ldots, a$. Thus,

$$f'(x) = \frac{1}{a} \sum_{p=1}^{a} f(x+\frac{p}{a}) e^{2\pi i a_o \frac{p}{a}}, \qquad (98)$$

which is the desired result.

If in a one-dimensional crystal the reflections with $h = a_o \pm an$ form a set of absences, it is clear that $f'(x) = 0$ for all values. The nature of the systematic absences in the reciprocal lattice is connected intimately with the notion of a subcell in the real crystal lattice. Corresponding to the absences in the one-dimensional reciprocal lattice described above, which repeat after a intervals, there is a subcell in real space whose length is 1/a of that of the true unit cell. Any of these subcell translations $t = p/a$ satisfies the requirement that $a.t$ is an integer.

The interpretation of a general three-dimensional set of absences, such as those occurring in the $Mg_{12}Ce$ reciprocal lattice, will now be discussed. Corresponding to the general three-dimensional arithmetic progression of reciprocal lattice indices given in equations 86, there is a three-dimensional subcell in real space with the property that x_α, y_α, and z_α, the components of any subcell translation $\underset{\sim}{t}_\alpha$ satisfy the equations

$$a_1 x_\alpha + b_1 y_\alpha + c_1 z_\alpha = j_1$$
$$a_2 x_\alpha + b_2 y_\alpha + c_2 z_\alpha = j_2 \qquad j_1, j_2, j_3 \text{ integers.} \quad (99)$$
$$a_3 x_\alpha + b_3 y_\alpha + c_3 z_\alpha = j_3.$$

Let $\rho(x,y,z)$ be a function with unit periodicity in each of the three variables and expressible in the three-dimensional Fourier series

$$\rho(x,y,z) = \sum_{h=-\infty}^{\infty} \sum_{k=-\infty}^{\infty} \sum_{l=-\infty}^{\infty} F_{hkl}\, e^{-2\pi i(hx+ky+lz)} \quad (100)$$

Then

$$F_{hkl} = \int_0^1 \int_0^1 \int_0^1 \rho(\xi,\eta,\zeta)\, e^{2\pi i(h\xi+k\eta+l\zeta)} \quad (101)$$

We wish to evaluate

$$\rho'(x,y,z) = \sum_{h=-\infty}^{\infty}{}' \sum_{k=-\infty}^{\infty}{}' \sum_{l=-\infty}^{\infty}{}' F_{hkl}\, e^{-2\pi i(hx+ky+lz)}, \quad (102)$$

where the primed summations indicate that only those values of (hkl) which satisfy equations 86 are to be included.

From equations 86, 101, and 102,

$$\rho'(x,y,z) = \sum_{n_1=-\infty}^{\infty} \sum_{n_2=-\infty}^{\infty} \sum_{n_3=-\infty}^{\infty} \left\{ \int_0^1 \int_0^1 \int_0^1 \rho(\xi,\eta,\zeta)\, e^{2\pi i (a_0 + a_1 n_1 + a_2 n_2 + a_3 n_3)\xi} \right.$$

$$\times e^{2\pi i (b_0 + b_1 n_1 + b_2 n_2 + b_3 n_3)\eta} e^{2\pi i (c_0 + c_1 n_1 + c_2 n_2 + c_3 n_3)\zeta} d\xi\, d\eta\, d\zeta \Big\}$$

$$\times e^{-2\pi i (a_0 + a_1 n_1 + a_2 n_2 + a_3 n_3) x} e^{-2\pi i (b_0 + b_1 n_1 + b_2 n_2 + b_3 n_3) y}$$

$$\times e^{-2\pi i (c_0 + c_1 n_1 + c_2 n_2 + c_3 n_3) z}. \qquad (103)$$

Because the functions, as before, are well-behaved, equation 103 may be rewritten

$$\rho'(x,y,z) = \int_0^1 \int_0^1 \int_0^1 e^{2\pi i [a_0(\xi - x) + b_0(\eta - y) + c_0(\zeta - z)]}$$

$$\times \sum_{n_1=-\infty}^{\infty} e^{2\pi i n_1 [a_1(\xi - x) + b_1(\eta - y) + c_1(\zeta - z)]} \sum_{n_2=-\infty}^{\infty} e^{2\pi i n_2 [a_2(\xi - x) + b_2(\eta - y) + c_2(\zeta - z)]} \qquad (104)$$

$$\times \sum_{n_3=-\infty}^{\infty} e^{2\pi i n_3 [a_3(\xi - x) + b_3(\eta - y) + c_3(\zeta - z)]}\, d\xi\, d\eta\, d\zeta.$$

Each of the summations in equation 104 is a Dirac δ-function which is non-zero when the term in the square bracket is equal to an integer. There can be a contribution to the overall expression only when all three sums are simultaneously non-zero, i.e., when the terms in each square bracket are simultaneously integers. Comparison of the contents of

the square brackets with equations 99 reveals that this occurs when and only when $(\xi - x)$, $(\eta - y)$, and $(\zeta - z)$ are the components x_α, y_α, and z_α of a subcell translation $\underset{\sim}{t}_\alpha$. Because

$$\int_0^1\int_0^1\int_0^1 \sum_{n_1=-\infty}^{\infty} e^{2\pi i n_1[a_1(\xi-x)+b_1(\eta-y)+c_1(\zeta-z)]} \sum_{n_2=-\infty}^{\infty} e^{2\pi i n_2[a_2(\xi-x)+b_2(\eta-y)+c_2(\zeta-z)]}$$

$$\times \sum_{n_3=-\infty}^{\infty} e^{2\pi i n_3[a_3(\xi-x)+b_3(\eta-y)+c_3(\zeta-z)]} d\xi\, d\eta\, d\zeta = 1, \qquad (105)$$

the weighting factor of each peak in the compound δ-function is $1/N$, where N is the number of subcells (and hence the number of δ-function peaks) in the true unit cell.* Thus, from equation 104,

$$\rho'(x,y,z) = \frac{1}{N} \sum_{\alpha=1}^{N} \rho(x+x_\alpha, y+y_\alpha, z+z_\alpha)\, e^{2\pi i(a_0 x_\alpha + b_0 y_\alpha + c_0 z_\alpha)}, \qquad (106)$$

where the summation is carried out over all subcell sites in the true unit cell. If vector notation is used, equation 106 can be made formally identical to equation 98. Thus

$$\rho'(\underset{\sim}{r}) = \frac{1}{N} \sum_{\alpha} \rho(\underset{\sim}{r} + \underset{\sim}{t}_\alpha)\, e^{2\pi i\, \underset{\sim}{h}_0 \cdot \underset{\sim}{t}_\alpha}, \qquad (107)$$

---

*N is the absolute value of the determinant $\begin{vmatrix} a_1 & a_2 & a_3 \\ b_1 & b_2 & b_3 \\ c_1 & c_2 & c_3 \end{vmatrix}$.

where $\underset{\sim}{h}_o$ is the constant reciprocal lattice vector in the arithmetic progression 86 whose components are a_o, b_o, and c_o. In this form the equation is valid regardless of dimensionality, if suitable projections are substituted for when the dimensionality of the absences is less than that of the crystal.

Equation 107 can be applied to a set of reciprocal lattice absences resulting in a set of simultaneous equations each having the form

$$\sum_{\alpha} \rho(\underset{\sim}{r} + \underset{\sim}{t}_{\alpha}) e^{2\pi i \underset{\sim}{h}_o \cdot \underset{\sim}{t}_{\alpha}} = 0, \qquad (108)$$

where $\underset{\sim}{h}_o$ in each equation is the reciprocal lattice vector of an absent reflection in the "asymmetric unit" in reciprocal space enclosed by the primitive reciprocal lattice vectors corresponding to the subcell. This finite set of equations involving the electron density ρ then contains all the conditions imposed by the absences upon the structure.

Equations of this type were applied to the $Mg_{12}Ce$ structure by setting $\underset{\sim}{r}$ equal to zero and successively substituting for $\underset{\sim}{h}_o$ the indices of absent reflections in the "asymmetric unit" in reciprocal space. This led to a set of simultaneous equations involving the quantities $(2p_\alpha - 1) = r_\alpha$, where p_α is the probability that the cerium atom at x,y site α is at z = 0. It was convenient to develop a set of equations for each possible space group, using the equalities among the p_α's imposed

by the symmetry relationships to reduce the number of unknowns. In no case could the set of unknowns be completely eliminated. It was possible, however, to relate the remaining unknowns to the amplitudes and phases of the contributions of the cerium atoms to the structure factors of those odd layer reflections which were not absent.

c. The structure factor for the odd layer reflections.

1. Separation of atoms into groups.

Owing to the fact that the x and y coordinates of the atoms in the $Mg_{12}Ce$ structure are at, or nearly at, special subcell positions, it is possible to treat the absences in its diffraction patterns in an alternate way which shows how absences in the contribution to the structure factor from one set of atoms leads to absences in the contributions from the other sets of atoms. The method which will be developed is less cumbersome to apply than the general theory of absences described above. Furthermore, since no assumptions are made involving the symmetry of the crystal, the results are applicable to all of the possible space groups.

The total structure factor for each odd layer reflection can be separated into the sum of the contributions from (1) the cerium atoms, (2) the magnesium atoms with subcell coordinates $0,0,\pm z_1$, (3) the magnesium atoms with subcell coordinates near $1/3,2/3,0$, etc., and (4) the magnesium atoms with subcell coordinates near $1/2,0,1/4$, etc. Expressions

will be derived for the contributions to the odd layer structure factors for each group of atoms, and it will be shown that if certain reasonable assumptions are made, the expression for the total structure factor can be simplified enormously.

ii. Contributions from the cerium atoms.

For the cerium site α in the x,y projection of the true unit cell, with coordinates x_α, y_α, let the probability that the cerium atom is located at z=0 be p_α. The probability that there is a cerium atom at z=1/2 is then $1-p_\alpha$. These probabilities can be equated to the average number of cerium atoms at each position. The contribution of the cerium atoms to the structure factors with odd l must be based on these averages. Since an odd index can be represented as 2n+1, where n is an integer, the contribution of the cerium atoms to the odd layer structure factors, $F_{Ce}(h,k)$, is

$$\sum_\alpha f_{Ce}\left\{p_\alpha e^{2\pi i[hx_\alpha+ky_\alpha+(2n+1)\cdot 0]}+(1-p_\alpha)e^{2\pi i[hx_\alpha+ky_\alpha+(2n+1)\cdot\frac{1}{2}]}\right\}, \qquad (109)$$

or

$$F_{Ce}(h,k) = \sum_\alpha f_{Ce}\,(2p_\alpha-1)\,e^{2\pi i(hx_\alpha+ky_\alpha)}. \qquad (110)$$

making the definitions

$$r_\alpha = 2p_\alpha-1, \qquad (111)$$

and

$$U(h,k) = \sum_{\alpha} r_{\alpha} e^{2\pi i (h x_{\alpha} + k y_{\alpha})}, \tag{112}$$

there results

$$F_{Ce}(h,k) = f_{Ce} U(h,k). \tag{113}$$

It will now be shown that the absolute magnitudes of the quantities U(h,k) may assume only a limited number of values. Let X_{α} and Y_{α} be the components of a subcell translation. Each set of cerium atom coordinates x_{α}, y_{α} can be written

$$x_{\alpha} = x_{o} + X_{\alpha}, \tag{114}$$

$$y_{\alpha} = y_{o} + Y_{\alpha} \quad , \tag{115}$$

where the quantities x_{o} and y_{o} are introduced to account for the possibility that the cerium atoms may not be on the origin of the projection of the true unit cell onto the x,y plane. (If the origin of the x,y projection coincides with a cerium site, then both x_{o} and y_{o} can be made zero, and the U's in each set, as well as their absolute values, can be equated.)

If the indices h_1,k_1 and h_2,k_2 of two odd layer reflections are related so that the vector $(h_2-h_1,\ k_2-k_1)$ is reciprocal to a subcell translation, i.e.,

$$(h_2-h_1)X_\alpha + (k_2-k_1)Y_\alpha = n \tag{116}$$

where n is an integer, then

$$\begin{aligned} U(h_2,k_2) &= \sum_\alpha r_\alpha e^{2\pi i(h_2x_\alpha + k_2y_\alpha)} \\ &= \sum_\alpha r_\alpha e^{2\pi i[(h_2-h_1)X_\alpha + (k_2-k_1)Y_\alpha + (h_2-h_1)x_o + (k_2-k_1)y_o + h_1x_\alpha + k_1y_\alpha]} \\ &= e^{2\pi i[(h_2-h_1)x_o + (k_2-k_1)y_o]} \sum_\alpha r_\alpha e^{2\pi i(h_1x_\alpha + k_1y_\alpha)} \\ &= e^{2\pi i[(h_2-h_1)x_o + (k_2-k_1)y_o]}\ U(h_1,k_1). \end{aligned} \tag{117}$$

Since the exponential of a purely imaginary quantity has an amplitude of unity, the absolute value of $U(h_2,k_2)$ is equal to the absolute value of $U(h_1,k_1)$. (In any case, the quantities x_o and y_o are rational submultiples of the unit cell dimensions, so that there will be periodicity in the actual values of U(h,k) as well.) A two-dimensional map in reciprocal space of the absolute values of the quantities U(h,k) thus has translational symmetry of precisely the same sort possessed by an electron density map of a crystal in real space, and it becomes possible to introduce the notion of a "unit cell" in reciprocal space. Referring to the reciprocal space plot of figure 1,

the unit cell origins are at the centers of the polygons about which the odd layer reciprocal points are arrayed. Furthermore Friedel's law dictates that the point symmetry of the absolute magnitude of any component of the structure factor must be the Laue symmetry of the diffraction pattern, which is p6m in the projection plane. The translation group and the point symmetry may be combined exactly as in real space to produce a space group in reciprocal space, and it is convenient to refer to an asymmetric unit in the reciprocal space map of the absolute values of U(h,k). Referring to figure 1, it will be seen that the non-equivalent reciprocal points with h,k indices 31, 30, and 22 are the only non-absent reflections occurring in one such asymmetric unit. The entire map of the magnitudes of U(h,k) can be described by specifying the quantities $|U(3,1)|$, $|U(3,0)|$, and $|U(2,2)|$. These quantities can be determined from the observed odd layer intensities after their relationship to the total structure factors has been developed. Table 15 shows the criteria for the three groups of reflections having the same values of $|\sum_{\alpha} h_{\alpha} e^{2\pi i(hx_{\alpha}+ky_{\alpha})}|$.

Table 15. Groups of odd layer reflections equivalent with respect to $|U(h,k)|$.

Prototype indices	Criterion: $(h-k)^2 \bmod 3 + (h^2+hk+k^2) \bmod 2$	Value of $\lvert\sum_{\alpha} h_{\alpha} e^{2\pi i(hx_{\alpha}+ky_{\alpha})}\rvert$
31	2	$\lvert U(3,1)\rvert$
30	1	$\lvert U(3,0)\rvert$
22	0	$\lvert U(2,0)\rvert$

iii. Contributions from the magnesium atoms of type I.

Evaluation of the contribution to the odd layer structure factors of the magnesium atoms at subcell coordinates $0,0,\pm z_1$ which shall henceforth be called the atoms of type I, is a simple matter. Each cerium atom has a pair of magnesium atoms in contact above and below, with the centers of the three atoms on a line parallel to the c axis of the crystal. Therefore, if p_α is the probability that a cerium atom is at $x_\alpha, y_\alpha, 0$, and $1-p_\alpha$ is the probability that a cerium atom is at $x_\alpha, y_\alpha, 1/2$, then the probability of finding a pair of magnesium atoms at $x, y, \pm z_1$ is p_α, and the probability of finding the pair at $x_\alpha, y_\alpha, 1/2 \pm z_1$ is $1-p_\alpha$. The contribution to the structure factor from the set of atoms, $F_{MgI}(h,k,l)$ can therefore be written as

$$\sum_\alpha f_{Mg}\left\{p_\alpha\left[e^{2\pi i(hx_\alpha+ky_\alpha+lz_1)}+e^{2\pi i(hx_\alpha+ky_\alpha-lz_1)}\right]\right.$$

$$\left.+[1-p_\alpha]\left[e^{2\pi i[hx_\alpha+ky_\alpha+l(\frac{1}{2}+z_1)]}+e^{2\pi i[hx_\alpha+ky_\alpha+l(\frac{1}{2}-z_1)]}\right]\right\}. \qquad (118)$$

Since l is odd,

$$e^{2\pi i l\cdot\frac{1}{2}} = -1, \qquad (119)$$

and 118 may be rewritten as

$$F_{MgI}(h,k,l) = \sum_{\alpha} f_{Mg}[p_\alpha - (1-p_\alpha)][e^{2\pi i(hx_\alpha + ky_\alpha + lz_1)} + e^{2\pi i(hx_\alpha + ky_\alpha - lz_1)}]$$

$$= 2f_{Mg}\cos 2\pi l z_1 \sum_{\alpha} (2p_\alpha - 1)\, e^{2\pi i(hx_\alpha + ky_\alpha)} \qquad (120)$$

Making use of definitions 111 and 112, it is found that

$$F_{MgI}(h,k,1) = 2f_{Mg}\cos 2\pi l z_1 U(h,k). \qquad (121)$$

It was mentioned in the description of the subcell structure that the configuration of the MgCeMg chains is the only feature which is affected grossly by the ambiguity of translation by $1/2\zeta_o$. The remaining ten atoms are shifted only slightly from their "ideal" positions at 1/3,2/3,0, and 1/2,0,1/4, etc. It is convenient to regard the structure as being largely described by the configuration of the MgCeMg chains, and to treat the shifts of the other atoms from their ideal positions as small perturbations needed to fit them into the framework of MgCeMg chains.

iv. Contributions from the magnesium atoms of type II.

The contributions to the odd layer structure factors from the magnesium atoms of type II, near the subcell positions 2(c) and 2(d) (1/3,2/3,0; 2/3,1/3,0; 1/3,2/3,1/2, and 2/3,1/3,1/2) will now be discussed. There are mirror planes

at z=0 and z=1/2 regardless of the ambiguities introduced by the possibility of translation by 1/2 $\underset{\sim}{c}_o$. The atoms under consideration must therefore have z coordinates of exactly zero or one-half, so that any displacements from the ideal positions must be in the x,y plane. These atoms are in the centers of equilateral triangles in a plane perpendicular to the c axis whose corners are occupied either by cerium atoms in the plane of the central atom, or by pairs of magnesium atoms, which belong to the ordered MgCeMg chains, above and below the plane of the central atom.

The displacement of these atoms from their "ideal" positions at the centers of the equilateral triangles depend principally only on whether cerium atoms or magnesium atom pairs occupy the corners. In calculating $F_{MgII}(h,k)$, the contribution of this group of atoms to the odd layer structure factors, the following assumptions will be made regarding their displacements from the centers of the triangles. If a central magnesium atom is surrounded symmetrically by three cerium atoms, or by three magnesium pairs, it will not be shifted. If the atom is surrounded by two cerium atoms and one magnesium pair, it will be displaced from the center of the triangle by a distance δ_1 toward the magnesium pair. If it is surrounded by one cerium atom and two magnesium pairs, it will be displaced away from the cerium atom by a distance δ_2. (The values of δ_1 and δ_2 have been established in the discussion of the subcell.)

Figure 6 shows that the triangles of atomic sites surrounding the magnesium atoms of type II can have either of two orientations. The corners of the triangles can have x,y coordinates of either x_α, y_α; $x_\alpha+1/12$, $y_\alpha+1/6$; and $x_\alpha-1/12$, $y_\alpha+1/12$, with the center of the triangle at $x_\alpha, y_\alpha+1/12$, or x_α, y_α; $x_\alpha+1/12$, $y_\alpha+1/6$, and $x_\alpha+1/6$, $y_\alpha+1/12$, with the center of the triangle at $x_\alpha+1/12$, $y_\alpha+1/12$. Using the assumptions made above, table 16 lists for both orientations the positions of the central atom for each possible arrangement of the cerium atoms and magnesium atom pairs at the corners of the triangles. (For each configuration denoted by capital letters in table 16, the assignment of cerium atoms or magnesium pairs to the corner sites a,b,c is the same for both orientations.) It should be noticed that configurations A and B, C and D, E and F, and G and H are complementary pairs with respect to interchange of cerium atoms and magnesium pairs. Since the MgCeMg chains are ordered along their length, if the configurations of a triangular site at z=0 is one member of such a pair, then the configuration of the triangular site immediately above the first at z=1/2 is the other member of the pair.

This complementarity makes it possible to deduce certain relationships concerning the contribution of the central magnesium atoms to the odd layer structure factors. For instance, if the configuration at a particular site at z=0 is of type A (and of type B at z=1/2) then neither the magnesium atom of

Table 16. Coordinates of the magnesium atoms of type I (central magnesium atoms) for different configurations of their ligands.

Designation of corner site	a	b	c		
Coordinates of corner site: Orientation 1	x_α, y_α	$x_\alpha+1/12$, $y_\alpha+1/6$	$x_\alpha-1/12$, $y_\alpha+1/12$		
Orientation 2	x_α, y_α	$x_\alpha+1/12$, $y_\alpha+1/6$	$x_\alpha+1/6$, $y_\alpha+1/12$		
Configuration				Orientation 1	Orientation 2
A	Ce	Ce	Ce	x_α, $y_\alpha+1/12$	$x_\alpha+1/12$, $y_\alpha+1/12$
B	Mg-Mg	Mg-Mg	Mg-Mg	x_α, $y_\alpha+1/12$	$x_\alpha+1/12$, $y_\alpha+1/12$
C	Ce	Mg-Mg	Mg-Mg	x_α, $y_\alpha+1/12+\delta_2$	$x_\alpha+1/12+\delta_2$, $y_\alpha+1/12+\delta_2$
D	Mg-Mg	Ce	Ce	x_α, $y_\alpha+1/12-\delta_1$	$x+1/12-\delta_1$, $y+1/12-\delta_1$
E	Mg-Mg	Ce	Mg-Mg	$x_\alpha-\delta_2$, $y_\alpha+1/12-\delta_2$	$x+1/12$, $y+1/12-\delta_2$
F	Ce	Mg-Mg	Ce	$x_\alpha+\delta_1$, $y_\alpha+1/12+\delta_1$	$x+1/12$, $y+1/12+\delta_1$
G	Mg-Mg	Mg-Mg	Ce	$x_\alpha+\delta_2$, $y_\alpha+1/12$	$x+1/12-\delta_2$, $y+1/12$
H	Ce	Ce	Mg-Mg	$x_\alpha-\delta_1$, $y+1/12$	$x+1/12+\delta_1$, $y+1/12$

type I ~~atom~~ at z=0 nor the atom at z=1/2 will be perturbed from its ideal position. Since the two atoms have the same x and y coordinates, and z coordinates differing by 1/2, their combined contribution to any odd layer structure factor will be zero. Furthermore, defining

$$
\begin{aligned}
S_{C_1\alpha} &= f_{Mg}\{e^{2\pi i[hx_\alpha + k(y_\alpha + \frac{1}{12} + \delta_2)]} - e^{2\pi i[hx_\alpha + k(y_\alpha + \frac{1}{12} - \delta_1)]}\} \\
S_{E_1\alpha} &= f_{Mg}\{e^{2\pi i[h(x_\alpha - \delta_2) + k(y_\alpha + \frac{1}{12} - \delta_2)]} - e^{2\pi i[h(x_\alpha + \delta_1) + k(y_\alpha + \frac{1}{12} + \delta_1)]}\} \\
S_{G_1\alpha} &= f_{Mg}\{e^{2\pi i[h(x_\alpha + \delta_2) + k(y_\alpha + \frac{1}{12})]} - e^{2\pi i[h(x_\alpha - \delta_1) + k(y_\alpha + \frac{1}{12})]}\} \\
S_{C_2\alpha} &= f_{Mg}\{e^{2\pi i[h(x_\alpha + \frac{1}{12} + \delta_2) + k(y_\alpha + \frac{1}{12} + \delta_2)]} - e^{2\pi i[h(x_\alpha + \frac{1}{12} - \delta_1) + k(y_\alpha + \frac{1}{12} - \delta_1)]}\} \\
S_{E_2\alpha} &= f_{Mg}\{e^{2\pi i[h(x_\alpha + \frac{1}{12}) + k(y_\alpha + \frac{1}{12} - \delta_2)]} - e^{2\pi i[h(x_\alpha + \frac{1}{12}) + k(y_\alpha + \frac{1}{12} + \delta_1)]}\} \\
S_{G_2\alpha} &= f_{Mg}\{e^{2\pi i[h(x_\alpha + \frac{1}{12} - \delta_2) + k(y_\alpha + \frac{1}{12})]} - e^{2\pi i[h(x_\alpha + \frac{1}{12} + \delta_1) + k(y_\alpha + \frac{1}{12})]}\},
\end{aligned}
\tag{122a-f}
$$

the combined contributions to the odd layer structure factors from the atoms at z = 0 and z = 1/2 at the center of the triangle whose corners have the coordinates given in table 16 can be tabulated for each configuration at z = 0 as follows. (Table 17)

The distinction between an ordered and a disordered crystal structure is that in the former, similarly located sites have the same configuration in every unit cell. This is of course not the case when there is disorder. The intensities of the Bragg peaks obtained from a disordered structure are related to the Fourier transform of the structure which is the average over all unit cells of the atomic configuration. This introduces what appears to be a powerful device for the treatment of disordered structures, (or at

Table 17. Contribution from pair of type II magnesium atoms at z=0 and z=½ to the odd layer structure factors.

Configuration* at z=0	Contribution	
	Orientation 1*	Orientation 2*
A	0	0
B	0	0
C	$S_{C_1\alpha}$	$S_{C_2\alpha}$
D	$-S_{C_1\alpha}$	$-S_{C_2\alpha}$
E	$S_{E_1\alpha}$	$S_{E_2\alpha}$
F	$-S_{E_1\alpha}$	$-S_{E_2\alpha}$
G	$S_{G_1\alpha}$	$S_{G_2\alpha}$
H	$-S_{G_1\alpha}$	$-S_{G_2\alpha}$

*See table 16.

least for disordered structures of the type being discussed in this thesis,) which may be called the method of ensemble averages. Consider an ensemble of equivalently located triangular sites, all corresponding to a particular α, in each unit cell of the crystal. Let the fraction of these sites having the configurations A, ...,H be n_A, ...,n_H. (This argument will be valid for both orientations of the triangles, so the numerical subscripts pertaining to the two orientations

will be dropped.) From table 17, the appropriately averaged scattering S_α from the magnesium atoms at the centers of the triangles at z=0 and z=½ is

$$S_\alpha = (n_C - n_D)S_{C\alpha} + (n_E - n_F)S_{E\alpha} + (n_G - n_H)S_{G\alpha} . \qquad (123)$$

The quantity r_α for a cerium site α has been defined as the probability of finding a cerium atom at x_α, y_α,0 minus the probability of finding a cerium atom at $x_\alpha, y_\alpha, 1/2$. An alternate definition, consistent with the notion of averaging the configuration over all unit cells, is that r_α is the fraction of unit cells having a cerium atom at $x_\alpha, y_\alpha, 0$ minus the fraction of unit cells having a pair of magnesium atoms above and below the point $x_\alpha, y_\alpha, 0$. Referring to table 16, there results

$$\begin{aligned} r_a &= n_A + n_C + n_F + n_H - n_B - n_D - n_E - n_F \\ r_b &= n_A + n_D + n_E + n_H - n_B - n_C - n_F - n_G \qquad (124a\text{-}c) \\ r_c &= n_A + n_D + n_F + n_G - n_B - n_C - n_E - n_H . \end{aligned}$$

(The quantities r in equations 124 depend of course on α, although this dependence is not explicitly denoted. A notation with α introduced in the subscript would have been cumbersome, or have produced ambiguities with the quantities r_α.) Defining

$$J_A = n_A - n_B$$
$$J_C = n_C - n_D \qquad (125a\text{-}d)$$
$$J_E = n_E - n_F$$
$$J_G = n_G - n_H ,$$

equations 124 become

$$r_a = J_A + J_C - J_E - J_G$$
$$r_b = J_A - J_C + J_E - J_G \qquad (126a\text{-}c)$$
$$r_c = J_A - J_C - J_E + J_G$$

Equations 126 have the solution

$$J_C = J_A - \tfrac{1}{2}(r_b + r_c)$$
$$J_E = J_A - \tfrac{1}{2}(r_a + r_c) \qquad (127a\text{-}c)$$
$$J_G = J_A - \tfrac{1}{2}(r_a + r_b).$$

Substitution of equations 125 and 127 into equation 123 gives

$$S_\alpha = J_A(S_{C\alpha} + S_{E\alpha} + S_{G\alpha}) - \tfrac{1}{2}[(r_b + r_c) S_{C\alpha} + (r_a + r_c) S_{E\alpha} + (r_a + r_b) S_{G\alpha}]. \qquad (128)$$

The quantity J_A for each triangular site is the difference between the fraction of those sites that have three cerium atoms at z = 0 and the fraction having three magnesium

pairs at z=0 (or three cerium atoms at z=½). Although the equilateral triangle is just large enough to accommodate a central magnesium atom with three cerium atoms at its corners if the sum of the standard magnesium and cerium metallic radii is taken, this configuration must still be regarded as unlikely. Due to the large ligancy of the cerium atoms in the structure, an interatomic distance somewhat larger than the standard radii sum is to be expected, and this is evidenced by the observed displacements of the central atom when it is not symmetrically surrounded. (From the analysis of the subcell data it was found that a likely distance between neighboring cerium and magnesium atoms is approximately 3.70 Å. This is considerably greater than 3.43 Å, the distance between the center and the apex of each triangle.) In the $TiBe_{12}$ structure (2), the atomic radii and the unit cell dimensions are such that configurations with three heavy (titanium) atoms at the corners of a triangle are virtually impossible. If such configurations are regarded as highly improbable, then J_A will be much smaller than the other J's, and as an approximation

$$S_\alpha \simeq -\tfrac{1}{2}[(r_b+r_c)S_{C\alpha}+(r_a+r_c)S_{E\alpha}+(r_a+r_b)S_{G\alpha}] \qquad (129)$$

More about this approximation will be mentioned later.

There are 96 equilateral triangles in the unit cell, each containing two central magnesium atoms (one at z=0 and one at z=½), or a total of 192 atoms contributing to $F_{MgII}(h,k)$.

There is one triangle of orientation 1, and one of orientation 2 in correspondence with each cerium x,y site indexed by α. Accordingly,

$$F_{MgII}(h,k) = \sum_{\alpha} (S_{1\alpha} + S_{2\alpha}), \tag{130}$$

where $S_{1\alpha}$ and $S_{2\alpha}$ are the quantities expressed in equation 129 with the subscripts denoting orientation included, can be written as follows with the use of equations 129 and 124, and the listing of coordinates of corner sites at the top of table 16.

$$\begin{aligned}
F_{MgII}(h,k) = \\
&-\tfrac{1}{2} f_{Mg} \sum_{\alpha} \{ n_{x_\alpha+\frac{1}{12}, y_\alpha+\frac{1}{6}} + n_{x_\alpha-\frac{1}{12}, y_\alpha+\frac{1}{12}} \} \{ e^{2\pi i[hx_\alpha + k(y_\alpha+\frac{1}{12}+\delta_2)]} - e^{2\pi i[hx_\alpha + k(y_\alpha+\frac{1}{12}-\delta_1)]} \} \\
&-\tfrac{1}{2} f_{Mg} \sum_{\alpha} \{ n_{x_\alpha, y_\alpha} + n_{x_\alpha-\frac{1}{12}, y_\alpha+\frac{1}{12}} \} \{ e^{2\pi i[h(x_\alpha-\delta_2) + k(y_\alpha+\frac{1}{12}-\delta_2)]} - e^{2\pi i[h(x_\alpha+\delta_1) + k(y_\alpha+\frac{1}{12}+\delta_1)]} \} \\
&-\tfrac{1}{2} f_{Mg} \sum_{\alpha} \{ n_{x_\alpha, y_\alpha} + n_{x_\alpha+\frac{1}{12}, y_\alpha+\frac{1}{6}} \} \{ e^{2\pi i[h(x_\alpha+\delta_2) + k(y_\alpha+\frac{1}{12})]} - e^{2\pi i[h(x_\alpha-\delta_1) + k(y_\alpha+\frac{1}{12})]} \} \\
&-\tfrac{1}{2} f_{Mg} \sum_{\alpha} \{ n_{x_\alpha+\frac{1}{12}, y_\alpha+\frac{1}{6}} + n_{x_\alpha+\frac{1}{6}, y_\alpha+\frac{1}{12}} \} \{ e^{2\pi i[h(x_\alpha+\frac{1}{12}+\delta_2) + k(y_\alpha+\frac{1}{12}+\delta_2)]} - e^{2\pi i[h(x_\alpha+\frac{1}{12}-\delta_1) + k(y_\alpha+\frac{1}{12}-\delta_1)]} \} \\
&-\tfrac{1}{2} f_{Mg} \sum_{\alpha} \{ n_{x_\alpha, y_\alpha} + n_{x_\alpha+\frac{1}{6}, y_\alpha+\frac{1}{12}} \} \{ e^{2\pi i[h(x_\alpha+\frac{1}{12}) + k(y_\alpha+\frac{1}{12}-\delta_2)]} - e^{2\pi i[h(x_\alpha+\frac{1}{12}) + k(y_\alpha+\frac{1}{12}+\delta_1)]} \} \\
&-\tfrac{1}{2} f_{Mg} \sum_{\alpha} \{ n_{x_\alpha, y_\alpha} + n_{x_\alpha+\frac{1}{12}, y_\alpha+\frac{1}{6}} \} \{ e^{2\pi i[h(x_\alpha+\frac{1}{12}-\delta_2) + k(y_\alpha+\frac{1}{12})]} - e^{2\pi i[h(x_\alpha+\frac{1}{12}+\delta_1) + k(y_\alpha+\frac{1}{12})]} \}.
\end{aligned} \tag{131}$$

The aspect crucial to the following development is that it is possible to express equation 131 in terms of the same quantities which are involved in the contributions from the

other groups of atoms in the structure. As an example, the first term,

$$-\tfrac{1}{2} f_{Mg} \sum_{\alpha} r_{x_\alpha+\frac{1}{12},\, y_\alpha+\frac{1}{6}}\, e^{2\pi i[hx_\alpha + k(y_\alpha+\frac{1}{12}+\delta_2)]},$$

in equation 131 will be re-evaluated this way.

$$-\tfrac{1}{2} f_{Mg} \sum_{\alpha} r_{x_\alpha+\frac{1}{12},\, y_\alpha+\frac{1}{6}}\, e^{2\pi i[hx_\alpha + k(y_\alpha+\frac{1}{12}+\delta_2)]} =$$

$$-\tfrac{1}{2} f_{Mg}\, e^{2\pi i[-\frac{h}{12} - k(\frac{1}{12}-\delta_2)]} \sum_{\alpha} r_{x_\alpha+\frac{1}{12},\, y_\alpha+\frac{1}{6}}\, e^{2\pi i[h(x_\alpha+\frac{1}{12}) + k(y_\alpha+\frac{1}{6})]} \qquad (132)$$

The summation on the right hand side of equation 132 is over the products of the value of r at each site in the x,y plane and the usual phase exponential involving the coordinates of that site. Since the summation is over all of the cerium sites in the plane,

$$\sum_{\alpha} r_{x_\alpha+\frac{1}{12},\, y_\alpha+\frac{1}{6}}\, e^{2\pi i[h(x_\alpha+\frac{1}{12}) + k(y_\alpha+\frac{1}{6})]} = \sum_{\alpha} r_{x_\alpha, y_\alpha}\, e^{2\pi i(hx_\alpha + ky_\alpha)} = U(h,k). \qquad (133)$$

Therefore,

$$-\tfrac{1}{2} f_{Mg} \sum_{\alpha} r_{x_\alpha+\frac{1}{12},\, y_\alpha+\frac{1}{6}}\, e^{2\pi i[hx_\alpha + k(y_\alpha+\frac{1}{12}+\delta_2)]}$$

$$= -\tfrac{1}{2} f_{Mg}\, e^{2\pi i[-\frac{h}{12} - k(\frac{1}{12}-\delta_2)]}\, U(h,k). \qquad (134)$$

In a similar fashion, U(h,k) can be factored out of each term in equation 131, resulting in

$$
\begin{aligned}
F_{Mg\,II}(h,k) = -\tfrac{1}{2} f_{Mg}\, U(h,k)\{ & e^{2\pi i[-\frac{h}{12}-k(\frac{1}{12}-\delta_2)]} - e^{2\pi i[-\frac{h}{12}-k(\frac{1}{12}+\delta_1)]} + e^{2\pi i[\frac{h}{12}+k\delta_2]} \\
& - e^{2\pi i[\frac{h}{12}-k\delta_1]} + e^{2\pi i[-h\delta_2+k(\frac{1}{12}-\delta_2)]} - e^{2\pi i[h\delta_1-k(\frac{1}{12}+\delta_1)]} \\
& + e^{2\pi i[h(\frac{1}{12}-\delta_2)-k\delta_2]} - e^{2\pi i[h(\frac{1}{12}+\delta_1)+k\delta_1]} + e^{2\pi i[h\delta_2+\frac{k}{12}]} \\
& - e^{2\pi i[-h\delta_1+\frac{k}{12}]} + e^{2\pi i[-h(\frac{1}{12}-\delta_2)-\frac{k}{12}]} - e^{2\pi i[-h(\frac{1}{12}+\delta_1)-\frac{k}{12}]} \\
& + e^{2\pi i[h\delta_2-k(\frac{1}{12}-\delta_2)]} - e^{2\pi i[-h\delta_1-k(\frac{1}{12}+\delta_1)]} + e^{2\pi i[-h(\frac{1}{12}-\delta_2)+k\delta_2]} \\
& - e^{2\pi i[-h(\frac{1}{12}+\delta_1)-k\delta_1]} + e^{2\pi i[\frac{h}{12}+k(\frac{1}{12}-\delta_2)]} - e^{2\pi i[\frac{h}{12}+k(\frac{1}{12}+\delta_1)]} \\
& + e^{2\pi i[-\frac{h}{12}-k\delta_2]} - e^{2\pi i[-\frac{h}{12}+k\delta_1]} + e^{2\pi i[h(\frac{1}{12}-\delta_2)+\frac{k}{12}]} \\
& - e^{2\pi i[h(\frac{1}{12}+\delta_1)+\frac{k}{12}]} + e^{2\pi i[-h\delta_2-\frac{k}{12}]} - e^{2\pi i[h\delta_1-\frac{k}{12}]}\}.
\end{aligned}
\tag{135}
$$

The expression for $F_{MgII}(h,k)$ can be reduced to a much less cumbersome form if the substitution

$$
g(n) = \cos 2\pi n(\tfrac{1}{24}+\delta_1) - \cos 2\pi n(\tfrac{1}{24}-\delta_2) \tag{136}
$$

is made. The application of equation 136 and trigonometric manipulation to equation 135 results in

$$
\begin{aligned}
& F_{Mg\,II}(h,k) = \\
& 2 f_{Mg}\left[\cos 2\pi \frac{h+2k}{24}\, g(k) + \cos 2\pi \frac{h-k}{24}\, g(h+k) + \cos 2\pi \frac{2h+k}{24}\, g(k)\right] U(h,k),
\end{aligned}
\tag{137}
$$

which is the final, and easily calculated expression to be derived in this section.

v. Contributions from the magnesium atoms of type III.

Thus far, it has been possible to express the contributions to the odd layer structure factors in terms of previously determined positional parameters and the quantities U(h,k) for every group of atoms except those forming the graphite type layers near the planes z=1/4 and z=3/4. The contributions for this last group, III, of atoms will now be discussed. It is again possible to relate the probabilities and magnitudes of the displacements of each of these atoms from their ideal positions to the quantities r for the neighboring cerium sites.

The presence of mirror planes in the structure at z = 0 and z = $\frac{1}{2}$ requires that each pair of atoms of type III near z = 1/4 and z = 3/4 have the same x and y coordinates. The displacement of these atoms is determined principally by the configurations of the two MgCeMg chains nearest to the pair of atoms. In figure 8 cross-sections through the plane x=y in the subcell show the four possible configurations of the MgCeMg chains and the displacements of the type III atoms which would be expected if only the MgCeMg chains shown influenced their positions. A more complete analysis of the effect on the displacements of the group III atoms by all of their ligands indicates that there are interactions from the

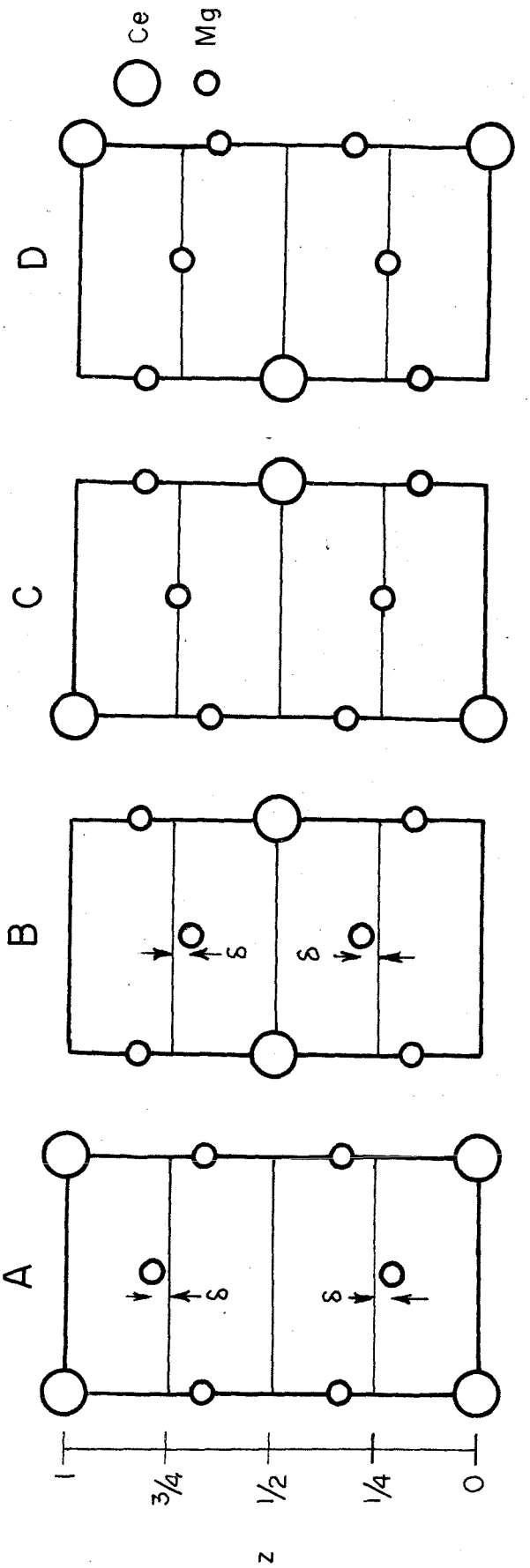

FIGURE 8. CONFIGURATIONS SHOWING DISPOSITION OF MAGNESIUM ATOMS OF TYPE III.

second nearest pair of MgCeMg chains due to their effect on the configuration of the magnesium atoms of type II. The second order interactions in some configurations can produce small horizontal displacements of the type II atoms. (These displacements could account for the shape of the peak on the (hk0) Fourier projection at 1/2,0, and yet produce no contributions to the odd layer structure factors with small l, as such pairs of atoms are separated by very nearly $1/2\underset{\sim}{c}_o$.) The complete expressions produced by the more rigorous treatment cannot be simplified by methods similar to those used in the discussion of the other groups of atoms. However, unless l is large, the simple treatment pictorialized by figure 8 results in a good approximation to the contribution to the odd layer structure factors given by the complete analysis.

Figure 8 indicates that if x_1,y_1 and x_2,z_2 are the x,y coordinates of the left hand and right hand MgCeMg chains, respectively, then $\frac{1}{2}(x_1+x_2)$, $\frac{1}{2}(y_1+y_2)$ are the x,y coordinates of the pair of magnesium atoms of type III. The z coordinates of these atoms are $1/4-\delta$ and $3/4+\delta$ in configuration A, $1/4+\delta$ and $3/4-\delta$ in B, and 1/4 and 3/4 in both C and D. The contributions from the type III atoms to the odd layer structure factors $F_{MgIII}(h,k,l)$ can therefore be tabulated as follows. If $n_A,..,n_D$ now represent the fraction of equivalent sites in an ensemble of unit cells that have configurations A,..,D respectively, then the effective scattering S from the type III atoms in the site under consideration is

Table 18. Contributions to $F_{MgIII}(h,k,l)$.

Configuration	Contribution
A	$2 f_{Mg} (-1)^{\frac{l-1}{2}} (\sin 2\pi l\delta) e^{\pi i [h(x_1+x_2) + k(y_1+y_2)]}$
B	$-2 f_{Mg} (-1)^{\frac{l-1}{2}} (\sin 2\pi l\delta) e^{\pi i [h(x_1+x_2) + k(y_1+y_2)]}$
C	0
D	0

$$S = (n_A - n_B) \cdot 2 f_{Mg} (-1)^{\frac{l-1}{2}} (\sin 2\pi l\delta) e^{\pi i [h(x_1+x_2) + k(y_1+y_2)]} . \qquad (138)$$

But from figure 8,

$$r_{x_1,y_1} = n_A + n_C - n_B - n_D$$
$$r_{x_2,y_2} = n_A + n_D - n_B - n_C , \qquad (139a,b)$$

so that

$$\tfrac{1}{2}(r_{x_1,y_1} + r_{x_2,y_2}) = n_A - n_B , \qquad (140)$$

and

$$S = (f_{x_1,y_1} + f_{x_2,y_2}) f_{Mg} (-1)^{\frac{l-1}{2}} (\sin 2\pi l\delta)\, e^{\pi i[h(x_1+x_2)+k(y_1+y_2)]} \qquad (141)$$

Figure 9 illustrates the relationship between the scattering from a single pair of type III atoms and the scattering from the entire group. Corresponding to each MgCeMg site at x_α, y_α there are three sites in the x,y plane for atoms of type III. The first of these, denoted in figure 9 by split circles, is situated between the MgCeMg chains at x_α, y_α and $x_\alpha + 1/12, y_\alpha + 1/6$; the second, denoted by open circles, between chains at x_α, y_α and $x_\alpha - 1/12$, $y_\alpha + 1/12$, and the third, denoted by closed circles, between chains at x_α, y_α and $x_\alpha + 1/6$, $y_\alpha + 1/12$. The total contribution of the type III atoms is the sum over α of the quantities S given in equation 141 for each of the three sets of sites, or

$$F_{Mg\,III}(h,k,l) =$$
$$(-1)^{\frac{l-1}{2}} f_{Mg} \sin 2\pi l\delta \Big\{ \sum_\alpha (f_{x_\alpha, y_\alpha} + f_{x_\alpha+\frac{1}{12}, y_\alpha+\frac{1}{6}})\, e^{\pi i[h(2x_\alpha+\frac{1}{12})+k(2y_\alpha+\frac{1}{6})]}$$
$$+ \sum_\alpha (f_{x_\alpha, y_\alpha} + f_{x_\alpha-\frac{1}{12}, y_\alpha+\frac{1}{12}})\, e^{\pi i[h(2x_\alpha-\frac{1}{12})+k(2y_\alpha+\frac{1}{12})]}$$
$$+ \sum_\alpha (f_{x_\alpha, y_\alpha} + f_{x_\alpha+\frac{1}{6}, y_\alpha+\frac{1}{12}})\, e^{\pi i[h(2x_\alpha+\frac{1}{6})+k(2y_\alpha+\frac{1}{12})]} \Big\}. \qquad (142)$$

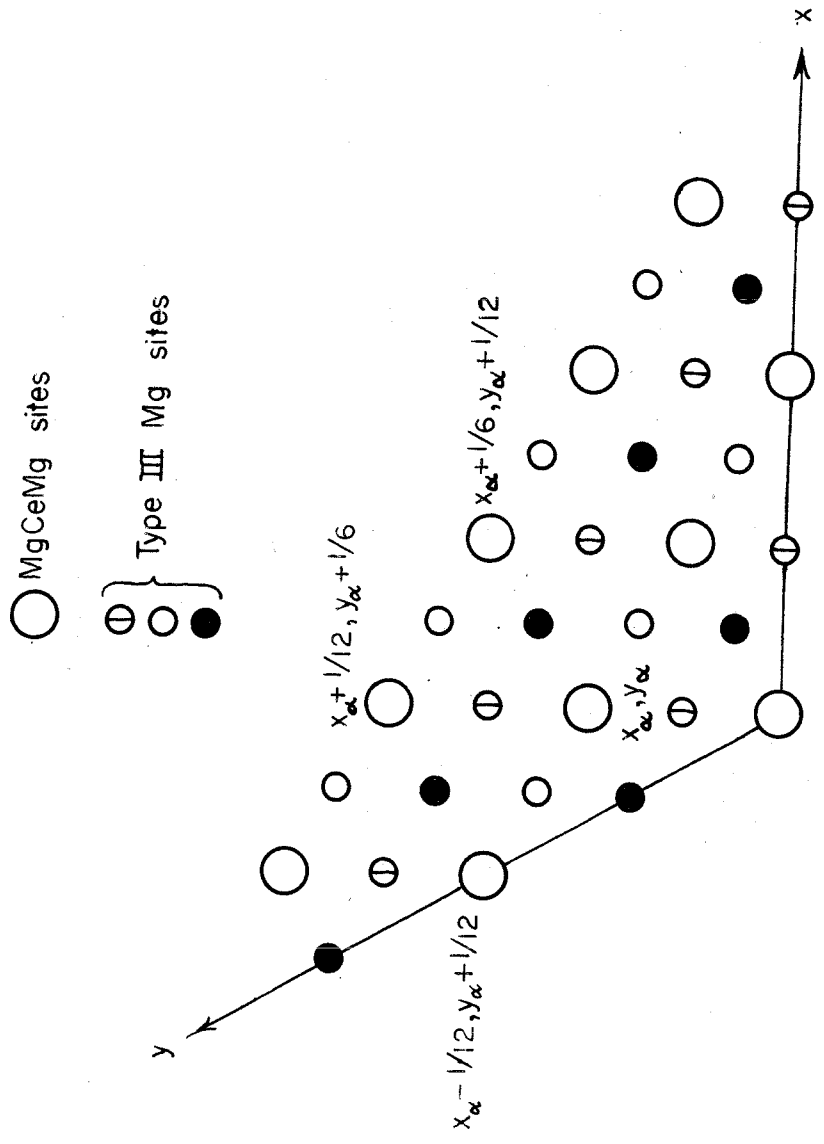

FIGURE 9. PROJECTION ONTO THE (x,y) PLANE SHOWING SOME SITES OF MgCeMg CHAINS AND ATOMS OF TYPE III.

By appropriately factoring the exponentials out of the summation, equation 142 may be rewritten

$$F_{Mg\,III}(h,k,\ell) = (-1)^{\frac{\ell-1}{2}} \sin 2\pi\ell\delta \Big\{ e^{2\pi i\left(\frac{h}{24}+\frac{k}{12}\right)} \sum_{\alpha} h_{x_\alpha, y_\alpha}\, e^{2\pi i[hx_\alpha + ky_\alpha]}$$
$$+ e^{-2\pi i\left(\frac{h}{24}+\frac{k}{12}\right)} \sum_{\alpha} h_{x_\alpha+\frac{1}{12}, y_\alpha+\frac{1}{6}}\, e^{2\pi i[h(x_\alpha+\frac{1}{12})+k(y_\alpha+\frac{1}{6})]}$$
$$+ e^{-2\pi i\left(\frac{h}{24}-\frac{k}{24}\right)} \sum_{\alpha} h_{x_\alpha, y_\alpha}\, e^{2\pi i[hx_\alpha + ky_\alpha]}$$
$$+ e^{2\pi i\left(\frac{h}{24}-\frac{k}{24}\right)} \sum_{\alpha} h_{x_\alpha-\frac{1}{12}, y_\alpha+\frac{1}{12}}\, e^{2\pi i[h(x_\alpha-\frac{1}{12})+k(y_\alpha+\frac{1}{12})]}$$
$$+ e^{2\pi i\left(\frac{h}{12}+\frac{k}{24}\right)} \sum_{\alpha} h_{x_\alpha, y_\alpha}\, e^{2\pi i[hx_\alpha + ky_\alpha]}$$
$$+ e^{-2\pi i\left(\frac{h}{12}+\frac{k}{24}\right)} \sum_{\alpha} h_{x_\alpha+\frac{1}{6}, y_\alpha+\frac{1}{12}}\, e^{2\pi i[h(x_\alpha+\frac{1}{6})+k(y_\alpha+\frac{1}{12})]} \Big\} f_{Mg}. \qquad (143)$$

By the same argument that was used to justify equation 133, every summation over α in equation 143 can be equated to U(h,k). Therefore, the final expression for the contributions of the group III magnesium atoms is simply

$$F_{Mg\,III}(h,k,\ell) =$$
$$2(-1)^{\frac{\ell-1}{2}} f_{Mg} \sin 2\pi\ell\delta \left[\cos 2\pi\left(\frac{h+2k}{24}\right) + \cos 2\pi\left(\frac{h-k}{24}\right) + \cos 2\pi\left(\frac{2h+k}{24}\right)\right] U(h,k). \qquad (144)$$

The expression for the total structure factor for an odd layer reflection is

$$F(h,k,l) = F_{Ce}(h,k) + F_{MgI}(h,k,l) + F_{MgII}(h,k) + F_{MgIII}(h,k,l). \qquad (145)$$

Referring to equations 113, 121, 137, and 144, equation 145 may be written

$$F(h,k,l) = \mathrm{I\!I} f_{Ce} + f_{Mg}\{2\cos 2\pi l z_1 + 2[\cos 2\pi(\tfrac{h+2k}{24})g(h) + \cos 2\pi(\tfrac{h-k}{24})g(h+k) + \cos 2\pi(\tfrac{2h+k}{24})g(k)]$$
$$+ 2(-1)^{\frac{l-1}{2}} \sin 2\pi l\delta[\cos 2\pi(\tfrac{h+2k}{24}) + \cos 2\pi(\tfrac{h-k}{24}) + \cos 2\pi(\tfrac{2h+k}{24})]\} \mathrm{I\!I}\, U(h,k). \qquad (146)$$

The essential feature of equation 146 is that this formulation of F(h,k,l) where l is odd contains U(h,k) as a factor. As is shown by equation 113, U(h,k) is closely related to the contribution to the odd layer structure factors from the cerium atoms. Equation 146 therefore indicates that if the odd layer contribution from the cerium atoms satisfies the observed absences, then the total structure factors must comply with the observed absences also. It should be noted that it is erroneous to attempt to justify the assumptions and approximations made in the development of equations 137 and 144* by arguing that deviations of the actual contributions to the structure factor from those stated in these equations will result in net contributions which violate the observed set of absences. It has already been discussed how small deviations from an ideal structure can alter the intensities of the reflections which are observable in the ideal structure,

---

*Namely, that there are no configurations with three cerium atoms at the corners of an equilateral triangle, and that the disposition of the type III magnesium atoms are determined only by the configuration at the two nearest MgCeMg sites.

and still not cause new reflections to appear.

Another important property of the expression for F(h,k,l) becomes evident when it is written in the form

$$F(h,k,l) = F_{Mg\,II}(h,k) + \{f_{Ce} + f_{Mg}[2\cos 2\pi l z_1 + 2(-1)^{\frac{l-1}{2}} \sin 2\pi l \delta(\cos 2\pi \tfrac{h+2k}{24} + \cos 2\pi \tfrac{h-k}{24} + \cos 2\pi \tfrac{2k+h}{24})]\} U(h,k). \qquad (147)$$

The expression contained between the braces in equation 147 involves the indices h and k only as the trigonometric functions of their rational multiples times 2π . For a given l, there are therefore only a finite number of groups of indices (h,k) such that the quantity between the braces is constant for each group, with the exception of changes in f_{Ce} and f_{Mg} due to normal decline. This conclusion can also be deduced if it is considered that each cerium atom, and each magnesium atom of type I or III which contributes to the odd layer structure factors has subcell x and y coordinates which are integral multiples of 1/2. Thus the combined structure factor contribution from these groups of atoms must show normal decline in the h,k plane along the subcell reciprocal vectors [2,0], etc.

This result has another interesting consequence. Thus far, it has been assumed that since no violations to the system of absences on the odd layers were observed, even at large Bragg angles, these absences had to be rigorous extinctions.

It is now apparent that for the absent reflections, U(h,k) can have a small but finite value without causing any of the reflections to be observable. (It is estimated that any U(h,k) larger in absolute value than four percent of U(3,1) would have caused reflections to appear where none were observable.) In the treatment which follows, the occupancy probabilities for the cerium sites are related in a simple fashion to the quantities U(h,k). Except in the computation of the probable errors, contributions from the absent reflections will be neglected. The resulting structures will be such that the calculated structure factors for the absent reflections are rigorously zero. Merely by including small terms in equation 165 which represent the unobserved reflections, the resulting array of probabilities is modified slightly in such a way that the calculated intensities of the observable reflections remain the same, and the intensities of the other reflections have a finite, but unobservable value. Neglecting the unobserved terms, which is equivalent to assuming that they are truly zero, has no effect on the forthcoming treatment, except making the equations therein somewhat more compact.

There are eight groups of indices (h,k) for which odd layer reflections are observable, each corresponding to a point in the asymmetric unit in reciprocal space. The pertinent information about each of these groups is summarized in table 19 below.

Table 19. Groups of reflections having equal values of

$$2\cos 2\pi l z_1 + 2(-1)^{(l-1)/2}\left(\cos 2\pi\frac{h+2k}{24} + \cos 2\pi\frac{h-k}{24} + \cos 2\pi\frac{2h+k}{24}\right)\sin 2\pi l\delta \equiv G.$$

Group	Prototype indices (h,k)	Values of G	Value of |U(h,k)|
1	31	$2\cos 2\pi l z_1 + 1.7321(-1)^{(l-1)/2}\sin 2\pi l\delta$	|U(3,1)|
2	70	$2\cos 2\pi l z_1 - 2.7673(-1)^{(l-1)/2}\sin 2\pi l\delta$	|U(3,1)|
3	50	$2\cos 2\pi l z_1 - 0.6968(-1)^{(l-1)/2}\sin 2\pi l\delta$	|U(3,1)|
4	30	$2\cos 2\pi l z_1 + 2.8284(-1)^{(l-1)/2}\sin 2\pi l\delta$	|U(3,0)|
5	41	$2\cos 2\pi l z_1$	|U(3,0)|
6	71	$2\cos 2\pi l z_1 - 2.8284(-1)^{(l-1)/2}\sin 2\pi l\delta$	|U(3,0)|
7	60	$2\cos 2\pi l z_1 - 2(-1)^{(l-1)/2}\sin 2\pi l\delta$	|U(2,2)|
8	22	$2\cos 2\pi l z_1 + 2(-1)^{(l-1)/2}\sin 2\pi l\delta$	|U(2,2)|

The fact that large groups of reflections have identical contributions from the cerium atoms and the magnesium atoms of types I and III makes it possible to test the validity of equation 137, which expresses the contribution to the odd layer structure factors from the type II magnesium atoms. The largest set of odd layer reflections as tabulated above which are readily observable is group 1. It is apparent from the odd layer Weissenberg photographs that the intensities of the group 1 reflections deviate from a normal decline. Since the geometrical part of the structure factor contributions from the cerium atoms and the magnesium atoms of types I and III are constant within each reflection group, the deviations from normal decline are due to the contributions from the atoms of type II. Furthermore, if two corresponding groups of reflections having different values of l are compared, it is observed that the intensities of two reflections having the same values of h and k differ from the other members of their respective groups in the same way. This confirms that the deviations within each group from the normal decline are caused by the type II magnesium atoms, inasmuch as these are the only atoms in the structure with the exception of the cerium atoms for which the contributions to the odd layer structure factors are independent of l.

It should now be possible to correlate the deviations from the normal decline with the geometrical structure factor contributions from the type II atoms, using the numerical

values of the positional parameters δ_1 and δ_2 for these atoms determined in the treatment of the subcell structure. Using the values

$$\delta_1 = 0.0121 \qquad (148a,b)$$

$$\delta_2 = 0.0067,$$

equation 136 becomes

$$(n) = \cos 2\pi n(0.0537) - \cos 2\pi n(0.0350). \qquad (149)$$

Tabulated below are qualitative intensities for group 1 reflections which occur at nearly the same Bragg angles, together with computed values for $H = \cos 2\pi \frac{h+2k}{24} g(h) + \cos 2\pi \frac{h-k}{24} \times g(h+k) + \cos 2\pi \frac{2h+k}{24} g(k)$, which is proportional to the geometrical structure factor contributions from the type II atoms. Comparison of the calculated quantities H with the observed values of the intensities reveals that although the formulation for the contribution of the type II atoms is in fair agreement with the observed deviations from normal decline, there are still striking discrepancies, e.g., the reversal of the order of the intensities with the indices 45,4,1 and 41,12,1. It was thought that these discrepancies could be removed by adjusting the positional parameters δ_1 and δ_2, but it was found that no reasonable values of these parameters gave better agreement. Because the dis-

Table 20. Calculated contributions and observed intensities of the type II magnesium atoms for some odd layer reflections.

Indices h,k	Observed intensity	H	Indices h,k	Observed intensity	H
21,4	S	0.168	45,4	M	-0.243
17,12	M	-0.717	41,12	MW	-0.097
13,20	S	1.462	37,20	M	1.395
9,28	MW	-1.244	33,28	VW	-1.382
			29,36	VW	0.551
33,4	MS	0.205			
29,12	M	-0.592	57,4	MW	-0.565
25,20	MS	1.386	53,12	W	0.443
21,28	MW	-1.406	49,20	MW	1.309
17,36	MW	0.382	45,28	W	-2.190

Intensity scale

S - strong.
MS - medium strong
M - medium
MW - medium weak
W - weak
VW - very weak

placements of the type II magnesium atoms from their ideal positions are such a small fraction of the true unit cell dimension, that H is rather insensitive to changes in them, even for large values of the Miller indices. A possible explanation of the discrepancy is that equation 137 is slightly in error because triangular arrays of cerium atoms actually occur to some extent in the structure.

d. Interpretation of the data by differential analysis.

Due to the fact that the contribution of the type II magnesium atoms to the odd layer reflections is independent of l except for the form factors of the atoms, it is possible to bypass the complications introduced by the presence of the triangular arrays. For example, if the geometrical part of F(h,k,l) is subtracted from that of F(h,k,3), there is no contribution from the type II atoms in the difference. Thus, from equation 146,

$$\frac{F(h,k,3)}{f_{Mg}(h,k,3)} - \frac{F(h,k,1)}{f_{Mg}(h,k,1)} =$$

$$\left[\frac{f_{Ce}(h,k,3)}{f_{Mg}(h,k,3)} - \frac{f_{Ce}(h,k,1)}{f_{Mg}(h,k,1)} + 2(\cos 6\pi z_1 - \cos 2\pi z_1) - 2(\sin 6\pi\delta + \sin 2\pi\delta)A(h,k)\right]U(h,k), \quad (150)$$

where

$$A(h,k) = \cos 2\pi\left(\frac{h+2k}{24}\right) + \cos 2\pi\left(\frac{h-k}{24}\right) + \cos 2\pi\left(\frac{2h+k}{24}\right). \quad (151)$$

With the possible exception of the terms $\frac{f_{Ce}(h,k,3)}{f_{Mg}(h,k,3)} - \frac{f_{Ce}(h,k,1)}{f_{Mg}(h,k,1)}$, the expression inside the brackets on the right hand side of equation 150 is a constant for each of the eight groups of reflections listed in table 19. It will now be shown that to a good approximation, the remaining terms add up to a quantity which is independent of h and k. (In many structures, linear combinations of the geometrical parts of structure factors result in expressions which are simpler to interpret than the structure factors themselves. Complications are introduced into such analysis if the atoms in the structure have dissimilar form factors. The method to be described generally eliminates these complications provided that the crystal has orthogonal axes.) The following empirical relationship between the atomic scattering factors of magnesium and cerium takes into account the different shapes and atomic numbers of the atoms, and is valid over a wide range of $\sin\theta/\lambda$.

$$f_{Ce} \approx \left(4.82 + 4.96 \frac{\sin^2\theta}{\lambda^2}\right) f_{Mg}. \qquad (152)$$

Therefore,

$$\frac{f_{Ce}(h,k,3)}{f_{Mg}(h,k,3)} - \frac{f_{Ce}(h,k,1)}{f_{Mg}(h,k,1)} = 4.96\left(\frac{\sin^2\theta_{hk3}}{\lambda^2} - \frac{\sin^2\theta_{hk1}}{\lambda^2}\right). \qquad (153)$$

Since in the hexagonal system

$$\frac{\sin^2\theta_{hkl}}{\lambda^2} = \frac{h^2+hk+k^2}{4d^2_{100}} + \frac{l^2}{4d^2_{001}} \quad , \tag{154}$$

$$\frac{\sin^2\theta_{hk3}}{\lambda^2} - \frac{\sin^2\theta_{hk1}}{\lambda^2} = \frac{3^2}{4d^2_{001}} - \frac{1^2}{4d^2_{001}} = \frac{2}{d^2_{001}} = 0.0191 \tag{155}$$

for the $Mg_{12}Ce$ lattice. Thus from equations 153 and 155,

$$\frac{f_{Ce}(h,k,3)}{f_{Mg}(h,k,3)} - \frac{f_{Ce}(h,k,1)}{f_{Mg}(h,k,1)} = 4.96 \times 0.0191 = 0.947, \tag{156}$$

for all values of h and k. Equation 150 now becomes

$$\frac{F(h,k,3)}{f_{Mg}(h,k,3)} - \frac{F(h,k,1)}{f_{Mg}(h,k,1)} = [0.0947 + 2(\cos 6\pi z_1 - \cos 2\pi z_1) - 2(\sin 6\pi\delta + \sin 2\pi\delta)A(h,k)]\,U(h,k). \tag{157}$$

Using the values $z_1 = 0.353$ and $\delta = 0.035$ determined in the analysis of the subcell data, the quantity $\frac{F(h,k,3)}{f_{Mg}(h,k,3)} - \frac{F(h,k,1)}{f_{Mg}(h,k,1)}$ is

evaluated below in terms of U(h,k) for each of the eight groups of reflections.

Table 21. Interpretation of $\frac{F(h,k,3)}{f_{Mg}(h,k,3)} - \frac{F(h,k,1)}{f_{Mg}(h,k,1)}$.

Group	$\frac{F(h,k,3)}{f_{Mg}(h,k,3)} - \frac{F(h,k,1)}{f_{Mg}(h,k,1)}$	$\frac{\lvert F(h,k,3)\rvert}{f_{Mg}(h,k,3)} - \frac{\lvert F(h,k,1)\rvert}{f_{Mg}(h,k,1)}$
1	1.726 U(h,k)	1.726 |U(3,1)|
2	5.465 U(h,k)	5.465 |U(3,1)|
3	3.744 U(h,k)	3.744 |U(3,1)|
4	0.815 U(h,k)	0.815 |U(3,0)|
5	3.165 U(h,k)	3.165 |U(3,0)|
6	5.515 U(h,k)	5.515 |U(3,0)|
7	4.827 U(h,k)	4.827 |U(2,2)|
8	1.503 U(h,k)	1.503 |U(2,2)|

The inclusion of the expressions involving absolute values in table 21 is justified because it follows from the treatment of the odd layer structure factors in the previous section that all structure factors associated with the same U(h,k) have the same phase, and because $\frac{|F(h,k,3)|}{f_{Mg}(h,k,3)}$ is greater than

$\frac{|F(h,k,1)|}{f_{Mg}(h,k,1)}$. Thus, a method is arrived at by which the three quantities $|U(3,1)|$, $|U(3,0)|$, and $|U(2,2)|$, which are fundamental to the description of the disorder probabilities, can be evaluated from the observed odd layer intensity data. The accuracy of the evaluation suffers because the quantity $\frac{|F(h,k,3)|}{f_{Mg}(h,k,3)} - \frac{|F(h,k,1)|}{f_{Mg}(h,k,1)}$ is a small difference between larger numbers, but this disadvantage is more than overcome by the fact that for each group containing a large number of reflections the observed quantity is a constant, and statistical accuracy can be achieved by a simple averaging process. Furthermore, the method has the advantage that if there are any residual contributions to the odd layer structure factors from the magnesium atoms of type III which have not been accounted for in equation 144, they will not affect the averaged values of $|U(h,k)|$. Such contributions will be positive for some values of (h,k) within each group and negative for others, and will tend to cancel each other when averaged over a large number of reflections.

The odd layer intensity data was taken principally from hk1 and hk3 molybdenum Weissenberg photographs. Scale factors were correlated with the even layer data using true cell h0 (subcell hh) precession photographs. As was mentioned previously, the crystals are sufficiently small so that there is no appreciable absorption correction when molybdenum radiation is used, and since the intensities of the odd layer reflections are considerably smaller than those of the even

layer reflections, it was not necessary to correct for extinction. (Only the strongest even layer reflections showed effects due to extinction.) The data were corrected for the Lorentz and polarization factors, the temperature factor was divided out, and the absolute values of the structure factors were computed. In fixing the scale factor the even layer structure factors were given values 48 times those listed previously since they were in reference to the true unit cell, which contains 48 subcells. Table 22 lists the eight groups of odd layer reflections, the values of the indices (h,k) for which data were obtainable, the values of $|F(h,k,3)|$ and $|F(h,k,1)|$ in electrons, and

$$|U(h,k)| = \frac{1}{M}\left[\frac{|F(h,k,3)|}{f_{Mg}(h,k,3)} - \frac{|F(h,k,1)|}{f_{Mg}(h,k,1)}\right], \qquad (158)$$

where M is the multiplier for each group of reflections given in table 21.

The computed values of $|U(h,k)|$ should be equal to $|U(3,1)|$ for each value of (h,k) in groups 1,2, and 3, to $|U(3,0)|$ in groups 4,5, and 6, and to $|U(2,2)|$ in groups 7 and 8. The average values and probable errors for these quantities are given in table 23.

The quantity

$$\frac{\sum\left|\frac{|F(h,k,3)|}{f_{Mg}(h,k,3)} - \frac{|F(h,k,1)|}{f_{Mg}(h,k,1)} - M|U(h,k)|\right|}{\sum\left|\frac{|F(h,k,3)|}{f_{Mg}(h,k,3)} - \frac{|F(h,k,1)|}{f_{Mg}(h,k,1)}\right|},$$

Table 22. The odd layer intensity data.

Group	Indices h	k	|F(h,k,3)|	|F(h,k,1)|	|U(h,k)|
1	7	5	609	497	10.9
	9	4	710	570	13.2
	11	4	605	398	17.4
	12	5	751	608	13.3
	12	7	787	637	14.4
	11	9	738	600	16.9
	20	1	871	757	13.1
	20	3	836	655	17.3
	21	4	837	732	12.1
	23	4	444	259	18.5
	17	12	651	611	6.3
	25	3	361	379	0.1
	19	12	698	507	22.3
	20	13	852	841	4.1
	20	15	586	488	13.5
	19	17	716	638	11.2
	29	7	691	650	7.8
	28	9	566	499	10.2
	31	5	669	588	12.6
	33	4	752	675	13.2
	29	12	623	602	6.2
	23	21	640	543	16.7
	31	12	480	368	17.8
	36	5	668	646	5.1
	25	20	748	693	12.3
	33	11	617	587	6.2
	36	7	628	576	11.6
	35	9	603	468	21.1
	27	20	485	358	20.4
	28	21	615	581	7.8
	44	1	536	604	-8.4
	27	25	530	400	23.3
	44	3	538	383	28.4
	37	15	516	443	15.1
	36	17	704	631	16.0
	45	4	699	698	3.9
	36	19	375	359	3.0
	37	20	806	751	15.4
	31	29	521	468	10.5

Table 22.--continued

Group	Indices h	k	|F(h,k,3)|	|F(h,k,1)|	|U(h,k)|
2	17	0	886	464	11.0
	15	3	932	431	13.7
	17	7	951	609	10.1
	16	9	914	421	14.1
	24	7	927	525	13.5
	23	9	974	501	16.3
	25	8	1101	685	15.3
	31	0	753	357	13.3
	32	1	946	602	13.4
	25	15	635	237	16.2
	24	17	884	552	14.4
	41	0	738	542	2.8
	32	15	673	339	16.5
	31	17	761	432	14.0
	33	16	778	619	9.7
	41	7	794	612	10.4
	40	9	750	427	18.7
	33	23	701	467	14.7
	32	25	858	612	15.6
3	8	3	696	547	6.4
	13	3	652	310	12.2
	13	8	945	724	9.5
	19	0	854	563	11.9
	19	5	896	640	11.6
	24	5	823	624	10.3
	21	11	927	611	15.7
	29	0	708	507	11.0
	27	8	596	390	11.5
	21	16	680	529	9.8
	32	3	704	517	11.6
	24	19	653	454	13.7
	37	3	590	405	12.4
	32	13	734	695	6.4
	37	8	777	685	7.7
	29	19	795	557	15.0
	43	5	645	506	12.1
	29	24	703	583	10.7
	35	21	669	430	21.3
4	3	5	263	235	7.1
	11	5	219	137	14.2
	11	8	299	246	11.0
	21	0	319	305	5.6

Table 22.--continued

Group	Indices h	k	|F(h,k,3)|	|F(h,k,1)|	|U(h,k)|
	21	3	231	245	0
	19	13	263	208	13.9
	19	16	187	186	2.5
5	7	4	270	209	3.9
	9	3	269	219	2.6
	13	4	254	184	3.3
	13	7	299	241	3.2
	12	9	335	287	2.8
	19	1	326	196	6.3
	19	4	332	188	7.1
	20	5	287	172	6.1
	20	11	159	185	-0.9
	21	12	246	275	-0.8
	21	15	198	213	-0.4
	20	17	213	232	-0.6
6	15	9	237	141	2.7
	17	8	338	166	4.8
	23	8	343	195	5.0
	25	7	301	209	3.4
	24	9	306	219	3.3
7	8	2	459	284	4.9
	18	0	382	277	3.5
	14	8	390	271	3.9
	18	6	402	276	4.3
	24	6	402	212	7.2
	22	10	348	210	5.5
	32	2	276	208	3.2
	24	18	221	255	-1.1
8	6	6	263	237	3.9
	10	4	269	227	4.3
	12	6	309	230	8.0
	10	10	323	254	7.4
	20	2	339	306	4.4
	18	12	197	213	-0.6
	20	14	238	268	-2.0

Table 23. Values of $|U(h,k)|$.

$$|U(3,1)| = 12.9 \pm 0.5$$
$$|U(3,0)| = 3.4 \pm 0.4$$
$$|U(2,2)| = 3.9 \pm 0.5$$

---

which is analogous in this treatment to the R factor, has a value of 0.281. This figure is in reasonable accord with the R factor for the even layer data in view of the fact that the quantities $|F(h,k,3)|/f_{Mg}(h,k,3)$ and $|F(h,k,1)|/f_{Mg}(h,k,1)$ are on an average approximately 3.3 times greater than their difference.

e. Evaluation of the disorder probabilities for hexagonal space groups.

The evaluation of the three quantities $|U(3,1)|$, $|U(3,0)|$ and $|U(2,2)|$ represents the last stage in the treatment of the odd layer data. The final step in the description of the $Mg_{12}Ce$ structure is to determine the values of r_α for each cerium site in the x,y plane. If the actual, rather than the absolute values of $U(h,k)$ were known, the quantities r_α could be easily determined. It should be noted that the expression for $U(h,k)$,

$$U(h,k) = \sum_\alpha r_\alpha e^{2\pi i(hx_\alpha + ky_\alpha)}, \qquad (112)$$

is formally identical to that for the hk0 structure factor from a configuration of point atoms with atomic numbers r_α. There follows from the Fourier summation theorem that

$$\sum_{h,k} U(h,k) e^{-2\pi i(hx+ky)} = \sum_\alpha r_\alpha \delta(x-x_\alpha)\delta(y-y_\alpha), \qquad (159)$$

where δ is the Dirac delta function. The left hand side of equation 159 may be expressed in an alternate way because of the periodicities in the indices of the odd layer reflections which are present and in the quantities U(h,k). In accord with these periodicities, for every reflection with indices (h_j,k_j) that is present on the odd layers, there are also present reflections with the indices

$$\begin{aligned} h &= h_j + 4n_1 + 8n_2 \\ k &= k_j + 4n_1 - 4n_2, \end{aligned} \qquad (160a,b)$$

where n_1 and n_2 are integers. (The parts of equations 160 dependent on n_1 and n_2 are merely the transformation between the true cell and subcell indices given previously.) It has already been shown that if there is a cerium site at the origin of the x,y plane, then $U(h_j+4n_1+8n_2,\ k_j+4n_1-4n_2) = U(h_j,k_j)$ for all values of n_1 and n_2. It is advantageous in this treatment to arbitrarily make the x,y origin coincide with a cerium site even at the expense of not having it coincide with the three- or sixfold axis. Equation 159 can

then be rewritten as

$$\sum_j \sum_{n_1,n_2} U(h_j,k_j)\, e^{-2\pi i[(h_j+4n_1+8n_2)x + (k_j+4n_1-4n_2)y]}$$

$$= \sum_\alpha r_\alpha \delta(x-x_\alpha)\,\delta(y-y_\alpha), \qquad (161)$$

where the summation indexed by j is over those reflections contained in a single "unit cell" in reciprocal space of the kind that has been described previously. The double summation in equation 161 can be factored, resulting in

$$\{\sum_j U(h_j,k_j)\, e^{-2\pi i(h_j x + k_j y)}\}\{\sum_{n_1,n_2} e^{-2\pi i[(4n_1+8n_2)x + (4n_1-4n_2)y]}\}$$

$$= \sum_\alpha r_\alpha \delta(x-x_\alpha)\,\delta(y-y_\alpha). \qquad (162)$$

It can be recognized that the quantity $\sum_{n_1,n_2} e^{-2\pi i[(4n_1+8n_2)x+(4n_1-4n_2)y]}$ is a function of x and y having Dirac delta function contributions whenever $(4n_1+8n_2)x + (4n_1-4n_2)y$ is an integer, i.e., at all sites x_α, y_α. Thus

$$\sum_{n_1,n_2} e^{-2\pi i[(4n_1+8n_2)x + (4n_1-4n_2)y]} = \frac{1}{|N|}\sum_\alpha \delta(x-x_\alpha)\delta(y-y_\alpha), \qquad (163)$$

where N is the constant of proportionality equal to the determinant of the transformation and has the absolute value 48.

(See the general discussion of periodic absences in the reciprocal lattice.) It is now permissible to write equation 162 as

$$\sum_{\alpha}\left[\frac{1}{48}\sum_{j}U(h_j,k_j)e^{-2\pi i(h_j x_\alpha + k_j y_\alpha)}\right]\delta(x-x_\alpha)\delta(y-y_\alpha)$$

$$=\sum_{\alpha} r_\alpha\,\delta(x-x_\alpha)\delta(y-y_\alpha), \qquad (164)$$

from which follows the expression for the solution of the quantities r_α in terms of U(h,k):

$$r_\alpha=\frac{1}{48}\sum_{j}U(h_j,k_j)e^{-2\pi i(h_j x_\alpha + k_j y_\alpha)}. \qquad (165)$$

Two reflections having the same value of $|U(h,k)|$ can have different values of $U(h,k)$. There are phase relationships between the values of $U(h,k)$ for such reflections which vary according to the space group of the structure. Thus, before equation 165 can be applied, it is necessary to discuss the various possible space groups. This involves only the specification of the two-dimensional symmetry of the array of values r_α in the x,y plane. As was mentioned previously, the space groups which are consistent with the observed absences and the hexagonal symmetry of the reciprocal lattice are $D_{3h}^{1} = C\bar{6}m$, $D_{3h}^{3} = C\bar{6}2m$, $C_{6v}^{1} = C6mm$, $D_{6}^{1} = C62$, $D_{6}^{6} = C6_32$, and $D_{6h}^{1} = C6/mmm$. The space groups C_{6v}^{1}, D_{6}^{1}, and D_{6}^{6} can now

be eliminated, inasmuch as they do not contain the horizontal mirror planes which are present in the structure. To each of the remaining space groups there corresponds a plane group which represents the symmetry of the assignment of r_α values to the cerium sites in the x,y plane. Thus, the plane groups p3m1, p31m, and p6m correspond respectively to the space groups D^1_{3h}, D^3_{3h}, and D^1_{6h} (11). Either of the two possible arrangements of the cerium sites as shown in figures 5 and 6 are consistent with the symmetry of the plane group p31m. Only the arrangement as in figure 5 is consistent with p3m1 and p6m. The assignment of cerium sites as per figure 5 in plane group p31m can be quickly eliminated. The equalities which must be valid among the quantities r_α in a structure having this symmetry cause the sine part of the contribution from the cerium atoms to the structure factor to vanish for every odd layer reflection which is present. This implies that such a structure is centrosymmetric. The addition of a center of symmetry to the non-centrosymmetric plane group p31m reduces it to the plane group p6m. The three possibilities which remain are p3m1 and p6m with the assignment of cerium atoms as per figure 5, and p31m with the assignment as per figure 6.

The computations for the centrosymmetric arrangement p6m, corresponding to the space group D^1_{6h} = C6/mmm were carried out as follows. In a centrosymmetric space group the point and Laue symmetry of the reciprocal lattice are identical. It thus results in D^1_{6h} that the quantities U(h,k) themselves

can be placed in the three groups. The h and k indices of the non-absent reflections occurring in one "unit cell" in reciprocal space, and the corresponding values of U(h,k) are tabulated below. It is observed in table 24 that for every index h,k which occurs in the reflection groups (3,1)

Table 24. Reflections in the "unit cell" in reciprocal space and values of U(h,k) in D_{6h}^1.

Indices	U(h,k)
3,1;-3,-1;1,-4;-1,4;4,-3;-4,3	$U(3,1) = \pm\|U(3,1)\|$
3,0;-3,0;0,3;0,-3;3,-3;-3,3	$U(3,0) = \pm\|U(3,0)\|$
2,2;-2,4;-4,2	$U(2,2) = \pm\|U(2,2)\|$

and (3,0), the index $\bar{h},\bar{k}$ also appears. Therefore, for space group D_{6h}^1 equation 165 becomes

$$\rho_\alpha = \frac{1}{48}\{2U(3,1)[\cos 2\pi(3x_\alpha+y_\alpha) + \cos 2\pi(x_\alpha-4y_\alpha) + \cos 2\pi(4x_\alpha-3y_\alpha)]$$
$$+ 2U(3,0)[\cos 2\pi\cdot 3x_\alpha + \cos 2\pi\cdot 3y_\alpha + \cos 2\pi(3x_\alpha-3y_\alpha)]$$
$$+ U(2,2)[e^{-2\pi i(2x_\alpha+2y_\alpha)} + e^{-2\pi i(-2x_\alpha+4y_\alpha)} + e^{-2\pi i(-4x_\alpha+2y_\alpha)}]\} \qquad (166)$$

Table 25 lists representative x,y coordinates of the equivalent cerium sites in space group D_{6h}^1.

Table 25. Coordinates of the cerium sites in D_{6h}^{1}.

Designation	Multiplicity	Coordinates (x_α, y_α)
A	1	0,0
B	2	1/3,2/3; etc.
C	3	0,1/2; etc.
D	6	1/4,0; etc.
E	6	7/12,1/6; etc.
F	6	1/2,1/4; etc.
G	6	1/3,1/6; etc.
H	6	1/6,1/12; etc.
I	12	5/12,1/12; etc.

Straightforward substitution of the coordinates x ,y given in table 25 into equation 166 results in the following expressions for the quantities r_α.

$$r_A = \tfrac{1}{8}U(3,1) + \tfrac{1}{8}U(3,0) + \tfrac{1}{16}U(2,2)$$

$$r_B = -\tfrac{1}{16}U(3,1) + \tfrac{1}{8}U(3,0) + \tfrac{1}{16}U(2,2)$$

$$r_C = -\tfrac{1}{24}U(3,1) - \tfrac{1}{24}U(3,0) + \tfrac{1}{16}U(2,2)$$

$$r_D = \tfrac{1}{24}U(3,1) + \tfrac{1}{24}U(3,0) - \tfrac{1}{48}U(2,2)$$

$$r_E = \tfrac{1+2\sqrt{3}}{48}U(3,1) - \tfrac{1}{24}U(3,0) - \tfrac{1}{48}U(2,2)$$

$$r_F = -\tfrac{1}{24}U(3,1) - \tfrac{1}{24}U(3,0) - \tfrac{1}{48}U(2,2) \qquad (167a\text{-}1)$$

$$r_G = \tfrac{1}{48}U(3,1) - \tfrac{1}{24}U(3,0) + \tfrac{1}{16}U(2,2)$$

$$r_H = \tfrac{1-2\sqrt{3}}{48}U(3,1) - \tfrac{1}{24}U(3,0) - \tfrac{1}{48}U(2,2)$$

$$r_I = -\tfrac{1}{48}U(3,1) + \tfrac{1}{24}U(3,0) - \tfrac{1}{48}U(2,2). \qquad (167a\text{-}i)\ (\text{cont.})$$

Only the absolute values of U(3,1), U(3,0), and U(2,2) (which are real for a centrosymmetric space group) are known, so that there are a total of $2^3 = 8$ choices of signs possible. But as mentioned in connection with the elimination of ordered solutions, there is a redundancy of $\underset{\sim}{o}/2$ in the choice of the z origin which can be removed by arbitrarily fixing the sign of one of the quantities U(h,k). Therefore the sign of U(3,1) was made positive, and numerical values of $r_A, \ldots, r_I$ were calculated for the 2^2 arrangements of signs. The results are shown in table 26. Probable errors for r_A and r_B are also listed. None of the sets of values for the quantities r_α given in table 26 is a satisfactory solution because the equation

$$r_\alpha = 2p_\alpha - 1 , \qquad (111)$$

where p_α is a probability, implies that r_α cannot be greater than 1 or less than -1. Every assignment of signs in the table gives rise to a value for r_A or r_B which strays from these limits by more than the probable errors can explain.

Table 26. Values of r_α for the various choices of signs in D_{6h}^1.

	Choice of signs			
	$U\{3,1\}=12.9$ $U\{3,0\}=3.4$ $U(2,2)=3.9$	$U\{3,1\}=12.9$ $U\{3,0\}=3.4$ $U(2,2)=-3.9$	$U\{3,1\}=12.9$ $U\{3,0\}=-3.4$ $U(2,2)=3.9$	$U\{3,1\}=12.9$ $U\{3,0\}=-3.4$ $U(2,2)=-3.9$
r_A	2.28±0.11	1.79±0.11	1.43±0.11	0.94±0.11
r_B	-0.14±0.08	-0.63±0.08	-0.99±0.08	-1.48±0.08
r_C	-0.54	-0.92	-0.15	-0.64
r_D	0.60	0.76	0.32	0.48
r_E	0.98	1.14	1.26	1.42
r_F	-0.76	-0.60	-0.48	-0.32
r_G	0.37	-0.12	0.66	0.17
r_H	0.44	0.60	0.72	0.89
r_I	-0.21	-0.05	-0.49	-0.33

It is evident that the space group D_{6h}^1 is not the symmetry of the structure, and that there is a criterion for the acceptability of the remaining possible space groups. When values of r_α are computed for the space groups D_{3h}^1 and D_{3h}^3 it is found that for every possible solution, there are some r_α's which are markedly more than 1 or less than -1. The method of solution for the r_α's in space group D_{3h}^3 is similar to that in D_{6h}^1, because it can be shown that with the proper

choice of origin U(3,1) and U(2,2) are real, and that U(3,0) is purely imaginary, so that again only four assignments of phases need be considered. In space group D^1_{3h} the quantities U(h,k) are complex numbers, but manipulation of the phases resulted in solutions which were only slightly less objectionable than those for D^1_{6h}. Something fundamental is wrong.

f. Modified interpretation of the reciprocal lattice.

The foregoing has been an admittedly involved but correct analysis of the reciprocal lattice depicted in figure 1. It can be inferred from the failure of the preceding treatment to give acceptable solutions that there is some subtlety about the diffraction phenomena which has been overlooked until now. Acceptable solutions can be obtained if there is a phenomenon akin to but not identical with twinning in the specimens of $Mg_{12}Ce$ used in this investigation. In a truly single crystal, the probabilities of translation of the MgCeMg chains would be periodically and coherently arrayed over the entire domain of the aggregate. The curious disorder exhibited by the structure will later be shown to be intimately associated with the growth of the crystal. Because the MgCeMg chains are ordered along their length (parallel to the sixfold axis) it will suffice in discussing the relation between crystal growth and the disorder to consider only the component of growth in the plane perpendicular to the sixfold axis. It is reasonable that this component of

growth should be in a hexagonal spiral around a screw dislocation.* If the array of probabilities becomes incoherent with those in the previous section each time the direction of growth in the plane changes, then there result six domains of coherent probability arrays as illustrated in figure 10, rather than one domain as in a truly single crystal.

The consequences of such a mode of growth on the structure of the crystal and its x-ray diffraction pattern are as follows. Within each domain the structure obviously has less than hexagonal symmetry. Since this decreased symmetry pertains only to the array of probabilities describing the disorder, and the configuration of the reciprocal lattice layers with l even is quite independent of the features of the disorder, the symmetry of the diffraction phenomena from a single domain remains very nearly hexagonal for the even layers. The odd layer diffraction patterns from opposing sextants in figure 10 coincide, so that such an aggregate will give three interpenetrating odd layer reciprocal lattices.

In a naturally grown aggregate, there will be an equal amount of material in each of the six domains, so that its x-ray diffraction patterns will show sixfold symmetry throughout the reciprocal lattice. On the other hand, a fragment of such an aggregate will not in general maintain an equal distribution of the domains. The x-ray diffraction data with l even from such a specimen should still have hexagonal sym-

---

*An excellent photograph of a polygonal growth spiral can be found on the cover of the March 1955 issue of Scientific American magazine.

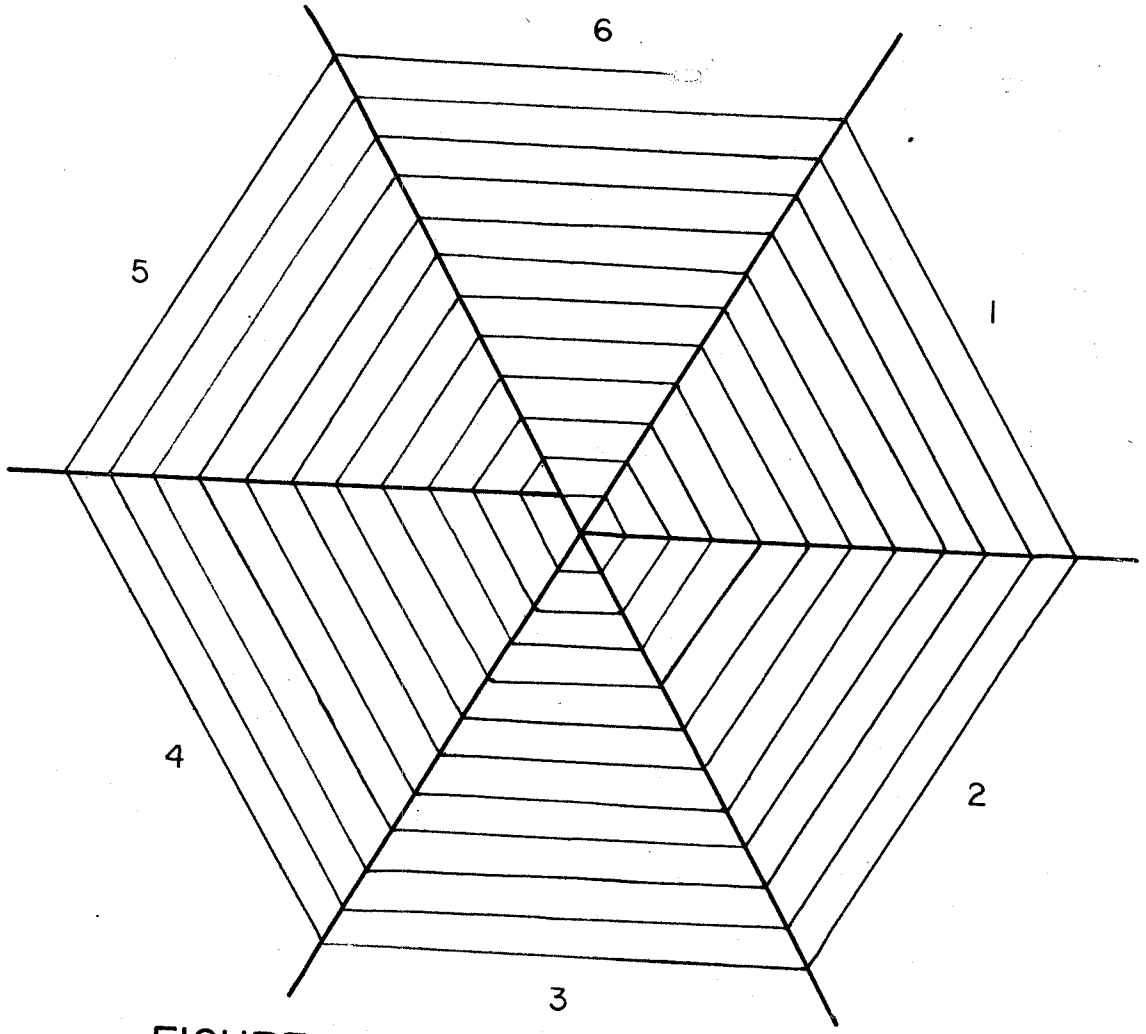

FIGURE 10. DOMAINS WITHIN WHICH THE DISORDER PROBABILITIES ARE COHERENT.

metry, but on the odd layers there will be three equivalent reciprocal lattices rotated 120° to eachother which differ in the overall intensities of their reflections. This describes precisely what was observed upon reinspection of some of the diffraction photographs prepared earlier. The bulk of the odd layer intensity data were obtained from equi-inclination Weissenberg photographs with constant l, made from a crystal specimen that was a completely formed needle. There was no noticeable deviation from hexagonal symmetry on these photographs. A set of precession photographs with constant l was made with the same crystal used to obtain the subcell (hhl) Weissenberg data. These photographs were not used for intensity measurements, so that their deviations from hexagonal symmetry were not observed previously. A careful examination of the photographs showed that those with l even still retained full hexagonal symmetry, but that those with l odd showed systematic differences in the intensities of supposedly symmetry-equivalent reflections. The internal consistency of the intensities of three subsets of the odd layer reflections corresponded to the reciprocal lattice illustrated below. Figure 11 shows the subset of the lattice depicted in figure 1 which corresponds to the correct reciprocal lattice of the structure. The new lattice has the Laue symmetry corresponding to the orthorhombic holohedry D_{2h} = 2/mmm. The new unit cell retains the original orientation of the c axis and one of the a axes.

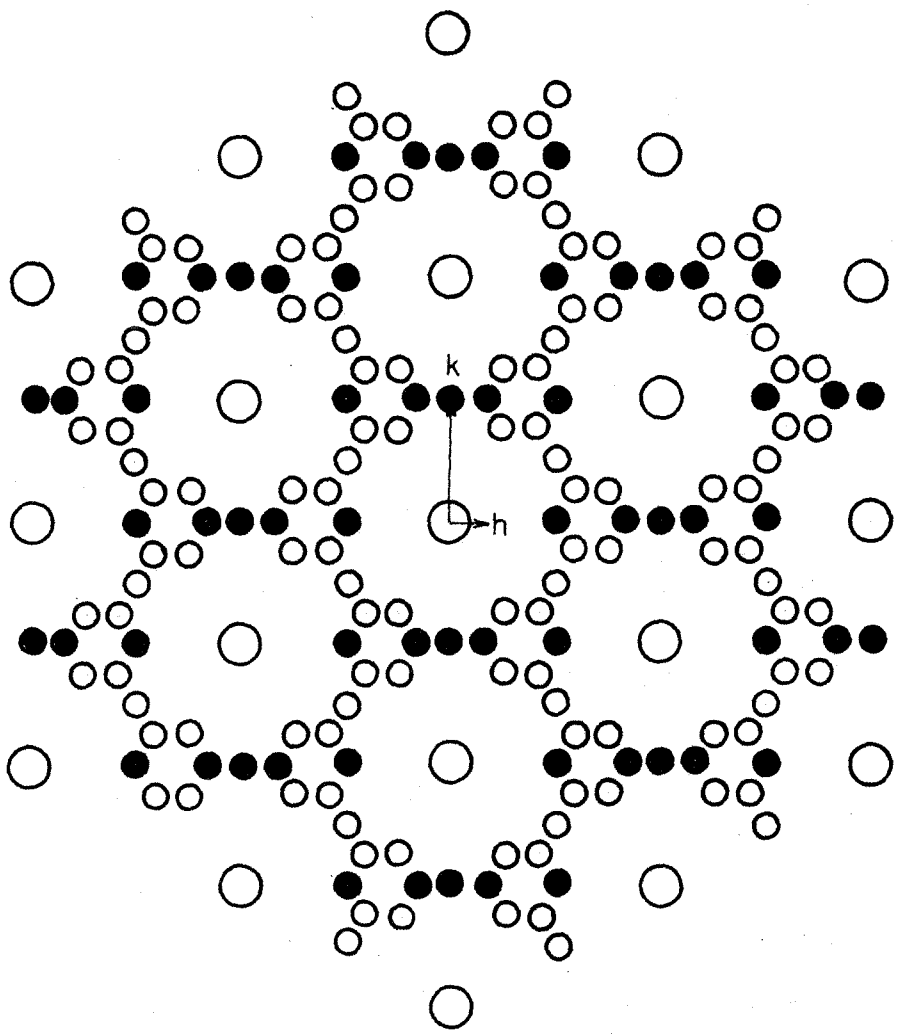

FIGURE 11. RECIPROCAL LATTICE OF REDUCED SYMMETRY FOR $Mg_{12}Ce$.

Legend

○ Even layer lattice points.

● Odd layer lattice points reciprocal to a single domain.

○ Odd layer lattice points from other domains.

The unit cell contains 12 cerium atoms. It was mentioned that at the onset of this investigation an attempt was made to resolve the observed diffraction data into a set of simpler interpenetrating reciprocal lattices. Although the mode of resolution described above was recognized at that time, it was not considered further because it eliminated neither the non-space group absences nor the necessity of large unit cell dimensions. The "twinning" reported for $MoBe_{12}$ and postulated for $TiBe_{12}$ (18) is probably due to the same phenomenon described here.

It is fortunate that this altered version of the reciprocal lattice requires only trifling revisions of the interpretations which have been made until now. The discussion of the subcell structure remains intact. In the section where ordered configurations were eliminated by considering subsets of the odd layer diffraction data it was assumed that the structure possessed hexagonal symmetry. Ordered structures are therefore now possible, but they can be excluded by simple methods. In the sections deriving the expression for the odd layer structure factors in terms of U(h,k), the only information used involving the symmetry of the structure was the existence of horizontal mirror planes. The positional parameters were referred to the hexagonal axes, but since it is possible to describe the orthorhombic structure in this system also (although it is now non-primitive), the quantities U(h,k) still have the same significance as

before. It is desirable however to refer both U(h,k) and the Miller indices to the primitive orthorhombic cell with dimensions $a_o = 35.63 \pm 0.01$ Å, $b_o = 10.284 \pm 0.003$ Å, and $c_o = 10.284 \pm 0.003$ Å. The transformation equations relating the subcell indices (H,K,L) to the true cell indices (h,k,l) are now

$$h = 6H + 6K$$
$$k = H - K \qquad (168a\text{-}c)$$
$$l = L$$

The reflections in the "asymmetric unit" of the odd layer reciprocal plane have the indices 50, 30, and 60, corresponding respectively to the hexagonal indices 31, 30, and 22. If the quantities U(h,k) are to refer to the new unit cell the former values should be divided by 4, since in establishing the relationship between the even and odd layer structure factors it was assumed that there were 48 rather than 12 subcells in the true unit cell. Furthermore, it must be realized that in accord with the present notion of the crystal growth, the even layer reflections are produced by the entire aggregate, whereas each odd layer reflection is produced by only one-third of the aggregate. Since the scattering from an individual domain is to be considered, the measured odd layer intensities are too small relative to the even layer intensities by a factor of three.

Therefore an additional factor of $\sqrt{3}$ should be included in the conversion of the quantities U(h,k) from the old to the new axial system. The new values of $|U(h,k)|$ and their probable errors which are equal to the former values multiplied by $\sqrt{3}/4$, are tabulated below.

Table 27. Values of $|U(h,k)|$ in the orthorhombic system.

Hexagonal Index class	Orthorhombic Index class	$\|U(h,k)\|$
3,1	5,0	5.6 ± 0.2
3,0	3,0	1.5 ± 0.2
2,2	6,0	1.7 ± 0.2

Equation 165 which relates the values of r_α for each cerium site to the quantities U(h,k) is still valid if the factor of 1/48 (which is the reciprocal of the number of cerium sites in the unit cell) is changed to 1/12.

g. Evaluation of the disorder probabilities for orthorhombic space groups.

It is now necessary to enumerate the possible space groups for the structure that are consistent with the orthorhombic system. As before, this involves merely the discussion

of the two-dimensional symmetry of the array of p_α's in the x,y plane. Because this array cannot be centered, it suffices to consider only the primitive rectangular plane groups, which are pm, plm, pg, plg, pmm, pmg, pgm, and pgg (11). Because the y coordinates of the cerium sites in the new unit cell are either 0 or 1/2, there must be mirror lines perpendicular to the b axis, so that the plane groups pm and pg can be eliminated inasmuch as they correspond respectively to pmm and pgm. In addition, pmg, plg, and pgg must be discarded, since in combination with the aforementioned mirror lines they result in centering or halving of the unit cell edge depending on the coordinate of the glide line. The remaining plane groups are plm, pgm, and pmm corresponding respectively to the space groups P2mm = C_{2v}^1, Pcmm = D_{2h}^5, and Pmmm = D_{2h}^1. Table 28 shows the positions of equivalent cerium sites for each of these symmetry groups.

Plane group pgm can be discussed simply. For if the quantity U(6,0) is computed according to equation 112 and the coordinates in table 28b there results

$$U(6,0) = \sum_\alpha r_\alpha e^{2\pi i \cdot 6 \cdot x_\alpha} = r_A\left(e^{2\pi i\cdot 6\cdot 0} + e^{2\pi i\cdot 6\cdot \frac{1}{12}}\right) + r_B\left(e^{2\pi i\cdot 6\cdot \frac{1}{6}} + e^{2\pi i\cdot 6\cdot \frac{11}{12}}\right)$$
$$+ r_C\left(e^{2\pi i\cdot 6\cdot \frac{1}{3}} + e^{2\pi i\cdot 6\cdot \frac{3}{4}}\right) + r_D\left(e^{2\pi i\cdot 6\cdot \frac{1}{2}} + e^{2\pi i\cdot 6\cdot \frac{7}{12}}\right) + r_E\left(e^{2\pi i\cdot 6\cdot \frac{2}{3}} + e^{2\pi i\cdot 6\cdot \frac{5}{12}}\right)$$
$$+ r_F\left(e^{2\pi i\cdot 6\cdot \frac{5}{6}} + e^{2\pi i\cdot 6\cdot \frac{1}{4}}\right) \equiv 0. \qquad (168)$$

Table 28. Plane coordinates of the cerium sites in plm, pgm, and pmm

	Site designation	Multiplicity	Coordinates
a. plm (acentrosymmetric)	A	1	0,0
	B	1	1/6,0
	C	1	1/3,0
	D	1	1/2,0
	E	1	2/3,0
	F	1	5/6,0
	G	1	1/12,1/2
	H	1	1/4,1/2
	I	1	5/12,1/2
	J	1	7/12,1/2
	K	1	3/4,1/2
	L	1	11/12,1/2
b. pgm (center at 1/12,1/4)	A	2	0,0;1/12,1/2
	B	2	1/6,0;11/12,1/2
	C	2	1/3,0;3/4,1/2
	D	2	1/2,0;7/12,1/2
	E	2	2/3,0;5/12,1/2
	F	2	5/6,0;1/4,1/2
c. pmm (center at 0,0)	A	1	0,0
	B	1	1/2,0
	C	2	1/6,0;5/6,0
	D	2	1/3,0;2/3,0
	E	2	1/12,1/2;11/12,1/2
	F	2	1/4,1/2;3/4,1/2
	G	2	5/12,1/2;7/12,1/2

That U(6,0) is identically zero is inconsistent with the observed intensity data, so that pgm may be dismissed as a possible symmetry for the array of cerium sites.

The symmetry plm, corresponding to the space group C_{2v}^1 cannot be eliminated, since D_{2h}^1 is a special case of C_{2v}^1, and the structure must possess as symmetry one of these space groups or the other. The solution in space group C_{2v}^1 will be presented in terms of the observable quantities |U(h,k)| and the phases of U(3,0) and U(5,0), which in this space group are in general complex numbers. It is, of course, impossible to observe these phases directly, and since continuously varying values may be assigned to them, the number of solutions in this space group is infinite. It will be shown, however, that none of the solutions corresponds to an ordered structure. The reflections in the "unit cell" in reciprocal space are 30, $\bar{3}$0, 50, $\bar{5}$0, and 60. Thus, from equation 165 with the factor 1/12 substituted for 1/48,

$$\rho_\alpha = \tfrac{1}{12}\left[U(3,0)\,e^{-2\pi i\cdot 3x_\alpha} + U(-3,0)\,e^{2\pi i\cdot 3x_\alpha} + U(5,0)\,e^{-2\pi i\cdot 5x_\alpha}\right.$$

$$\left. + U(-5,0)\,e^{2\pi i\cdot 5x_\alpha} + U(6,0)\,e^{-2\pi i\cdot 6x_\alpha}\right]. \qquad (169)$$

From the definition of U(h,k) in equation 112, it is evident that U(3,0) = U^*(-3,0) and U(5,0) = U^*(-5,0), where the asterisk denotes the complex conjugate. Furthermore, since

the x coordinates of all of the cerium sites are multiples of 1/12, U(6,0) must be real. In order to remove the ambiguity associated with the position of the origin in the z direction, U(6,0) can arbitrarily be made positive. If the following definitions are made,

$$\frac{|U(3,0)|}{12} = X = 0.46, \quad \frac{|U(5,0)|}{12} = Y = 0.125, \quad \frac{|U(6,0)|}{12} = Z = 0.14, \tag{170a-c}$$

then

$$\frac{U(3,0)}{12} = Xe^{i\theta_3}, \quad \frac{U(-3,0)}{12} = Xe^{-i\theta_3}$$

$$\frac{U(5,0)}{12} = Ye^{i\theta_5}, \quad \frac{U(-5,0)}{12} = Ye^{-i\theta_5}$$

$$\text{and} \quad \frac{U(6,0)}{12} = Z \tag{171a-e}$$

In equations 170a-d, θ_3 and θ_5 are the indeterminate phase angles associated with U(3,0) and U(5,0). From equations 169 and 171 it follows that

$$\rho_\alpha = X\left[e^{-i(2\pi\cdot 3x_\alpha - \theta_3)} + e^{i(2\pi\cdot 3x_\alpha - \theta_3)}\right] + Y\left[e^{-i(2\pi\cdot 5x_\alpha - \theta_5)} + e^{i(2\pi\cdot 5x_\alpha - \theta_5)}\right] + Ze^{-2\pi i\cdot 6x_\alpha}$$

$$= 2X\cos(2\pi\cdot 3x_\alpha - \theta_3) + 2Y\cos(2\pi\cdot 5x_\alpha - \theta_5) + Ze^{-2\pi i\cdot 6x_\alpha} \tag{172}$$

Substitution of the x coordinates of the cerium sites listed in table 26a into equation 172, followed by trigonometric manipulation, results in the solution below of the quantities r_α in terms of the knowns X, Y, and Z, and the unknowns θ_3 and θ_5.

$$r_A = 2X\cos\theta_3 + 2Y\cos\theta_5 + Z$$

$$r_B = -2X\cos\theta_3 + 2Y(\tfrac{1}{2}\cos\theta_5 - \tfrac{\sqrt{3}}{2}\sin\theta_5) + Z$$

$$r_C = 2X\cos\theta_3 - 2Y(\tfrac{1}{2}\cos\theta_5 + \tfrac{\sqrt{3}}{2}\sin\theta_5) + Z$$

$$r_D = -2X\cos\theta_3 - 2Y\cos\theta_5 + Z$$

$$r_E = 2X\cos\theta_3 - 2Y(\tfrac{1}{2}\cos\theta_5 - \tfrac{\sqrt{3}}{2}\sin\theta_5) + Z$$

$$r_F = -2X\cos\theta_3 + 2Y(\tfrac{1}{2}\cos\theta_5 + \tfrac{\sqrt{3}}{2}\sin\theta_5) + Z$$

$$r_G = 2X\sin\theta_3 - 2Y(\tfrac{\sqrt{3}}{2}\cos\theta_5 - \tfrac{1}{2}\sin\theta_5) - Z$$

$$r_H = -2X\sin\theta_3 + 2Y\sin\theta_5 - Z$$

$$r_I = 2X\sin\theta_3 + 2Y(\tfrac{\sqrt{3}}{2}\cos\theta_5 + \tfrac{1}{2}\sin\theta_5) - Z$$

$$r_J = -2X\sin\theta_3 + 2Y(\tfrac{\sqrt{3}}{2}\cos\theta_5 - \tfrac{1}{2}\sin\theta_5) - Z$$

$$r_K = 2X\sin\theta_3 - 2Y\sin\theta_5 - Z$$

$$r_L = -2X\sin\theta_3 - 2Y(\tfrac{\sqrt{3}}{2}\cos\theta_5 + \tfrac{1}{2}\sin\theta_5) - Z. \qquad (173a\text{-}1)$$

It is simple to show that no choice of θ_3 and θ_5 can result in values of r_α corresponding to ordered structures. For from equations 173,

$$r_A + r_D = 2Z \qquad (174)$$

In an ordered structure, each r_α can have the value 1 or -1, so that $r_A + r_D$ could be equal only to 2, 0, or -2, which is inconsistent with the datum 2Z = 0.28 obtained from the observed intensities. It should be noted that because the space group C_{2v}^1 is polar as well as non-centrosymmetric it is an improbable symmetry for the structure of an intermetallic compound.

There remains only the possibility that the symmetry of the structure corresponds to the orthorhombic holohedry D_{2h}^1 = Pmmm. The solution of equation 165 in this space group, which follows, results in a unique acceptable set of values r_α. Due to the presence of a center of symmetry at the origin of the unit cell in space group D_{2h}^1 all of the quantities U(h,k) will be real. It follows from this and the definition of U(h,k) in equation 112 that in D_{2h}^1, U(3,0) = U(-3,0), and U(5,0) = U(-5,0). Equation 165 can therefore be written

$$r_\alpha = \tfrac{1}{12}\left[U(3,0)\left(e^{-2\pi i\cdot 3x_\alpha} + e^{2\pi i\cdot 3x_\alpha}\right) + U(5,0)\left(e^{-2\pi i\cdot 5x_\alpha} + e^{2\pi i\cdot 5x_\alpha}\right) + U(6,0)\, e^{-2\pi i\cdot 6x_\alpha}\right]$$

$$= \tfrac{1}{12}\left[2U(3,0)\cos 2\pi\cdot 3x_\alpha + 2U(5,0)\cos 2\pi\cdot 5x_\alpha + U(6,0)\, e^{-2\pi i\cdot 6x_\alpha}\right]. \qquad (175)$$

From equation 175 and the x coordinates in table 28c, there results

$$
\begin{aligned}
r_A &= \tfrac{1}{6}U(3,0) + \tfrac{1}{6}U(5,0) + \tfrac{1}{12}U(6,0) \\
r_B &= -\tfrac{1}{6}U(3,0) - \tfrac{1}{6}U(5,0) + \tfrac{1}{12}U(6,0) \\
r_C &= -\tfrac{1}{6}U(3,0) + \tfrac{1}{12}U(5,0) + \tfrac{1}{12}U(6,0) \\
r_D &= \tfrac{1}{6}U(3,0) - \tfrac{1}{12}U(5,0) + \tfrac{1}{12}U(6,0) \\
r_E &= -\tfrac{\sqrt{3}}{12}U(5,0) - \tfrac{1}{12}U(6,0) \\
r_F &= -\tfrac{1}{12}U(6,0) \\
r_G &= \tfrac{\sqrt{3}}{12}U(5,0) - \tfrac{1}{12}U(6,0)
\end{aligned}
\qquad (176a\text{-}g)
$$

Of the eight possible choices of signs for U(3,0), U(5,0) and U(6,0) only two are independent when the ambiguities associated with the position of the origin are removed. First, it is possible to make the sign of U(5,0) positive to remove the ambiguity in the origin of z. Second, it is observed that a translation by $1/2\underset{\sim}{a}_o$ carries sites A into B, C into D, E into G, and F into themselves. In equations 176, changing the sign of U(6,0) (symbolized by $U(6,0) \longrightarrow -U(6,0)$) results in $r_A \rightarrow -r_B$, $r_C \rightarrow -r_D$, $r_E \rightarrow -r_G$, and $r_F \rightarrow -r_F$. Therefore, solutions with the same sign of U(3,0) and different signs of U(6,0) are not independent, but correspond to the same configuration with the origin translated by $1/2\underset{\sim}{a}_o + 1/2\underset{\sim}{c}_o$. It suffices then to consider only the assignments

$$U(3,0) = 1.5 \quad U(5,0) = 5.6 \quad U(6,0) = 1.7$$

and

$$U(3,0) = -1.5 \quad U(5,0) = 5.6 \quad U(6,0) = 1.7 .$$

The numerical values of r_α corresponding to these choices of signs are shown in table 29.

Table 29. Values of r_α for the choices of signs in D_{2h}^1.

	CHOICE OF SIGNS	
	1. $U(3,0)=1.5$, $U(5,0)=5.6$, $U(6,0)=1.7$	2. $U(3,0)=-1.5$, $U(5,0)=5.6$, $U(6,0)=1.7$
r_A	1.32±0.06	0.82±0.06
r_B	-1.04±0.06	-0.54±0.06
r_C	0.36±0.04	0.86±0.04
r_D	-0.07±0.04	-0.57±0.04
r_E	-0.95±0.04	-0.95±0.04
r_F	-0.14±0.03	0.14±0.03
r_G	0.67±0.04	0.67±0.04

The value of r_A in the first choice of sign deviates from the allowed limits ($-1 \leq r \leq 1$) by far more than the estimated deviations in the quantities $|U(h,k)|$ permit. Assignment 1 there-

fore cannot be correct. However, the values of r_α in assignment 2 are all greater than -1 and less than 1. This assignment is attractive because it is the unique non-polar solution for which the resulting probabilities are physically realizable. It follows from equation 111 that the probability p_α that the cerium atom at site α is at z=0 is given by

$$p_\alpha = 1/2 + 1/2r_\alpha \quad . \tag{177}$$

The values of p_α corresponding to assignment 2 are listed below.

Table 30. Unique non-polar solution for the probabilities p_α .

Space group D_{2h}^1

Cerium site	p_α
A	0.91
B	0.23
C	0.93
D	0.21
E	0.03
F	0.42
G	0.83

Figure 12 depicts how the subcells are positioned in the x,y plane of the true unit cell and shows the probabilities p_α for each cerium site.

The (hk3) reflections for the odd reciprocal lattice layer with the greatest overall intensity. If the structure is indeed centrosymmetric, it follows when numerical parameters are inserted in equation 146 that the sign of F(h,k,3) is the same as that of U(h,k). Therefore, the signs of the (hk3) reflections consistent with the solution presented in table 30 are determinate. Although it was not attempted, a generalized Fourier projection using the (hk3) data is thus feasible, and would serve the following purpose. The solution presented above would be further confirmed if the resulting peak shapes and positions (especially those of the type II magnesium atoms) appear proper. In addition an analysis of the projection could possibly provide information about the contingent probabilities associated with the structure.

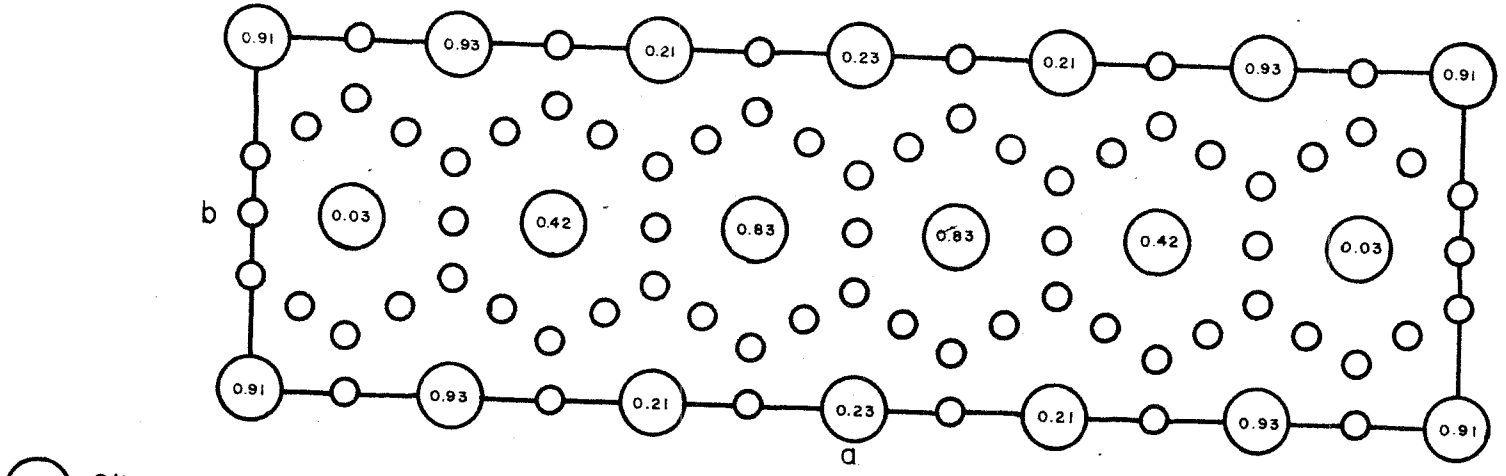

FIGURE 12. PROJECTION OF THE $Mg_{12}Ce$ STRUCTURE ONTO THE (x,y) PLANE OF THE ORTHORHOMBIC UNIT CELL.

"Ideal" positions of the Mg atoms of types II and III are shown.
Probabilities p_α that the Ce atoms are at z=0 are computed for space group D^1_{2h}.

H. Discussion of the causes of large repeat distances and periodic disorders, with reference to the $Mg_{12}Ce$ structure.

At the conclusion of the interpretation of the diffraction data with l even, the aspects of the arrangement of the atoms in the $Mg_{12}Ce$ structure were discussed. The treatment of the odd layer diffraction data showed that a specific type of disorder was present, and that a unit cell of large dimensions was required to specify the array of disorder probabilities encountered. The discussion in this concluding section will not be restricted to the disorder occurring in $Mg_{12}Ce$. Rather, an attempt will be made to treat the nature of long repeat distances in a fairly general fashion, and to relate the disorders in some other structure to that found in the $Mg_{12}Ce$ structure.

The simplest cause of large unit cell dimensions is that the structure consists of large molecules. In metals the notion of a "molecule" rarely arises. However, in many intermetallic compounds packing requirements and the attainment of favorable electron-atom ratios necessitate that a large number of atoms be placed in the unit cell, leading to long lattice spacings.

There is still a class of metallic structures in which the reasons for the large repeat distances are not obvious. These are structures for which simpler configurations involving the same atoms and atomic ratios can, and often do exist. (Superlattice structures are an example.) It is remarkable

that two equivalent atoms separated by the long lattice spacings encountered can somehow contrive to behave in an equivalent way when atomic interactions are basically short-ranged. The overall aim of this section is to present some examples showing how short range interactions can transmit the information ensuring the similarity of remote sites, without the agency of intervening equivalent sites which would be present in a structure having small unit cell dimensions.

It is necessary first to discuss how far the "short range" atomic interactions are effective. Radial distribution studies on single crystals of disordered $AuCu_3$ show that short range order results in deviations from randomness as far away as the tenth nearest neighbor (19). But this does not imply that the range of forces extends to the tenth nearest neighbor. As will be shown later, such a result can be accounted for even by nearest neighbor interactions. Another way that information about the range of interactions can be obtained is from the examination of ordered structures. If, for example, a one-dimensional crystal consisting of two types of atoms A and B has the structure AAABBBAAABBB...., it must be concluded that the interactions extend at least as far as the third nearest neighbor. This can be appreciated by considering that in the growth of the crystal, a knowledge of the types of the last two atoms to be deposited is insufficient to determine the type of atom that will be deposited next. Reference to the sequence of growth shows that if the

last two atoms were both of type B then either a type A atom or a type B atom can be deposited next. However, the rules in table 31 which are based on a knowledge of the last three atoms to be deposited is sufficient to determine the growth of the crystal. In this and in the following examples, the configurations listed in parentheses would occur only as defects in the structure. The types of next atoms deposited for such configurations have been chosen so that the structure heals itself immediately.

Table 31. Rules determining the growth of the AAABBB structure

Configuration of last three atoms deposited	Type of next atom deposited
AAA	B
AAB	B
ABB	B
BBB	A
BBA	A
BAA	A
(ABA)	A
(BAB)	B

It should be noted that the interactions deduced from the observation of such ordered structures result in certainties, and not probability relationships about the deposition of the next atom. A most remarkable structure has been reported for the orthorhombic phase of the intermetallic compound CuAu (20). The atoms are arranged at the points of a distorted face-centered cubic lattice. The overall structure can be described as resulting from stacking layers of four types A, B, C and D in the sequence ABABABABCDCDCD-CDCD to form a single unit cell. No less than ninth nearest neighbor interactions ($\sim$17 Å range) are required to produce this configuration. Interactions of considerably shorter range generally suffice to determine other structures.

Similar reasoning can be applied to show that structures can arise which have repeat distances considerably longer than the range of interactions within them. Such structures are most conveniently discussed using the theory of Markov chains (21). The growth of a one-dimensional ordered structure will be considered. It will be supposed that there are k kinds of atoms $a_1,\ldots,a_k$ in the structure, and that the type of atom deposited at the nth lattice point is determined completely by the configuration of the m most recently deposited atoms, i.e., on the configuration of the atoms at the lattice points n-m, n-m+1,...n-1. In terms of probability language, the specification that the configuration of these m lattice points is a particular arrangement

of the kinds of atoms a_i is equivalent to stating that a particular event E takes place at the n-1st trial. If k is the number of kinds of atoms which can be at each lattice point, and m is the number of lattice points which are specified, then the number p of possible events E is

$$p = k^m \ . \tag{178}$$

These statements can be made more clear if a simple example is given. Let there be three kinds of atoms (k=3), denoted by A,B, and C. Only the configuration of these atoms at the two most recently deposited lattice points (m=2) will determine which kind of atom is deposited at the next lattice point. Then the n-1st trial, which specifies the configuration at the n-2nd and n-1st lattice points, can result in $3^2=9$ outcomes E_{n-1} which are listed below in table 32.

Table 32. Outcomes of E_{n-1} for k=3, m=2.

Outcome number	Atom at lattice point n-2	Atom at lattice point n-1
1	A	A
2	A	B
3	A	C
4	B	A
5	B	B
6	B	C
7	C	A
8	C	B
9	C	C

The usefulness of this method of notation is that according to the laws of crystal growth, the outcome of event E_n is determined completely by the outcome of event E_{n-1}. It should be noted that only k rather than k^m outcomes are possible for E_n, once E_{n-1} is specified. Thus, in the previous example, if the event E_{n-1} had outcome number 1, namely that there are A atoms at lattice point n-2 and n-1, then the event E_n can have only the three outcomes listed in table 33. Which of the k outcomes for the event E_n will result once the outcome of the event E_{n-1} is established is determined completely by the particular law relating to the growth of the crystal.

Table 33. Outcomes of E_n given that the outcome of E_{n-1} was an A atom at lattice points n-2 and n-1.

Outcome number	Atom at lattice point n-1	Atom at lattice point n
1	A	A
2	A	B
3	A	C

The important property of these laws is that if the outcome of E_{n-1} is i implies that the outcome of E_n is j, the relationship that j follows i is independent of n. Thus, in the example given, if outcome number 1 (configuration AA) in the n-1st trial implies outcome number 2 (configuration AB) in the nth trial, then every time the configuration AA occurs in the structure, a B atom follows immediately. Since the growth law determines the structure of the crystal completely, the entire configuration (in an infinite crystal) following any one pair of atoms AA is the same as that following any other pair of atoms AA. Now, any infinite structure which can be brought into self-coincidence by a translation is periodic. It is through this mechanism in the growth of a one-dimensional crystal that periodicity is introduced.

A simple relationship exists between k,m, and the maximum period the structure can display. It is evident that the crystal can grow without repeating itself only as long as none of the events E occurs more than once, because the configuration of the crystal is the same following each identical event E. But the number of different events E is limited by equation 178. Since the numbering of each event increases by one each time an atom is deposited, the longest sequence of atoms that can be deposited without a repeat is also k^m. Restating this result, the maximum number of atoms in the unit cell of a one-dimensional crystal is equal to k^m, where k is the number of kinds of atoms in the structure, and m

is the number of nearest neighbors over which interactions extend.

Certain laws of crystal growth result in structures which have a smaller periodicity than the maximum. For instance, the structure AAABBB.... has a periodicity of only 6 as compared with the maximum $2^3=8$. Reference to table 31 shows that the two configurations placed in parentheses do not occur if the laws of crystal growth are obeyed, and this accounts for the reduced periodicity. Growth laws in which all of the k^m events E materialize before any single E occurs twice correspond to irreducible Markov chains. An example of such a growth law, in which there are two kinds of atoms and fourth nearest neighbor interactions is shown in table 34 and illustrates how a structure of large periodicity can result from a shorter ranged interaction. A unit cell grown according to the "instructions" presented in table 34 has the configuration AABAABBABABBBBAA.

Another example will now be presented which is closer to physical reality. The possible structures resulting from the closest packing of spheres will be enumerated up to a certain complexity of interactions required to produce the configurations. The structures can be derived by stacking planar layers of hexagonal close packed spheres. There are three possible orientations for any given plane, which are usually denoted by A,B, and C. In order to avoid redundancy in the choice of origin (e.g. ABCABC...and BACBAC.... are

Table 34. A growth law producing maximum periodicity for the case k=2, m=4.

Configuration of the last four atoms deposited	Type of new atom deposited
AAAA	B
AAAB	A
AABA	A
AABB	A
ABAA	B
ABAB	B
ABBA	B
ABBB	B
BAAA	A
BAAB	B
BABA	B
BABB	B
BBAA	A
BBAB	A
BBBA	A
BBBB	A

both cubic closest packing) and to implicitly introduce the requirement that no two consecutive layers can have the same orientation, an altered notation of the layer type will be used. If a layer has the same surroundings above and below, as in hexagonal closest packing, it will be denoted as H, and if it has different surroundings above and below, as in cubic closest packing, it will be denoted as C. All of the resulting structures can be described by an infinite sequence of the letters C and H. The laws governing the growth of the crystal shall be limited in complexity by requiring that whether a layer is C or H is determined completely by the configuration (C or H) of the preceding two layers. The derivation of sequences of C or H from such growth laws is isomorphous logically to the formation of structures having two kinds of atoms with second nearest neighbor interactions. Since k=2 and m=2, the greatest periodicity which can result in the sequence of letters C and H is four. (This does not imply that this is the periodicity of the arrangement of layers. For example, the cubic closest packed structure which in the present notation is represented as CCCC····, with a periodicity of one, has a periodicity of three in its arrangement of layers ABCABC····.) The sequences with various periodicities up to four are easily enumerated.

The two sequences with unit periodicity are shown in tables 35 and 36 along with the growth laws producing them (The parentheses around configurations have the same significance as in table 31.) There is only one sequence with a

Table 35. Closest packing of spheres. Sequence HHHH.... .

Configuration of two successive layers	Configuration of next layer
HH	H
(HC)	H
(CH)	H
(CC)	H

Table 36. Closest packing of spheres. Sequence CCCC.... .

Configuration of two successive layers	Configuration of next layer
(HH)	C
(HC)	C
(CH)	C
CC	C

periodicity of two, since HCHC···· is equivalent to CHCH···· in an infinite crystal. The growth law for such a sequence is tabulated below. In an infinite crystal there are two non-equivalent sequences of period 3. They are HCHHCH····, and CHCCHC···· , as shown in tables 38 and 39. The sequence CCCHCCCH···· has a periodicity of four but it is not admissible here, since at one stage in its growth the configuration CC requires that a C layer follows, while at another stage the same configuration requires that an H layer follows. This is contrary to the simple types of interactions assumed. The only acceptable sequence with a periodicity of four, as tabulated below, is CHHCCHHC···· . It thus results that there are six closest packed structures which are derivable from the interaction range assumed. It is interesting to note that they are hexagonal closest packing (HHHH····), cubic closest packing (CCCC····), and the four closest packed structures (CHCH····, HCHHCH···· , CHCCHC····, and CHHCCHHC····) involving two non-equivalent kinds of spheres with the same radius (22).

Thus far, the laws discussed have dictated with certainty the next stage of the growth of the crystal, leading to ordered structures. There are many instances, however, where the growth laws are expressions of probability, rather than of certainty. For example, in a structure with k=2 and m=2, the configuration AB may result in the subsequent deposition of an A atom in seven-tenths of the instances and in the deposi-

Table 37. Closest packing of spheres. Sequence CHCH···· .

Configuration of two successive layers	Configuration of next layer
(HH)	C
HC	H
CH	C
(CC)	H

Table 38. Closest packing of spheres. Sequence HCHHCH···· .

Configuration of two successive layers	Configuration of next layer
HH	C
HC	H
CH	H
(CC)	H

Table 39. Closest packing of spheres. Sequence CHCCHC.... .

Configuration of two successive layers	Configuration of next layer
(HH)	C
HC	C
CH	C
CC	H

Table 40. Closest packing of spheres. Sequence CHHCCHHC.... .

Configuration of two successive layers	Configuration of next layer
HH	C
HC	C
CH	H
CC	H

tion of a B atom in three-tenths of the instances. The resulting structure will of course be disordered. Analysis of such growth laws gives rise to relationships between the probabilities of occupancy at the various sites in the lattice. These relationships can vary in complexity. For example, the distribution of isotopic atoms in an elemental crystal is essentially independent of the lattice position. On the other hand, the array of probabilities in the $Mg_{12}Ce$ structure represents a complicated situation. It will be shown, nevertheless, that the analysis of fairly simple kinds of growth laws can result in structures which resemble that of $Mg_{12}Ce$. Three examples will be presented in order of increasing complexity. In each case, the resulting solutions are probability relationships similar to those occurring in known structures.

The first case to be discussed will be the growth of a one-dimensional crystal consisting of two types of atoms A and B, and where the probability of whether an A or a B atom is deposited at the nth lattice site depends only on the type of atom already present at the (n-1)st lattice site. If an A atom is present at the (n-1)st lattice point, let the probability that an A atom is deposited at the nth lattice point be α , and the probability that a B atom is deposited be $1-\alpha$. If a B atom is present at the n-1st lattice point, let these probabilities be β and $1-\beta$, respectively. The notations A and B need not be restricted to

atoms. For example, identical one-dimensional periodic chains of atoms may be arranged to form a two-dimensional structure. If some of these chains are translated in the structure with respect to the others by one-half of their period, a sequence of the letters A and B can be used to describe the resulting configuration. (Translated and untranslated chains can be labelled A and B respectively.) The array of MgCeMg chains in the $Mg_{12}Ce$ structure is a three-dimensional configuration of precisely this nature. Two sequences of the letters A and B which are related by the interchange of all the A's with B's describe identical structures of this sort, one configuration merely being translated with respect to the other by one-half of the periodicity along the chain. Because of this equivalence, a reciprocity relationship is induced in the laws governing the growth of such a structure. If a certain configuration implies that an A chain (or atom) will be deposited next with a probability p, then the configuration formed from the first by the interchange of A's and B's implies that a B chain (or atom) will be deposited with the probability p. In the case now being discussed, this relationship implies that

$$\alpha = 1 - \beta. \qquad (179)$$

In each of the examples which will be presented, it will be assumed that the reciprocity relationship holds.

Let p_n be the probability of event A at the nth lattice site. The following table is therefore valid in the discussion of the first case. Corresponding to the growth law in table 41 is a difference equation relating the probability of occurrence of A (or B) at lattice sites (n-1) and n. In this simple example, this equation is readily derivable by the ordinary probability considerations. In the other cases to be discussed, considerations involving contingent probabilities make the formulation of the corresponding difference equations by the usual probability calculus more difficult. In order to avoid these difficulties, the same method of ensemble averaging that was used to derive the expressions for the odd layer structure factor contributions from groups of atoms in the $Mg_{12}Ce$ structure will be employed. Consider an ensemble of crystals growing according to the law in table 41. The growth of each crystal has proceeded up to the (n-1)st

Table 41. Growth law for case 1.

Occupancy at (n-1)st site	p_n Probability of A at nth site	$1-p_n$ Probability of B at nth site
A	α	$1-\alpha$
B	$1-\alpha$	α

lattice site. Let the fraction of crystals with an A event at site n-1 be m_A, and the fraction with a B event at site n-1 be m_B. If the total number of crystals in the ensemble is N (where N is very large), then the number of crystals that will have an A event at sites n-1 and n is $Nm_A\alpha$, and the number of crystals that will have a B event at site n-1 and an A event at site n is $Nm_B(1-\alpha)$. Since the probability of finding an A event at site n is the fraction of those crystals having an A event at this site,

$$p_n = m_A\alpha + m_B(1-\alpha) \quad . \tag{180}$$

Since

$$m_B = 1 - m_A \ , \tag{181}$$

$$p_n = 1-\alpha + (2\alpha -1)m_A \ . \tag{182}$$

In accord with the notion that the probability of an event in the fraction of times it occurs in an ensemble,

$$m_A = p_{n-1} \tag{183}$$

Substitution of equation 183 into 182 results in the desired difference equation

$$p_n = 1-\alpha + (2\alpha -1)p_{n-1} \ . \tag{184}$$

Equation 184 can be made homogeneous by the same substitu-

tion

$$p_i = 1/2 - 1/2\, r_i \tag{185}$$

that was so useful in discussing the odd layer diffraction data in the $Mg_{12}Ce$ structure. When this substitution is made, 184 becomes

$$r_n - (2\alpha - 1) r_{n-1} = 0. \tag{186}$$

It can be verified by substitution that the linear difference equation of degree A

$$\sum_{i=0}^{A} C_i r_{n-A+i} = 0 \tag{187}$$

has the solution

$$r_n = \sum_{j=0}^{A} Q_j R_j^n, \tag{188}$$

where each R_j is one of the A roots of the algebraic equation

$$\sum_{i=0}^{A} C_i x^i = 0\ , \tag{189}$$

and each Q_j is an arbitrary constant (which may be fitted to satisfy the initial conditions).

The algebraic equation corresponding to the first degree difference equation 186 is

$$x - (2\alpha - 1) = 0, \tag{190}$$

so that the solution is

$$r_n = Q(2\alpha - 1)^n. \tag{191}$$

Since α is a probability, $2\alpha - 1$ is a number which can be between -1 and 1. Thus a crystal following the growth law in table 41 has the following behavior. If it is known that lattice site zero is occupied by an A atom, then $r_o = 2p_o - 1 = 1$, and substitution into equation 191 shows that $Q = 1$. Unless α is zero or one, the absolute value of $2\alpha - 1$ is less than one, so that for sufficiently large values of n, r_n is very nearly equal to zero. This implies that at large distances from the site at which an A event is known to have occurred, the probability of finding an A event is equal to one-half, and is hence equal to the probability of finding a B event. In other words, the correlation effects vanish at long distances. If α is either zero or one, the absolute value of $2\alpha - 1$ is equal to one, so that the correlation function r_n is undamped. These instances correspond of course to ordered structures. If α is only slightly greater than zero, there will be a tendency for successive sites to have alternating configurations. This is the sort of short range order that was found in the radial distribution investigation of $AuCu_3$ (19).

Reference to equation 169 shows that the values of r in the $Mg_{12}Ce$ structure are the sums of exponentials of quantities proportional to the coordinates of the cerium sites (which would be proportional to n in a one-dimensional structure). Equation 169 differs from 191 in that the exponents in the former are purely imaginary, and combine to form undamped trigonometric functions. The quantities r associated with a row of cerium sites parallel to the a axis of the crystal thus vary trigonometrically along the row. It will be shown that similar trigonometric modulation results in one-dimensional growth when the probabilities associated with deposition at the nth lattice site depend on the configuration at the (n-1) st and (n-2)nd sites. Again assuming the reciprocity relationship to be valid in a structure containing two types of atoms A and B let the growth law be as shown in table 43. Defining m_1-m_4 as the fraction of crystals in an ensemble having the configurations 1-4, respectively, the following relationships are evident from table 42 and from the considerations made about probabilities in the discussion of case 1.

$$p_{n-2} = m_1 + m_3 \tag{192}$$

$$p_{n-1} = m_1 + m_4 \tag{193}$$

$$p_n = \alpha m_1 + (1-\alpha)m_2 + \beta m_3 + (1-\beta)\, m_4 . \tag{194}$$

Table 42. Growth law for case 2.

Configuration number	Occupancy at (n-2)nd site	Occupancy at (n-1)st site	p_n Probability of A at the nth site
1	A	A	α
2	B	B	$1-\alpha$
3	A	B	β
4	B	A	$1-\beta$

Since

$$m_1 + m_2 + m_3 + m_4 = 1 , \tag{195}$$

the following equations are also valid.

$$1 - p_{n-2} = m_2 + m_4 \tag{192'}$$

$$1 - p_{n-1} = m_2 + m_3 \tag{193'}$$

$$1 - p_n = (1-\alpha)m_1 + \alpha m_2 + (1-\beta)m_3 + \beta m_4 \tag{194'}$$

Since $r_1 = 2p_1 - 1 = p_1 - (1-p_1)$, subtracting 192' from 192, 193' from 193, and 194' from 194 results in

$$r_{n-2} = (m_1 - m_2) + (m_3 - m_4) \tag{196}$$

$$r_{n-1} = (m_1-m_2)-(m_3-m_4) \tag{197}$$

$$r_n = (2\alpha-1)(m_1-m_2)+(2\beta-1)(m_3-m_4) \tag{198}$$

It should be noted that in equations 196, 197, and 198, the quantities m occur only in the combinations (m_1-m_2) and (m_3-m_4). Equations 196 and 197 can therefore be used to eliminate the m's in equation 198, resulting in the homogeneous difference equation

$$r_n + (\beta-\alpha)r_{n-1} + (1-\alpha-\beta)r_{n-2} = 0 \tag{199}$$

The algebraic equation corresponding to 199 is

$$x^2 + (\beta-\alpha)x + (1-\alpha-\beta) = 0 \tag{200}$$

If the substitutions

$$1-\alpha-\beta = \theta^2 \tag{201}$$

$$\alpha-\beta = 2\theta\cos\frac{2\pi}{g} \tag{202}$$

are made, equation 200 becomes

$$x^2 - 2\theta\left(\cos\frac{2\pi}{g}\right)x + \theta^2 = 0, \tag{203}$$

which can be factored as follows.

$$x^2 - 2\theta\left(\cos\frac{2\pi}{q}\right)x + \theta^2 = x - \theta x e^{\frac{2\pi i}{q}} - \theta x e^{-\frac{2\pi i}{q}} + \theta^2$$
$$= \left(x - \theta e^{\frac{2\pi i}{q}}\right)\left(x - \theta e^{-\frac{2\pi i}{q}}\right) = 0 \qquad (204)$$

The roots of this equation are $\theta e^{\frac{2\pi i}{q}}$ and $\theta e^{-\frac{2\pi i}{q}}$, so that the solution to the difference equation 199 is

$$r_n = Q_1\left(\theta e^{\frac{2\pi i}{q}}\right)^n + Q_2\left(\theta e^{-\frac{2\pi i}{q}}\right)^n \qquad (205)$$

For the proper initial conditions, $Q_1 = Q_2$, and equation 205 becomes

$$r_n = 2Q_1\theta^n \cos\frac{2\pi n}{q} \qquad (206)$$

Equation 206 shows that for the growth law stated in table 42, the quantity r can be a trigonometric function of n which is damped exponentially by the factor θ^n. The damping constant θ and the periodicity q of the modulation depend on the probabilities α and β which appear in the growth law. The only solutions in which the trigonometric function is undamped have θ equal to 1 or -1. Reference to equation 201 shows that this situation can result only when α and β are zero, which corresponds to an ordered structure of periodicity four. For damped solutions, however, the periodicity can be made arbitrarily large. It can be shown that if the lattice grown according to this law is

regularly spaced, its x-ray diffraction pattern will consist of sharp diffraction maxima with intensities proportional to the square of the average scattering factor of the A and B atoms (or configurations), with broadened satellite reflections on each side of the sharp maxima. The intensities of the satellites are proportional to the square of the difference between the scattering factors of A and B, and have their maxima 1/qth the distance between the sharp maxima. Structures showing such phenomena have been reported. For example, when the intermetallic compound Cu_4FeNi_3 is heated at 650°C for one hour, diffuse sidebands develop which are similar to those discussed above (23).

The odd-layer reflections produced by the $Mg_{12}Ce$ structure are sharp, indicating that there is little or no damping of the trigonometric probability modulation waves. It may be that growth laws which depend on more than second nearest neighbors can produce undamped or very slightly damped modulation. Such situations are difficult to treat with the methods used here. Another way by which undamped solutions might result is by increasing the dimensionality of the growth. The problem of long range order is in general associated with the transmission of information from one point in the lattice to another. As the number of transmission paths increases greatly as the dimensionality is raised, more information could be transmitted from one point in the crystal to another, leading perhaps to undamped modu-

lation of the type being discussed. The third case to be discussed in this section will treat a two-dimensional growth problem which results in exponentially damped correlation in one direction as in equation 191, and in undamped trigonometric modulation in a direction normal to the first.

As the difficulties rapidly mount with increasing complexity of the crystal growth laws, an especially simple two-dimensional case will be presented. The growth of a two-dimensional rectangular lattice whose sites are indexed by k and ℓ will be treated. Once again, either of two configurations A and B will be deposited at each site. It will be assumed in this example that $p_{k\ell}$, the probability of deposition of an A configuration at site $k\ell$, depends only on the occupancy of sites k-2, ℓ; k-1, ℓ, and k,ℓ-1. If the reciprocity relationship is assumed, the growth law is expressible as in table 43.

In addition, it will be assumed that

$$\alpha - \beta - \gamma + \delta = 0. \tag{206}$$

The sole reason for imposing this restriction on the probabilities α, β, γ, and δ is that it enables the resulting difference equation to be solved by methods similar to those used in the previous cases. Define $m_1 \cdots m_8$ as the fraction of ensembles having configurations 1...8 as in table 43. By methods identical to those used to deduce equations 196,

Table 43. Growth law for case 3.

Configuration number	Occupancy at site			$p_{k,\ell}$ Probability of A at site k,ℓ
	$k-2,\ell$	$k-1,\ell$	$k,\ell-1$	
1	A	A	A	α
2	B	B	B	$1-\alpha$
3	A	A	B	β
4	B	B	A	$1-\beta$
5	A	B	A	γ
6	B	A	B	$1-\gamma$
7	A	B	B	δ
8	B	A	A	$1-\delta$

197, and 198, it is found that

$$r_{k-2,\ell} = (m_1-m_2)+(m_3-m_4)+(m_5-m_6)+(m_7-m_8) \tag{207}$$

$$r_{k-1,\ell} = (m_1-m_2)+(m_3-m_4)-(m_5-m_6)-(m_7-m_8) \tag{208}$$

$$r_{k,\ell-1} = (m_1-m_2)-(m_3-m_4)+(m_5-m_6)-(m_7-m_8)\ , \tag{209}$$

and

$$r_{k\ell} = (2\alpha-1)(m_1-m_2)+(2\beta-1)(m_3-m_4)+(2\gamma-1)(m_5-m_6)+(2\delta-1)(m_7-m_8). \tag{210}$$

Equations 207, 208, and 209 have the solutions

$$(m_3-m_4) = \tfrac{1}{2}(r_{k-2,\ell}+r_{k-1,\ell}) - (m_1-m_2) \tag{211}$$

$$(m_5-m_6) = \tfrac{1}{2}(r_{k-2,\ell}+r_{k,\ell-1}) - (m_1-m_2) \tag{212}$$

$$-(m_7-m_8) = \tfrac{1}{2}(r_{k-1,\ell}+r_{k,\ell-1}) - (m_1-m_2). \tag{213}$$

Substituting equations 211, 212, and 213 in 210 and collecting terms results in

$$r_k = (2\alpha-2\beta-2\gamma+2\delta)(m_1-m_2)+(\beta+\gamma-1)r_{k-2,\ell}+(\beta-\delta)r_{k-1,\ell} + (\gamma-\delta)r_{k,\ell-1}. \tag{214}$$

In view of assumption 206, equation 214 can be rewritten

$$(\beta+\gamma-1)r_{k-2,\ell} + (\beta-\delta)r_{k-1,\ell}+(\gamma-\delta)r_{k,\ell-1}-r_{k,\ell} = 0. \tag{215}$$

Equation 215 is separable if the substitution

$$r_k = X_k Y_\ell \tag{216}$$

is made, resulting in

$$(\beta+\gamma-1)X_{k-2}Y_\ell+(\beta-\delta)X_{k-1}Y_\ell+(\gamma-\delta)X_kY_{\ell-1} - X_kY_\ell = 0. \tag{217}$$

Division of equation 217 by X_kY_ℓ gives

$$(\beta+\gamma-1)\frac{X_{k-2}}{X_k}+(\beta-\delta)\frac{X_{k-1}}{X_k}+(\gamma-\delta)\frac{Y_{\ell-1}}{Y_\ell}-1 = 0, \tag{218}$$

or

$$1 - (\gamma-\delta)\frac{Y_{\ell-1}}{Y_\ell} = (\beta+\gamma-1)\frac{X_{k-2}}{X_k} + (\beta-\delta)\frac{X_{k-1}}{X_k} \qquad (218')$$

Since the left hand side of equation 218' is a function of ℓ only, and the right hand side a function of k only, each side must be independent of k and ℓ , and therefore equal to a constant K. Equation 218' is thus resolved into two equations: 219 involving the variation of $r_{k,\ell}$ in the direction, and 220 involving the variation in the k direction

$$1 - (\gamma-\delta)\frac{Y_{\ell-1}}{Y_\ell} = K \qquad (219)$$

$$(\beta+\gamma-1)\frac{X_{k-2}}{X_k} + (\beta-\gamma)\frac{X_{k-1}}{X_k} = K \qquad (220)$$

Equation 219 will be solved first. It can be rewritten

$$Y_\ell - \frac{\gamma-\delta}{1-K} = 0, \qquad (221)$$

and referring to case 1, has the solution

$$Y_\ell = Q_0\left(\frac{\gamma-\delta}{1-K}\right)^\ell \qquad (222)$$

Equation 220 may be rewritten

$$X_k + \frac{\delta-\beta}{K} X_{k-1} + \frac{1-\beta-\gamma}{K} X_{k-2} = 0. \qquad (223)$$

The solution of this equation, which is identical to that presented in case 2 is

$$X_k = Q_1(\theta e^{\frac{2\pi i}{\ell}})^k + Q_2(\theta e^{-\frac{2\pi i}{\ell}})^k, \qquad (224)$$

where now

$$\frac{1-\beta-\gamma}{K} = \theta^2, \qquad (225)$$

and

$$\frac{\delta-\beta}{K} = 2\theta \cos\frac{2\pi}{\ell}. \qquad (226)$$

The composite solution, from equations 216, 222, and 224

$$n_{k,\ell} = Q_0 \left(\frac{\gamma-\delta}{1-K}\right)^\ell (Q_1\theta^k e^{\frac{2\pi i k}{\ell}} + Q_2\theta^k e^{-\frac{2\pi i k}{\ell}}). \qquad (227)$$

It should be observed that constant Q_0 can be incorporated into Q_1 and Q_2 and therefore eliminated from equation 227 without loss of generality. Specification of the initial con-

ditions for a particular solution of case 3 requires fixing three arbitrary constants, for example, r_{11}, r_{21}, and r_{20}. It was the elimination of Q_0 in equation 227 that necessitated the introduction of the constant K into the solution. If $Q_1=Q_2=Q$ in equation 227, then

$$r_{k,\ell} = 2Q\left(\frac{\gamma-\delta}{1-K}\right)\theta^k \cos\frac{2k}{q}. \tag{228}$$

Some numerical values can be inserted in equation 228 that result in an array of probabilities somewhat like those shown in figure 12 which depicts the projection of the $Mg_{12}Ce$ structure onto the x,y plane. If the values for the probabilities α, β, γ, and δ required to specify the growth law in table 43 are 0.4, 1.0, 0.2, and 0.8 respectively, which satisfy restriction 206, and if Q = 1/2 and K = -0.2, then

$$\frac{\gamma-\delta}{1-K} = \frac{0.2-0.8}{1+0.2} = -\frac{1}{2}, \tag{229}$$

$$\theta^2 = \frac{1-\beta-\gamma}{K} = \frac{1-1.0-0.2}{-0.2} = 1, \tag{23}$$

and

$$2\theta\cos\frac{2\pi}{q} = \frac{\delta-\beta}{K} = \frac{0.8-1.0}{-0.2} = 1, \tag{231}$$

so that q = 6, and equation 228 becomes

$$r_{k,\ell} = \left(-\tfrac{1}{2}\right)^{\ell}\cos\frac{2\pi k}{6}. \tag{232}$$

Initial conditions which satisfy equation 232 are realizable, so the choice of 0 and K is justified. In the solution of the $Mg_{12}Ce$ structure represented in figure 12 there are six cerium sites along the rows parallel to the a axis for each cycle of trigonometric modulation. (The value of q in equation 232 was made 6 to be in accord with the $Mg_{12}Ce$ structure.) Furthermore, it should be noted that the negative damping factor in the ℓ direction is consistent with the proposed array of probabilities for the $Mg_{12}Ce$ structure. Where the probabilities p_α in one row of cerium sites ($y = 0$) are small, the probabilities at nearby sites in the neighboring row ($y = \frac{1}{2}$) are large, and vice-versa. (It must not be construed that the numerical values of α, β, γ, and δ given here are meant to represent deposition probabilities for the $Mg_{12}Ce$ structure. The numbers used above are convenient for calculation and give the desired values of θ^2 and q; other combinations would have sufficed.)

A growth law of the type treated in case 3 will not completely account for the array of probabilities found in $Mg_{12}Ce$. If the values of α, β, γ, δ, and K are such that there is no damping in the ℓ direction, then there necessarily results damping of the trigonometric modulation in the k direction which is no less than could have been obtained with the one-dimensional example. It is certainly reasonable to expect in structures such as $Mg_{12}Ce$ growth laws more complicated than those treated here. Cross-term interactions in two-

dimensional growth laws, which were neglected in case 3, might lead to solutions in which there is less damping.

A growth phenomenon which should not be neglected as a possible explanation of the disorder in $Mg_{12}Ce$ is the formation of ordered domains. The distribution of diffracted intensity from a disordered structure consisting of two types of atoms is related to the probabilities of finding A or B atoms at various distances from an atom known to be A or B. It will be shown that certain nearly ordered structures can lead to probability modulation which is virtually undamped even when the growth is one-dimensional. Consider the growth law shown in table 44 for a structure containing two types of atoms which dictates that each atom shall be unlike its

Table 44. Growth law leading to undamped modulation.

Configuration number	Configuration of three successive atoms	Next atom deposited
1	AAA	B
2	AAB	B
3	ABA	B
4	ABB	B
5	BAA	A
6	BAB	A
7	BBA	A
8	BBB	A

third nearest neighbor. This growth law differs from the other ordered laws discussed in that it corresponds to a

decomposable Markov chain. Depending on the initial configuration two distinct structures can occur, each of which will be repeated indefinitely if there are no defects (violations of the law). Initial configurations 3 and 6 in table 44 result in th ABABABAB···· structure, and the other configurations produce the AAABBBAAABBB···· structure. If there are occasional defects during the growth of the crystal, the structure will consist of ordered domains of each arrangement. If it is known that the atom at the nth site in the structure is A, there will be probability relationships involving the occupancy at other sites. Except in the neighborhood of a defect, there can be four sequences whose first member is A, namely AAABBBAAABBB····, AABBBAAABBBA····, ABBBAAABBBAA····, and ABABABABABAB···· . If the defects are appropriately random, each configuration will occur an equal number of times. Providing that this is the case, it is apparent upon examination of the four sequences that the array of quantities $r=p(A)-p(B)$ corresponding to the average is $1,0,0,-1,0,0,1,0,0,-1,0,0,\cdots$. That this is a trigonometric modulation leading to non-space group absences in the diffraction pattern can be appreciated if it is observed that the sequence of r's can be represented by the undamped function

$$r_n = \frac{2}{3}\cos\frac{2\pi n}{6} + \frac{1}{3}\cos\frac{2\pi n}{2}. \qquad (233)$$

The purpose of this final section has been to show how

when reasonable interactions during the growth of a crystal are assumed, complex structures can occur, which may possess in particular disorder of the type encountered in $Mg_{12}Ce$. Nevertheless, only when a growth law is found which is consistent with the known principles of the structure of metals, and which is shown to lead to an array of probabilities in agreement with the x-ray diffraction data, can the $Mg_{12}Ce$ structure be regarded as fully understood. Examples have been presented (tables 31, 34, and 35-40) showing how the analysis of ordered sequences or configurations can lead to sets of growth laws which describe the interactions of neighboring atoms. If a method could be found to analyze the probability arrays in disordered structures as complex as $Mg_{12}Ce$ into corresponding growth laws, a new way would be opened for the study of structural fundamentals.

II. Reaction Products of γ-Picoline and Iodine.*

A. Introduction.

A considerable body of experimental evidence has been collected concerning the complexes between pyridine and its homologs with iodine. The nature of these complexes has been the subject of some discussion. The main problem has been to determine whether the interactions between iodine and the organic base are strong enough to break the iodine-iodine bond, leading to ionization, or whether a covalent iodine molecule still exists in the addition compound. Since a knowledge of this distribution of iodine-iodine distances in the solid complex would be sufficient to resolve this problem, it was thought that an x-ray radial distribution analysis would be applicable, rather than a complete crystal structure determination (as suggested by Reid and Mulliken (24)), which would be enormously more laborious. Such questions as the relative spatial orientation of the iodine molecule with respect to the organic base are not answered by the radial distribution method, and fall outside the objectives of the present investigation.

The organic base γ-picoline was used rather than pyridine because its addition compounds with iodine were found to be

---

*This section is the text of a paper co-authored with Dr. Donald L. Glusker and submitted for publication in the Journal of Chemical Physics.

more stable. From the γ-picoline-iodine system it was possible to isolate two distinct compounds, both of which were investigated chemically, spectroscopically, and by the x-ray radial distribution method.

The first of these was a stable, water-soluble, alcohol-insoluble compound, (I), whose analysis corresponded to two moles of γ-picoline per mole of iodine (25a,b). The apparent anomalous behavior of this compound when compared with the complexes of iodine with the other picolines and with pyridine led to a search for another compound, essentially covalent, corresponding to the well-known solid pyridine-iodine complex reported by many workers (26). Other evidence which pointed to the existence of a second compound was that solutions of iodine in γ-picoline do not set solid until several hours after mixing, whereas the changes produced in the absorption frequencies of γ-picoline are immediate (25b). These changes in spectra are also entirely analogous to those observed in pyridine and the other picolines upon the addition of iodine. The second compound, (II), was isolated by the addition of water to a freshly prepared solution of iodine in excess γ-picoline. Its analysis corresponded to an equimolar addition compound between the iodine and the organic base.

The radial distribution method leads directly to information about the atomic configuration in a non-crystalline or powdered crystalline substance. Making the approximation

that the radial distribution of electrons associated with each atom in the structure is the same except for a constant factor, one may calculate from the distribution of intensity on an x-ray powder photograph or diffractometer tracing of the substance the weighted summation over each atom M in the molecule of the quantity $4\pi r^2 g_M(r)$, where $4\pi r^2 g_M(r)dr$ is the number of electrons associated with atoms lying within a spherical shell of radius r and of thickness dr surrounding a given atom M in the molecule. It is not necessary to index the powder photograph or to introduce any arguments concerning crystal symmetry or steric relationships as is done in other methods of structure analysis.

B. Compound (I). $C_{12}H_{14}N_2I_2$.

1. Experimental.

In the course of spectroscopic investigations on solutions of iodine in pyridine and its homologs, a saturated solution of resumblimed iodine in 99.77% pure γ-picoline (obtained from the National Chemical Research Laboratories, Teddington, England) was prepared under anhydrous conditions. It set to a solid mass after approximately two hours. The mixture was partially soluble in ethyl alcohol. The insoluble residue, (I), which proved to be water-soluble, and insoluble in the common organic solvents, was washed with ether and recrystallized from water-alcohol mixtures as a light brown microcrystalline solid. Its melting point is

223-4°C with decomposition, and its density approximately 1.9 gms./cm.^{3} Ether washings from a sample prepared by one of us two years previously were colorless, indicating that negligible dissociation had taken place during that time. Chemical analysis and equivalent weight determined from the freezing point depression of water solutions were consistent with an ionic formula $C_{12}H_{14}N_2I^+ I^-$. The analytical data for compound(I)are summarized in table 45. A precipitate of silver iodide is formed immediately upon the addition of acidified silver nitrate solution to an aqueous solution of (I).

Table 45. Composition and Molecular Weight of Compound (I).

$C_{12}H_{14}N_2I_2$

Analysis	% C	% H	% N	% I
Calculated	32.75	3.21	6.37	57.68
Found	34.32	3.34	6.25	56.05

Formula weight	440
Equivalent weight*	220
Cryoscopic equivalent weight	216

*Based on dissociation into two particles

For collecting the x-ray intensity data of compound (I), the conventional procedure of measuring the intensity distribution of an x-ray powder photograph with a recording micro-

photometer was used. The photographs were taken using filtered copper radiation (λK_α = 1.5418 Å). The intensities measured on the microphotometer tracing corrected in the usual fashion for absorption and polarization were plotted versus $s = 4\pi \sin\theta/\lambda$. The maximum value of s for which intensities were measurable on the powder photograph was 7.624 $Å^{-1}$ ($= s_{max}$).

2. Calculations.

The measured intensity distribution must be placed on an absolute scale, and the Compton scattering subtracted. This was accomplished by Warren's method (27a,b), which is based on equating the observed intensity at large values of s, where the structural features no longer influence the scattering, to the intensity distribution calculated for a random array of atoms. After the corrected intensity distribution, I(s), had been obtained, the radial distribution function was calculated (27a,b) according to the equation

$$4\pi r^2 \sum_M K_M [g_M(r) - g_o] = \frac{2r}{\pi} \int_o^\infty s\, i(s) \sin sr\, ds, \qquad (234)$$

where

$$i(s) = \left[\frac{I(s)}{N I_e \sum_M f_M^2} - 1 \right] \sum_M Z_M^2 \qquad (235)$$

In these equations, g_o is the average electron density in the substance,* f_m is the atomic scattering factor for the Mth atom in the molecule, N is the effective number of molecules in the x-ray beam, I_e is the intensity scattered by a classical free electron, and K_M is the effective weighting factor for the Mth atom, which was equated here to Z_M, the atomic number.

In practice, it is not possible to evaluate the integral in equation 234 to the limit $s = \infty$ but rather only to $s = s_{max}$. In order to decrease spurious detail in the calculated radial distribution function introduced by terminating the integral at s_{max} and by assigning too much weight to intensity measurements at large values of s, the following modified forms of equations 234 and 235 are used.

$$4\pi r^2 \sum_M K_M [g'_M(r) - g_o] = \frac{2r}{\pi} \int_0^{s_{max}} s\, i'(s) \sin sr\, ds, \qquad (234')$$

where

$$i'(s) = \left[\frac{I(s)}{N I_e \sum_M f_M^2} - 1 \right] e^{-B's^2} \sum_M Z_M^2. \qquad (235')$$

The introduction of the convergence factor $e^{-B's^2}$ broadens each peak in the radial distribution function due to a pair of atoms (i,j) without changing its area (28). The value of

*The quantity g_o refers to the average electron density within the individual particle of the substance, and not to the electron density of the gross sample, including its interstices. This point has been the subject of some confusion in other discussions of the x-ray radial distribution method.

of B' was chosen such that $e^{-B's^2}$ max is equal to one-tenth.

In this investigation the corrected intensity curve was separated into two parts: the set of discrete peaks corresponding to lines on the powder photograph, and a slowly varying curve through the bases of these peaks. In calculating the integral in equation 234' the slowly varying portion was divided into 100 equal intervals over the range of s. For each discrete peak, the value of s assigned was the closest integral multiple of $s_{max}/500$.

Values of si' (s) and the contributions from the discrete peaks adjusted to the same scale are shown in table 46. A scale factor of 26.9 has been introduced to bring the figure to a convenient range for the next stage of the calculation.

The integral in equation 234' was evaluated by the same punched card method as is used for electron diffraction computations carried out at the California Institute of Technology (29). The resulting function $4\pi r^2 \sum_M K_M \times [g_M(r)-g_o]$ has been plotted in figure 13 (curve A) together with the function $-4\pi r^2 \sum_M K_M g_o$ calculated from the empirical formula and measured density of the compound (curve B). The area enclosed between a peak at $r = r_A$ on curve A and the base curve B is approximately $\sum_{i,j} Z_i Z_j$, the sum over the molecule of the products of atomic numbers of atom pairs whose separations are sufficiently close to r_A to be included under the peak. Curve C is the calculated contribution to the differential radial distribution function for the pair

Table 46. Intensity Data for the Radial Distribution Analysis of Compound (I).

$C_{12}H_{14}N_2I_2$ $\quad E(s) = 26.9\ si'(s)/\sum_M Z_M^2$

	500s s_{max}	E(s)	500s s_{max}	E(s)	500s s_{max}	E(s)	500s s_{max}	E(s)
Continuous	5	-2	130	19	255	5	380	1
	10	-2	135	19	260	2	385	0
	15	-2	140	14	265	3	390	0
	20	-1	145	16	270	6	395	1
	25	1	150	12	275	8	400	0
	30	6	155	8	280	8	405	0
	35	9	160	9	285	9	410	0
	40	18	165	10	290	8	415	0
	45	20	170	9	295	7	420	0
	50	15	175	11	300	6	425	0
	55	12	180	6	305	8	430	0
	60	11	185	8	310	7	435	1
	65	12	190	8	315	6	440	1
	70	13	195	8	320	7	445	0
	75	16	200	10	325	8	450	-1
	80	18	205	10	330	9	455	0
	85	23	210	6	335	9	460	-1
	90	26	215	10	340	9	465	0
	95	28	220	6	345	8	470	0
	100	45	225	8	350	7	475	0
	105	31	230	5	355	5	480	0
	110	34	235	6	360	4	485	-1
	115	29	240	6	365	3	490	0
	120	24	245	5	370	2	495	-1
	125	19	250	3	375	1	500	-1
Discrete Portion	57	9	84	8	102	19	132	28
	68	2	92	23	115	42	141	16
	73	6	95	24	122	16	150	38

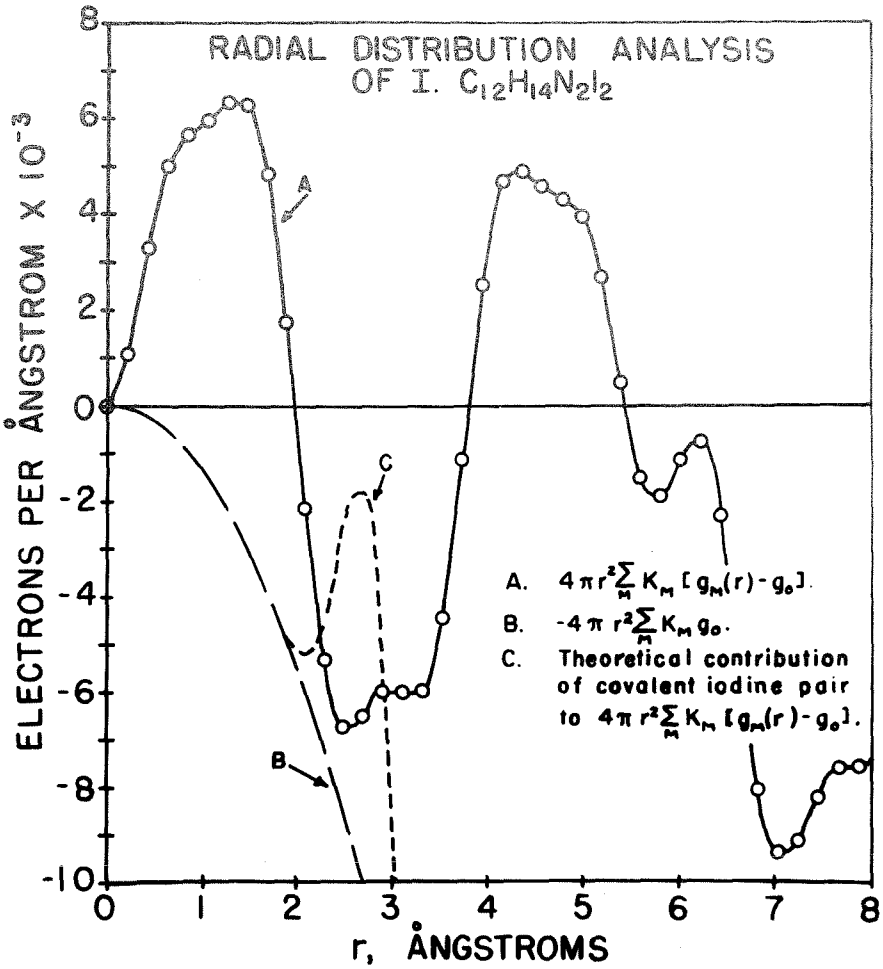
RADIAL DISTRIBUTION ANALYSIS
OF I. $C_{12}H_{14}N_2I_2$
ELECTRONS PER ÅNGSTROM X 10^{-3}
r, ÅNGSTROMS
A
B
C
A. $4\pi r^2 \sum_M K_M [g_M(r) - g_o]$.
B. $-4\pi r^2 \sum_M K_M g_o$.
C. Theoretical contribution of covalent iodine pair to $4\pi r^2 \sum_M K_M [g_M(r) - g_o]$.

FIGURE 13.

of iodine-iodine interactions in the neighborhood of 2.66 Å that must be present if covalent bonding exists between iodine atoms.

C. Compound (II). $C_6H_7NI_2$.

1. Experimental.

The obvious difference between the properties of compound (I) and those of the pyridine-iodine solid complex ($Py.I_2$) seemed to indicate that (I) was not the simple 1:1 complex, but something else. The compound $Py.I_2$ is precipitated by the addition of water to pyridine-iodine solutions. In an analogous fashion, it was attempted to isolate compound (II) by the addition of water to a solution of iodine in γ-picoline.

The following procedure was a satisfactory method for the isolation and purification of (II). To an excess of γ-picoline was added a saturated solution of iodine in ethanol. This was followed immediately by the addition of water. The precipitate was filtered and washed with water containing approximately 1% picoline. The compound was dried in a stream of nitrogen and stored in a refrigerator at 0°C. Under these conditions no noticeable decomposition took place over a period of one year. When compound (II) was left in a desiccator under nitrogen at room temperature, it decomposed to a tarry mass within two days. There are appreciable vapor pressures of picoline and iodine over the solid com-

pound. Compound (II) is soluble in most organic solvents, undergoing slow decomposition. When (II) is added to γ-picoline, it dissolves without decomposition, and the slow formation of (I) can be detected. Compound (II) can be crystallized from most solvents by evaporation. Table 47 lists the results of the chemical analysis of (II), which are consistent with the formula $C_6H_7NI_2$, corresponding to an equimolar addition product of iodine and picoline. No molecular weight was determined because the compound undergoes partial dissociation in solution. Compound (II) melts sharply at 83.2-83.4°C., and has a density of 2.45 gms./cm.^{3} at 20°C.

It was decided to investigate the applicability of a recording x-ray diffractometer for collecting the intensity data for the radial distribution analysis of (II). This instrument records the intensity of x-radiation scattered from a specimen directly as a function of the Bragg angle by means of a movable Geiger counter tube. In addition to being

Table 47. Composition of Compound (II).

$C_6H_7NI_2$

Analysis	% C	% H	% N	% I
Calculated	20.75	2.02	4.03	73.20
Found	19.49	1.84	3.60	75.01

more rapid than powder photography and subsequent microphotometry, the diffractometer method has the advantages that (with the proper type of specimens) the absorption correction is independent of the Bragg angle (2θ), and that the ratio of spuriously scattered to diffracted intensity is smaller than with the Debye-Scherrer technique. A General Electric model XRD-3 recording diffractometer was used with filtered copper radiation from an x-ray tube excited to 25 kilovolts peak at a space current of 15 milliamperes. Results satisfactorily free from the effects of preferred orientation of crystallites in the sample were obtained by using the mounting procedure described by McCreery (31), and the compound was sufficiently stable in air to permit scanning at the rate of 0.2 degrees of 2θ per minute. The diffraction pattern of (II) differed from that of (I) in that it consisted entirely of a series of discrete peaks on a monotonously varying background. Forty-nine peaks were observed to a value of $s_{max} = 4.518$ Å^{-1}.

2. Calculations

The procedure of calculating the radial distribution function when the intensity data is in the form of discrete peaks differs somewhat from the method used in computing the radial distribution function of compound (I) and has not previously been presented completely. For a scatterer giving discrete Bragg peaks, I(s), which appears in equation

235' can be written as

$$I(s) = I_{Bragg} + I'_{ind} \tag{236}$$

where I_{Bragg} is the discrete intensity distribution of the Bragg peaks, and I'_{ind} is the elastic scattering produced by the aperiodic component of the electron density in the crystal which is due to thermal vibrations. At large values of s, where the temperature factor has sufficiently reduced the intensities of the Bragg peaks, I'_{ind} approaches $NI_e\sum_M f_M^2$. If each atom in the structure has the same isotropic temperature factor e^{-Bs^2}, I'_{ind} can be approximated by

$$I'_{ind} \simeq NI_e(1-e^{-B\Delta^2})\sum_M f_M^2 . \tag{237}$$

Substituting equations 235', 236, and 237 in 234' results in

$$4\pi r^2\sum_M K_M[g'_M(r)-g_o] =$$

$$\frac{2r}{\pi}\left(\sum_M Z_M^2\right)\int_0^{\Delta_{max}} s\left[\frac{I_{Bragg}+NI_e(1-e^{-B\Delta^2})\sum_M f_M^2}{NI_e\sum_M f_M^2}-1\right]e^{-B'\Delta^2}\sin sr\,ds$$

$$\simeq \frac{2r}{\pi}\left(\sum_M Z_M^2\right)\left[\int_0^{\Delta_{max}} s\,\frac{I_{Bragg}}{NI_e\sum_M f_M^2}e^{-B'\Delta^2}\sin sr\,ds-\int_0^{\infty} s\,e^{-(B+B')\Delta^2}\sin sr\,ds\right]$$

$$= \frac{2r}{\pi}\left(\sum_M Z_M^2\right)\left[\int_0^{\Delta_{max}} s\,\frac{I_{Bragg}}{NI_e\sum_M f_M^2}e^{-B'\Delta^2}\sin sr\,ds-\frac{r\pi^{1/2}}{4(B+B')^{3/2}}e^{-\frac{r^2}{4(B+B')}}\right]. \tag{238}$$

Since $s = 4\pi\sin\theta/\lambda$, $ds = \frac{4\pi}{\lambda}\cos\theta d\theta$, and

$$\int_0^{s_{max}} s\,\frac{I_{Bragg}}{NI_e\sum_M f_M^2}\,e^{-B's^2}\sin sr\,ds = \int_0^{\theta_{max}} I_{Bragg}\,\frac{16\pi^2\sin\theta\cos\theta}{\lambda^2 NI_e\sum_M f_M^2}\,e^{-B's^2}\sin sr\,d\theta. \quad (239)$$

Because the function I_{Bragg} is in the form of narrow peaks having a sufficiently small range of θ, the other functions in the integral do not vary appreciably over a single peak, and the right-hand side of equation 239 can be expressed as the summation

$$\frac{16\pi^2}{\lambda^2}\sum_j \frac{\sin\theta_j\cos\theta_j}{NI_e\sum_M f_{Mj}^2}\,e^{-B's_j^2}A_j\sin s_j r\,,$$

where $A_j/NI_e\sum_M f_{Mj}^2$ is the ratio of the integrated counting rate for the jth. Bragg peak (in counts per second integrated over radians of Bragg angle) to the scattering due to an independent array of atoms. The summation indexed by j is over the observed Bragg peaks. Substituting this expression for the integral in equation 238 gives

$$4\pi r^2\sum_M K_M[g'_M(r)-g_o] = \frac{2r}{\pi}\left(\sum_M Z_M^2\right)\left[\sum_j C_j\sin s_j r - \frac{r\pi^{1/2}}{4(B+B')^{3/2}}\,e^{-\frac{r^2}{4(B+B')}}\right], \quad (240)$$

where

$$C_j = \frac{16\pi^2\mu'}{\lambda^2}\left(\frac{2m^2c^4R^2}{PAaI_0e^4}\right)\frac{\sin 2\theta_j\, e^{-B'\frac{\sin^2\theta_j}{\lambda^2}} A_j}{(1+\cos^2 2\theta_j)\sum_M f_{Mj}^2}. \qquad (241)$$

The diffractometer used was not sufficiently stable so that the scale factor could be reliably estimated by observing the counting rate at large angles. It is therefore necessary to introduce the quantity $\left(\frac{2m^2c^4R^2}{PAaI_0e^4}\right)$, which is the proportionality factor relating on an absolute basis the intensity scattered by a random array of atoms to the counting rate actually observed with the diffractometer. In this expression, e and m are respectively the charge and mass of the electron, c is the velocity of light, R is the distance between the scatterer and the detector, A is the cross-sectional area of the x-ray beam at its point of intersection with the specimen, a is the acceptance area of the detector, I_0 is the intensity of the x-radiation incident on the scatterer in ergs/cm.^{2}sec., and P is the detection efficiency of the Geiger tube in counts per erg. This constant of the instrumentation was determined by measuring the intensities diffracted by a sodium chloride standard. In equation 241, μ' is the molecular absorption coefficient

of the substance.

Equations 240 and 241 are the working expressions for the computation of the radial distribution function from diffractometer data consisting of discrete Bragg peaks. (Numerical values of $\sin 2\theta_j/(1+\cos^2 2\theta_j)$ were obtained from Buerger's tables (32).) For each of the observable Bragg peaks, the quantity $1030\ C_j$ is listed in table 48 with the corresponding frequency of the contribution, in units of $s_{max}/500$. The coefficient B in equation 240 was estimated by a modification of Wilson's method (33) to be 0.057Å^2, and the Fourier sum was evaluated by the same punched card method mentioned previously. The quantities $4\pi r^2 \sum_M K_M [s_M(r)-s_o]$ and $-4\pi r^2 \sum_M K_M s_o$ are plotted in figure 14 together with the theoretical contribution to the differential radial distribution function from a pair of iodine atoms separated by 2.66Å.

D. Interpretation of the Radial Distribution Curves.

A striking feature of both radial distribution curves (A in figures 13 and 14) is the peak between 4 and 5Å. The presence of such a peak indicates that more than the average amount of electron density is associated with atoms that have separations within this range. The region between 4 and 5Å is expected to be well populated in both compounds; the van der Waals contacts I···I, I···I^-, and I^-···I^- should all occur at about 4.3Å, and the van der Waals C···I contacts being at about 4Å, these and the next nearest non-bonded

Table 48. Intensity Data for the Radial Distribution Analysis of Compound (II)

$C_6H_7NI_2$

500s s_{max}	1030Cj	500s s_{max}	1030Cj	500s s_{max}	1030Cj	500s s_{max}	1030Cj	500s s_{max}	1030Cj
48	37	157	18	231	28	311	37	375	11
84	9	164	100	236	27	313	20	387	14
85	13	172	85	242	22	321	40	398	23
92	29	179	8	249	75	328	13	418	8
101	10	182	18	258	41	332	16	444	22
108	34	189	17	269	53	334	33	455	20
119	41	200	89	281	16	343	62	478	5
137	19	203	28	293	16	353	7	491	6
140	13	219	48	299	34	361	22	500	12
154	24	225	82	305	14	368	22		

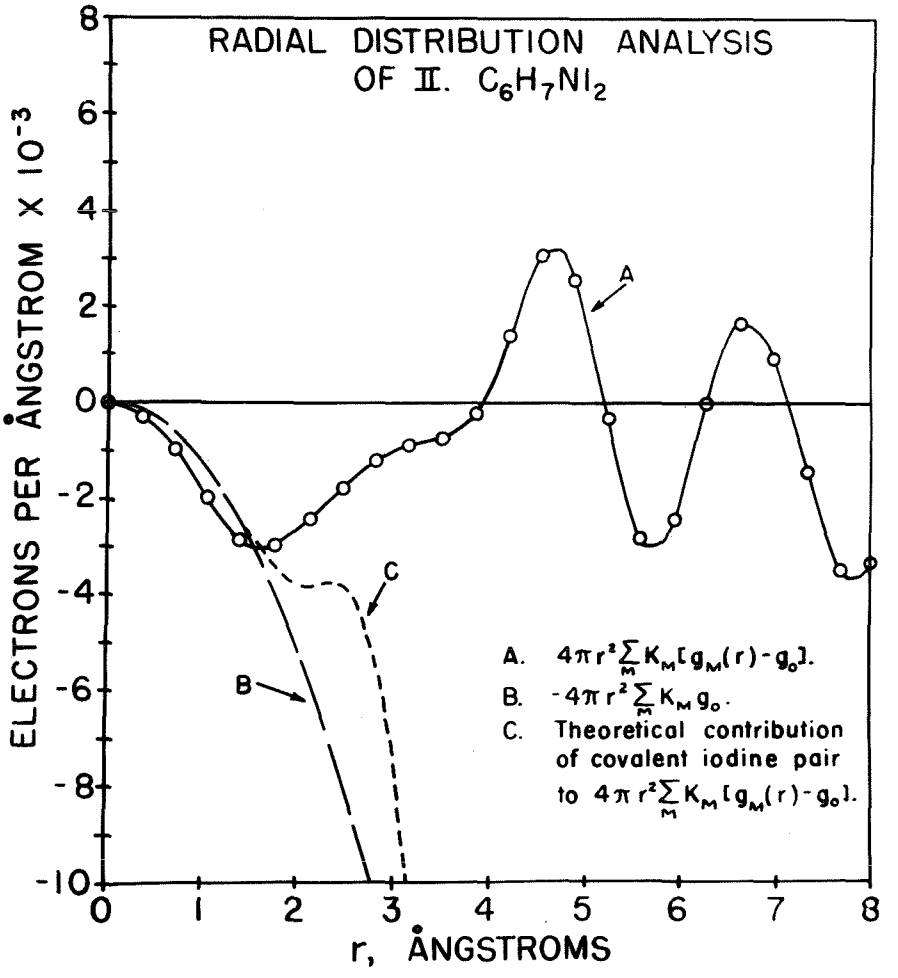
RADIAL DISTRIBUTION ANALYSIS
OF II. $C_6H_7NI_2$
ELECTRONS PER ÅNGSTROM X 10^{-3}
r, ÅNGSTROMS
A
B
C
A. $4\pi r^2 \sum_M K_M [g_M(r) - g_o]$.
B. $-4\pi r^2 \sum_M K_M g_o$.
C. Theoretical contribution of covalent iodine pair to $4\pi r^2 \sum_M K_M [g_M(r) - g_o]$.

FIGURE 14.

C···I will also fall in the interval from 4 to 5Å.

The curve for compound (I) (but not for compound (II)), has a prominent peak at 1.5Å. This peak is much too large to be due to the interactions near this distance, which are all between light atoms; it must be almost entirely the result of errors in the measured intensity distribution. Spurious peaks near the origin are sometimes encountered in radial distribution functions computed from electron diffraction data, and do not vitiate the validity of the function at larger values of r. They result from incorrect estimation of the average background, which is analogous to the function $NI_e \sum_M f_M^2$ in the present investigation. The error in the measured intensity distribution which would have to be present to produce the spurious peak was calculated as a function of s. The calculated error in i'(s) falls smoothly from a maximum value at s = 0 to nearly zero in the region of s that was used to establish the scale factor by Warren's method. This type of error, both in its variation with s and its magnitude, is what can reasonably be expected from misestimation of the absorption factor and from extraneous scattering by the walls of the capillary in which the specimen of compound (I) was mounted. The diffractometer technique used to collect the intensity data for compound (II) eliminates these errors, so that the radial distribution function for this compound has no false peak at the origin.*

*The erroneous variation of measured intensity for compound (I) is observable in the values of si'(s) presented in

From the radial distribution function it is possible to determine whether or not there are I-I interactions at about 2.66Å, and hence if there is covalent iodine-iodine bonding. Because the significant van der Waals separations in each structure are all longer than 3.5Å, the features in the radial distribution curves at smaller values of r must be due to predictable intramolecular interactions. The most significant points are displayed in table 49, in which the areas measured between the radial distribution curves A and the base parabolas B within limits of r corresponding to intramolecular interactions are compared with $\sum_{ij} Z_i Z_j$ as computed for all atoms i and j separated between these limits for covalent and ionic models of each compound. The range of r, from 1.9 to 3.0Å is chosen because it includes the region where the covalent iodine-iodine contributions would occur (See curves C, figures 13 and 14.), and because it is suffi-

---

table 46. These values are predominantly positive for intermediate values of s, whereas si'(s) should be a function which fluctuates around zero. In table 46, the observed deviations of the average values of si'(s) nearly coincide with the error term calculated by assuming that the peak at 1.5Å is spurious. Therefore, the errors in the measured intensity distribution are such that they will introduce the peak at 1.5Å without significantly affecting the features of the radial distribution curve at greater values of r. The minimum in the radial distribution function of compound (I) near 2.5Å, the presence of which is critical in the interpretation of the structure, cannot be appreciably in error. If it were, an error term would have to be introduced in the measured intensity distribution which oscillates through no less than three cycles in the observable range of s. No plausible experimental error could produce such a variation.

Table 49. Contributions between 1.9 and 3.0Å for covalent and ionic models of compounds (I) and (II). Interactions involving hydrogen are neglected.

Compound I.	Covalent I-I bond				
	Present		Absent		
	32 C-C	32x6x6	32 C-C	32x6x6	
	12 C-N	12x6x7	12 C-N	12x6x7	Area measured from figure 13
	4 N-I	4x7x53	4 N-I	4x7x53	
	4 C-I	4x6x53	4 C-I	4x6x53	
	2 I-I	2x53x53			
		10,030		4,412 Totals	3,900
Compound II	16 C-C	16x6x6	16 C-C	16x6x6	
	6 C-N	6x6x7	6 C-N	6x6x7	Area measured from figure 14
	2 N-I	2x7x53	2 N-I	2x7x53	
	4 C-I	4x6x53	4 C-I	4x6x53	
	2 I-I	2x53x53			
		8,460		2,806 Totals	8,400

ciently removed from the regions of the van der Waals interactions and the false peak in figure 13 discussed above. An ionic structure for compound (I) and a covalent structure for compound (II) are clearly indicated. For each compound, the discrepancy between the measured area on the radial distribution curve and the sum of the interactions in the alternative model significantly exceeds the reasonable limits of error.

E. Conclusions.

The data which have been collected by other workers and in the course of the present investigation lead us to propose the following sequence for the reaction of iodine with γ-picoline:

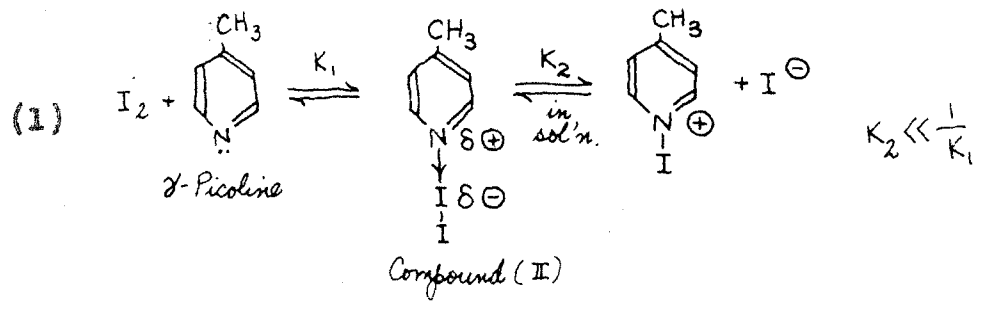

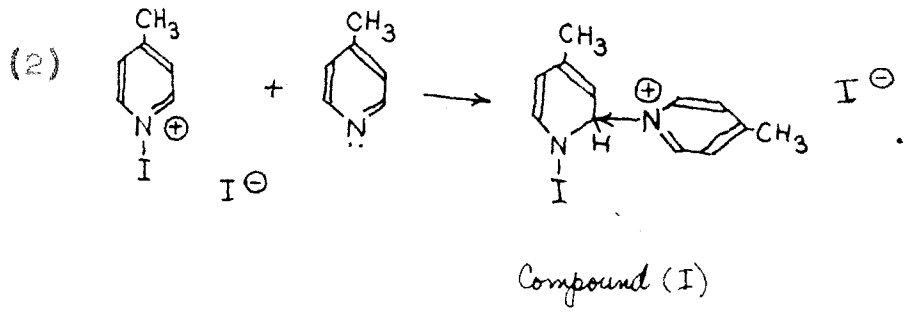

(The α addition of the second molecule of picoline to the ionized form of (II), as here indicated, seems reasonable in view of the resonance representation of (II) by several Lewis structures, including

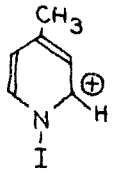

$I^{\ominus}$.)

The following evidence strongly supports the conclusion that (II) is a picoline-iodine addition complex analogous to the pyridine-iodine complex:

1. The changes in the infra-red spectra of pyridine and of γ-picoline caused by the addition of iodine are similar (25b).

2. After being stored for nearly a year at 0°C., compound (II) yielded an infra-red spectrum in carbon disulfide solution which was in all respects identical with that found for freshly prepared solution of iodine and γ-picoline in carbon disulfide. (The spectrum of the latter has previously been published (25b).)

3. Compound (II), like $Py.I_2$, is insoluble in water, and soluble with decomposition in most organic solvents. Its dilute solutions in carbon disulfide show the purple color characteristic of free iodine in this solvent. More concentrated solutions are brown in color, as is characteristic of complexed iodine. This behavior is consistent with the partial dissociation of the compound in accord with the law

of mass action.

Evidence for the existence of equilibria of the type K_2 in the pyridine system has been gathered in the following experiments:

1. Radioactive exchange experiments using I_2^{131} have shown the presence of PyI^+ ions in iodine-pyridine solutions (34).

2. Measurements of the electrical conductivity of pyridine-iodine solutions show a small initial conductivity which increases slowly with time (35). The initial value has been ascribed to a small concentration of PyI^+ and I^- ions in the solution, and the increase with time to reactions of iodine with the ring, or perhaps to those of the type shown in reaction (2) above. The occurrence of a slow chemical reaction between iodine and pyridine has been found by other workers also (36a,b).

References

1. Vogel, R., Z. anorg. Chem. 91, 277 (1915).

2. Raeuchle, R. F., and Rundle, R. E., Acta Cryst. 5, 85 (1952).

3. Raeuchle, R. F., Acta Cryst. 6, 107 (1953).

4. de Lange, J. J., Robertson, J. M., and Woodward, I., Proc. Roy. Soc. (London) A 171, 398 (1939).

5. Nelson, J. B., and Riley, D. P., Proc. Phys. Soc. (London) 57, 160 (1945).

6. Reddick, H. W., and Miller, F. H., "Advanced Mathematics for Engineers," John Wiley and Sons, New York, 362 (1947).

7. Rossi, A. Jandelli, Atti accad. naz. Lincei Rend. VI 19, 415 (1934).

8. X-Ray Diffraction Data Cards, American Society for Testing Materials, Philadelphia (1949).

9. Bergman, G., and Jaross, R. W., Acta Cryst. 8, 232 (1955).

10. Bunn, C. W., "Chemical Crystallography," Oxford, 244 (1946).

11. International Tables for X-Ray Crystallography, Kynoch Press, Birmingham, England, Volume 1 (1952).

12. Pauling, L., "The Nature of the Chemical Bond," Cornell Univ. Press, Ithaca, New York, 410 (1948).

13. Dunn, C. W., op. cit., 209.

14. Bergman, G., Waugh, J. L. T., and Pauling, L., Nature 169, 1057 (1952).

15. Haucke, W., Z. anorg. u. allgem. Chem. 244, 17 (1940).

16. Goldish, E., Thesis, California Institute of Technology (1956).

17. Florio, J. V., Baenziger, N. C., and Rundle, R. E., Acta Cryst. 9, 367 (1956).

18. Raeuchle, R. F., and von Batchelder, F. W., Acta Cryst. 8, 691 (1955).

19. Cowley, J. M., J. Appl. Phys. 21, 24 (1950).

20. Johansson, C. H., and Linde, J. O., Ann. Physik, 25, 1 (1936).

21. Feller, W., "An Introduction to Probability Theory and its Applications," John Wiley and Sons, New York, Volume 1, 307 (1950).

22. Pauling, L., op. cit., 378.

23. Daniel, V., and Lipson, H., Proc. Roy. Soc. (London) A 181, 368 (1943).

24. Reid, C., and Mulliken, R. S., J. Am. Chem. Soc. 46, 3869 (1954).

25a. Glusker, D. L., Thompson, H. W., and Mulliken, R. S., J. Chem. Phys. 21, 1407 (1953).

25b. Glusker, D. L., and Thompson, H. W., J. Chem. Soc. 471, (1955).

26. For example, see Chatelet, M., Compt. Rend. 196, 1421 (1933).

27a. Warren, B. E., and Gingrich, N. S., Phys. Rev. 46, 368 (1934).

27b. Klug, H. P., and Alexander, L. E., "X-ray Diffraction Procedures for Polycrystalline and Amorphous Materials," John Wiley and Sons, New York, 588 (1954).

28. Waser, J., and Schomaker, V., Revs. Mod. Phys. 25, 671 (1953).

29. Shaffer, P. A., Jr., Schomaker, V., and Pauling, L., J. Chem. Phys. 14, 659 (1946).

30. Klug, H. P., and Alexander, L. E., op. cit., 377.

31. McCreery, G. L., J. Am. Ceram. Soc. 32, 141 (1949).

32. Buerger, M. J., "Numerical Structure Factor Tables," Geological Society of America, New York, 116 (1941).

33. Wilson, A. J. C., Nature 150, 152 (1942).

34. Kleinberg, J., and Sattizahn, I., J. Am. Chem. Soc. 73, 1865 (1951).

35. Kortum, G., and Wilski, H., Z. Phys. Chem. 202, 35 (1953).

36a. Zingaro, R., Vander Werf, C., and Kleinberg, J., J. Am. Chem. Soc. 73, 88 (1951).

36b. Kleinberg, J., Colton, E., Sattizahn, J., and Vander Werf, C., J. Am. Chem. Soc. 75, 442 (1953).

Propositions

1. Modification of the emulsion type and/or the development process of x-ray film can result in a considerable decrease in the necessary exposure time.

2. It is proposed that the strong light-absorption shown by polyvinyl chloride after appropriate heat treatment is due to dehydrochlorination, with the formation of conjugated poly-ene systems $(-CH=CH-)_{\bar{n}}$, with $\bar{n}$ greater than for systems previously studied. Some experiments and applications are suggested.

3. Some fundamental errors have been made in the interpretation of the diffraction data with ℓ odd in the $TiBe_{12}$ structure (P-1). The ensemble averaging methods introduced in the discussion of the $Mg_{12}Ce$ structure would be especially useful for the correct solution of the $TiBe_{12}$ structure.

4. It would be worthwhile to attempt the solution of the difference equations corresponding to growth laws based on more complex interactions and perhaps higher dimensionality than those discussed previously (P-2), and to try to correlate the results with known disordered structures.

5. The x-ray absorption correction for cylindrical specimens when the equi-inclination technique is used can be

simply expressed in terms of the familiar equatorial absorption factor.

6. When Weissenberg cameras are used, data for the correction of errors in the measured diffraction intensities due to secondary extinction could feasibly be obtained directly from the film if the beam-stop assembly of the camera were suitably modified.

7a. It is proposed that most formulations which lead to general relationships between the phases in x-ray diffraction and which are based in part on the assumption that the atoms in a crystal structure do not overlap can, in principle, be reproven without this assumption.

b. As a consequence of the non-overlapping of atoms, it can be shown that the relationship

$$\sum_{hkl} I_{hkl}\, e^{-2\pi i(hu+kv+lw)} = \sum_{\alpha} S_{\alpha}(u,v,w)$$

is valid in a region about the (u,v,w) origin. The summation on the right hand side is over the atoms α in the unit cell, and $S_{\alpha}(u,v,w)$ is a known function for each atom. Because this equality obtains in a finite neighborhood about the origin it can be differentiated any number of times, leading to a series of relationships between the diffracted intensities which usefully augments the experimental data.

9. It is proposed that the formulation of the necessary and sufficient conditions for the sphericity of the atoms in a structure in terms of the diffraction phenomena would provide a powerful device for the solution of the phase problem. An approximate formulation which approaches this resembles the two-dimensional form of Sayre's equality (P-3), but generalized in that the restriction that the atoms be identical is removed.

9. If the definition of information as $k(\ln p)$ is made time-dependent, an interesting application of differential calculus to logic results in the analysis of surprise.

10. An intentional absurdity has been included above.

11. It is proposed that a stable compound (A) having the formula $C_{34}H_{66}$ could exist which would undergo the following reactions:

$$(A) + O_3 \longrightarrow C_{34}H_{66}O_3 \quad (B)$$

$$(B) \xrightarrow[H_2O]{H_3O^+} (C) + (D),$$

where (C) and (D) each contain 17 carbon atoms, and (D) is a hydrocarbon.

Appendix - Comments on Propositions

Proposition 3.

It was mentioned in the body of the thesis that some of the methods used in the solution of the $TlBe_{12}$ structure were incorrect. In addition, it is felt that the process by which the phases of the odd layer reflections were determined is not justifiable. In effect, relative odd layer intensities were used to calculate a set of relative values of r_α for each of the possible assignments of phases corresponding to a centrosymmetric structure. The criterion that all of the r_α's should be restricted in value between -1 and 1 was not considered. The resulting values of r_α obtained for each phase assignment were rounded off into simple rational fractions, and a set of odd layer structure factors corresponding to each solution was calculated. The assignment of phases which gave the best agreement between calculated and observed relative intensities was selected as the correct choice. Actually, if the r_α's were not rounded off, the calculated intensities would be identical for each assignment of phases, so that the decision method employed here has little foundation.

Because steric considerations make it nearly impossible for there to exist triangular configurations of titanium atoms all at z = 0 (or 1/2), the expression for the structure

factor analogous to equation 146 should be accurate.

Proposition 5.

It is well known that the absorption factor $A(\mu R,\theta)$ for equatorial diffraction from a cylindrical specimen is a function of two variables, namely the Bragg angle θ, and the product μR of the linear absorption coefficient and the radius of the specimen (P-4). Examination of figure P-1 shows that each path to and from a scattering element for the equi-inclination case has a length which is greater than the corresponding path-length for the equatorial case by a factor of $\sec\nu$ (where ν is the equi-inclination angle. It is evident that the expression for the absorption factor A for the equi-inclination case is given by the equation

$$A = A(\mu R \sec\nu, \tau/2), \qquad (P-1)$$

where τ is the projection of the deviation angle 2θ onto the equatorial plane.

Propositions 7 and 8.

Many attempts have been made to solve the phase problem in x-ray crystallography by deriving relationships between the phases that are generally applicable to all structures. If these relationships are to be general, they must be derivable from properties shared by every structure. The properties most commonly used in the derivation of these

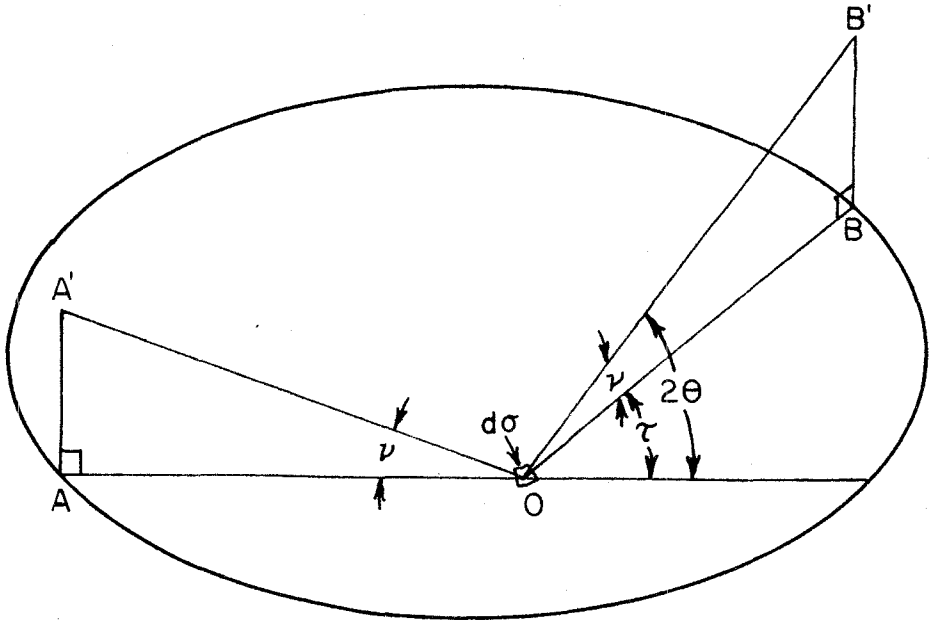

FIGURE P-I. PATHS TO AND FROM A DIFFRACTING ELEMENT $d\sigma$ IN A CYLINDRICAL SPECIMEN IN THE EQUATORIAL AND EQUI-INCLINATION CASES.

AOB is path in equatorial case. A'OB' is path in equi-inclination case.

AA' and BB' are on the boundary of the cylinder.

relationships are

1. that the electron density is everywhere positive,
2. that the atoms in the structure do not overlap, and
3. that the distribution of electron density associated with a single atom is approximately spherical.

Some of these relationships, such as the first inequality of Harker and Kasper (P-5)

$$|F_{hkl}|^2 \leqslant Z^2 \quad , \qquad \text{(P-2)}$$

where Z is the number of electrons in the unit cell, use only one of these properties (in this case property 1), while others, such as Sayre's equality (P-3) use all three. It is suggested here that the ultimate, and most powerful of these relationships would be the expression, in terms of the phases, of the necessary and sufficient conditions of each of the properties above. It will be shown below that such an expression for property 2 is easily discussed, and that it is possible to derive an approximate relationship that approaches the necessary and sufficient statement of property 3.

It is an interesting result that no further information about the phases is contained in the criterion that the atoms do not overlap than is already contained in the criterion that the electron density associated with each atom has the appropriate spherical distribution. This statement is a corollary of the theorem that if a choice of phases results in an electron density function which is the composite of

appropriately shaped peaks corresponding to each atom in the structure, there can be no overlapping of these peaks. The proof of this theorem follows. The correct choice of phases produces an electron density function which has properly shaped atomic peaks, with no overlapping. Suppose that the theorem is untrue, i.e., that a certain incorrect choice of phases results in an electron density function which preserves the proper peak shapes, but which exhibits overlapping of some of the peaks. The Patterson function corresponding to the latter electron density function is necessarily different from that corresponding to the former. Therefore the set of intensities corresponding to the latter function differs from the correct set of intensities. This is a contradiction, and the proof is completed.

The information relating to the non-overlapping of the atoms must then be contained in the relative intensities obtained in the diffraction experiments. If the neighborhood near the origin of the Patterson function consists solely of self-interaction terms, then around the origin,

$$\sum_{h,k,\ell} I_{hkl} e^{-2\pi i(hu+kv+lw)} = \sum_{\alpha} S_{\alpha}(u,v,w) , \qquad (P\text{-}3)$$

where the left hand side of equation P-3 is the Patterson function for a crystal having unit periodicity in each direction, and the right-hand side is the summation over the atoms α in the unit cell of the shape function $S_{\alpha}(u,v,w)$ for each

atom α produced by convoluting the electron density of the atom with itself. It can be shown that

$$S_\alpha(u,v,w) = \sum_{h,k,l} f^2_{\alpha,h,k,l} e^{-2\pi i(hu+kv+lw)}, \qquad \text{(P-4)}$$

where $f_{\alpha,h,k,l}$ is the form factor for atom α for the reflection with indices h,k,l. Equation P-3 can therefore be rewritten

$$\sum_{h,k,l} I_{hkl} e^{-2\pi i(hu+kv+lw)} = \sum_\alpha \sum_{h,k,l} f^2_{\alpha,h,k,l} e^{-2\pi i(hu+kv+lw)} \qquad \text{(P-5)}$$

Substituting in equation P-5 the values u=0, v=0, w=0 results in the relationship

$$\sum_{h,k,l} I_{hkl} = \sum_\alpha \sum_{h,k,l} f^2_{\alpha,h,k,l} \qquad \text{(P-6)}$$

which is the basis of the statistical method for obtaining the scale factor (P-6). Because equation P-5 is valid in a finite neighborhood about the origin, it may be differentiated any number of times, and the relationships that result upon setting u=0, v=0, w=0 are still valid. Thus, by differentiating equation P-5 twice with respect to u, there results

$$-4\pi^2 \sum_{h,k,l} h^2 I_{hkl} = \sum_\alpha \left(\frac{\partial^2 S_\alpha}{\partial u^2}\right)_{\substack{u=0 \\ v=0 \\ w=0}} = -4\pi^2 \sum_\alpha \sum_{h,k,l} h^2 f^2_{\alpha,h,k,l}. \qquad \text{(P-7)}$$

Many other relationships are similarly derivable.

The forthcoming derivation involving the sphericity of atoms is based on the fact that under the appropriate conditions, the atomic peaks in a generalized projection occur at the same coordinates as the peaks in a regular projection. Since the result is independent of the reciprocal lattice level over which the generalized projection summation is made, this can be the case only if the atoms have cylindrical symmetry about an axis parallel to the projection axis. But if this result is to be valid for all projection axes, the atoms must be cylindrically symmetrical with respect to every axis, i.e., they are spherically symmetrical. Unfortunately, the argument is not as clean-cut as it has been made to sound. Some objections will be presented below in the process of deriving from this notion a relationship between the structure factors.

It will be assumed that each atom in a structure has a similar, spherical shape, as implied by the equation

$$f_\alpha(\sin\theta/\lambda) = Z_\alpha f_o(\sin\theta/\lambda), \qquad \text{(P-8)}$$

where f_α is the form factor for the atom α, which varies with $\sin\theta/\lambda$, Z_α is the effective atomic number of the atom α, and $f_o(\sin\theta/\lambda)$ is a standard shape function describing the variation of the form factor with $\sin\theta/\lambda$. For such a structure, define U_{hkl} by

$$U_{hkl} = \frac{F_{hkl}}{f_o(\sin\theta/\lambda)} , \qquad \text{(P-9)}$$

where the value of $\sin\theta/\lambda$ corresponding to the indices hkl is used on the right hand side. If, in addition, the structure has a center of symmetry and unit periodicity, it can be shown (P-7) that

$$C'_{\ell_1}(x,y) \equiv \sum_{h,k} U_{hk\ell_1} \cos 2\pi(hx+ky) = \sum_{\alpha} Z_\alpha \, \delta(x-x_\alpha)\, \delta(y-y_\alpha) \cos 2\pi \ell_1 z_\alpha \qquad \text{(P-10)}$$

$$S'_{\ell_1}(x,y) \equiv \sum_{h,k} U_{hk\ell_1} \sin 2\pi(hx+ky) = \sum_{\alpha} Z_\alpha \, \delta(x-x_\alpha)\, \delta(y-y_\alpha) \sin 2\pi \ell_1 z_\alpha , \qquad \text{(P-11)}$$

where C'_{ℓ_1} and S'_{ℓ_1} are respectively the peak-sharpened sine and cosine generalized projections of order ℓ_1, and the δ's are Dirac delta-functions. The summations on the right-hand side of equations P-10 and P-11 are over the atoms α in the unit cell, with coordinates x_α, y_α, and z_α. If the peaks in the projection do not overlap, then it follows that

$$[C'_{\ell_1}(x,y)]^2 + [S'_{\ell_1}(x,y)]^2 = [C'_0(x,y)]^2 \qquad \text{(P-12)}$$

because

$$\cos^2 2\pi \ell_1 z_\alpha + \sin^2 2\pi \ell_1 z_\alpha = 1 \qquad \text{(P-13)}$$

for all values of ℓ_1 and z_α. In equation P-12, $C'_0(x,y)$ is

the sharpened cosine generalized projection of order zero, i.e., the ordinary peak-sharpened projection. Equation P-12, which is valid for all values of ℓ, no longer depends explicitly on the coordinates of the atoms in the structure, and can be used as a criterion for the correctness of a particular choice of signs to a subset of the structure factors. If it is suspected, for example, that all of the signs of the hk0 and hk4 reflections are known, the function on the left hand side of equation P-12 can be computed from the hk4 data, and the function on the right hand side from the hk0 data. If a few of the signs were incorrectly chosen, there will be discrepancies between the two functions.

Some objections to the method are as follows. In many space groups, there will necessarily be overlapping in the projections. Because the reciprocal lattice data, in any event, does not extend to infinity, it will be necessary, in practice, to apply an artificial convergence factor. This broadens the atomic peaks, and in addition to increasing the incidence of overlap, it makes the result somewhat inaccurate when the projection axis is not orthogonal to the other axes of the unit cell.

Equation P-12 can be stated in a different form which is more directly related to the quantities U_{hkl}. In a centrosymmetric structure, $U_{hk0} = U_{\bar{h}\bar{k}0}$, so that

$$S'_0(x,y) \equiv \sum_{h,k} U_{hk0} \sin 2\pi(hx+ky) = \tfrac{1}{2} \sum_{h,k} U_{hk0} [\sin 2\pi(hx+ky) + \sin 2\pi(-hx-ky)] = 0 \qquad \text{(P-14)}$$

It is therefore permissible to add $[S'_0(x,y)]^2 (=0)$ to the right hand side of equation P-12, obtaining

$$[C'_{\ell_1}(x,y)]^2 + [S'_{\ell_1}(x,y)]^2 = [C'_0(x,y)]^2 + [S'_0(x,y)]^2 \qquad \text{(P-15)}$$

With the use of equations P-10 and P-11 the left hand side of equation P-15 can be written

$$\left[\sum_{h,k} U_{hk\ell_1} \cos 2\pi(hx+ky)\right]\left[\sum_{H,K} U_{HK\ell_1} \cos 2\pi(Hx+Ky)\right] + \left[\sum_{h,k} U_{hk\ell_1} \sin 2\pi(hx+ky)\right]\left[\sum_{H,K} U_{HK\ell_1} \sin 2\pi(Hx+Ky)\right]$$

$$= \sum_{h,k} \sum_{H,K} U_{hk\ell_1} U_{HK\ell_1} [\cos 2\pi(hx+ky)\cos 2\pi(Hx+Ky) + \sin 2\pi(hx+ky)\sin 2\pi(Hx+Ky)]$$

$$= \sum_{h,k} \sum_{H,K} U_{hk\ell_1} U_{HK\ell_1} \cos 2\pi[(H-h)x + (K-k)y]. \qquad \text{(P-16)}$$

Making the substitutions

$$\eta = H-h$$
$$\kappa = K-k \qquad \text{(P-17)}$$

the left hand side of equation P-15 becomes

$$\sum_{\eta,k}\Big(\sum_{h,k} U_{hk\ell_1}\, U_{\eta+h,k+k,\ell_1}\Big)\cos 2\pi(\eta x+ky). \qquad \text{(P-18}$$

The commutation of the summations in these manipulations is justified when it is considered that the U's will be modified by a convergence factor which makes the summations finite. The right hand side of equation P-15 can be treated in the same fashion as the left hand side, with the substitution of the index 0 for ℓ_1 . Thus, equation P-15 can be rewritten

$$\sum_{\eta,k}\Big(\sum_{h,k} U_{hk\ell_1} U_{\eta+h,k+k,\ell_1}\Big)\cos 2\pi(\eta x+ky)=\sum_{\eta,k}\Big(\sum_{h,k} U_{hk0}\, U_{\eta+h,k+k,0}\Big)\cos 2\pi(\eta x+ky),$$

or

$$\sum_{\eta,k}\Big[\Big(\sum_{h,k} U_{hk\ell_1} U_{\eta+h,k+k,\ell_1}\Big)-\Big(\sum_{h,k} U_{hk0}\, U_{\eta+h,k+k,0}\Big)\Big]\cos 2\pi(\eta x+ky)=0. \qquad \text{(P-19)}$$

Since the coefficients in a cosine Fourier transform which is identically zero must all in turn be equal to zero, it follows that

$$\Big(\sum_{h,k} U_{hk\ell_1}\, U_{\eta+h,k+k,\ell_1}\Big)-\Big(\sum_{h,k} U_{hk0} U_{\eta+h,k+k,0}\Big)=0\ ,$$

or

$$\sum_{h,k} U_{hk\ell_1}\, U_{\eta+h,k+k,\ell_1}=\sum_{h,k} U_{hk0} U_{\eta+h,k+k,0}\ , \qquad \text{(P-20)}$$

which is the desired result. Equation P-21 is valid, within the limits imposed by the objections mentioned above, for all values of η, k and ℓ_1. It has the corollary

$$\sum_{\ell,k} U_{hk\ell_1} U_{\eta+h,k+k,\ell_1} = \sum_{h,k} U_{hk\ell_2} U_{\eta+h,k+k,\ell_2} \qquad \text{(P-21)}$$

for all ℓ_1 and ℓ_2. The equation is also valid in altered form for any other projection axis.

If the atoms in the structure are all equal, it can be shown that

$$\sum_{\ell k} U_{hk0} U_{\eta+h,k+k,0} = s(\eta,k) U_{\eta k 0}, \qquad \text{(P-22)}$$

where $s(\eta,k)$ is an appropriate shape function. This is Sayre's equality for a non-overlapping projection (P-3). As a consequence of equation P-20 it is evident that the self-convolution of the (hk0) reciprocal plane which appears on the left hand side of equation P-22 can be replaced by the self-convolution of any reciprocal lattice layer parallel to the (hk0) layer. This is a considerably stronger form of Sayre's relationship.

References for Propositions

P-1. Raeuchle, R. F., and Rundle, R. E., Acta Cryst. 5, 85 (1952).

P-2. Miller, A., Thesis, California Institute of Technology (1957).

P-3. Sayre, D., Acta Cryst. 5, 60 (1952).

P-4. Bradley, A. J., Proc. Phys. Soc. (London) 36, 879 (1935).

P-5. Harker, D., and Kasper, J.S., Acta Cryst. 1, 70 (1948).

P-6. Wilson, A. J. C., Nature 150, 152 (1942).

P-7. Lipson, H., and Cochran, W., "The Crystalline State, Volume III, The Determination of Crystal Structures," G. Bell and Sons, London, 221 (1953).